

[Catégorie]

SALP annual report (2017) of Mean Sea Level Activities

Reference: CLS-SPA-18-013
Nomenclature: SALP-RP-MA-EA-23189-CLS
Issue: 1.0
Date: 2018,Jan.22

CLS headquarters
11 rue Hermès
Parc technologique du Canal
31520 Ramonville Saint-Agne
FRANCE

Tel. +33 (0)5 61 39 47 00
Fax +33 (0)5 61 75 10 14
Mail: info@cls.fr
www.cls.fr

CLS Brest Le Ponant
Zone du technopôle de Brest Iroise
Avenue La Pérouse
29280 Plouzané
FRANCE

Tel. 33 (0)2.98.05.76.80
Fax 33 (0)2.98.05.76.90





Chronology Issues:

Issue:	Date:	Reason for change:	Author
1.0	19/01/2018	Creation	M. Ablain

People involved in this issue:

Written by (*):	Michael Ablain, Nicolas Taburet, Lionel Zawadzki, Remy Jugier, Maxime Vayre	Date + Initials:(visa or ref)
Checked by (*):		Date + Initial:(visa ou ref) [Checker]
Approved by (*):		Date + Initial:(visa ou ref) [Approver]
Application authorized by (*):		Date + Initial:(visa ou ref)

**In the opposite box: Last and First name of the person + company if different from CLS*

Index Sheet:

Context:	
Keywords:	[Mots clés]
Hyperlink:	

Distribution:



Company	Means of distribution	Names
CLS	Notification	



List of tables and figures

List of tables:

Table 1: Altimeter standards selected for the sea level calculation for the MSL AVISO indicator: the choice of these corrections can change in time or from a MSL group to another.	14
Table 2: GMSL relative bias between all the reference missions and all the complementary missions with several references: a) 0 in 1993 in the first column, b) TOPEX in the second column, c) the previous missions in the last column (only for reference missions).	15
Table 3: Global Mean sea level error budget for the main climate scales established by (Ablain et al, 2015)	21
Table 4: Modelling of altimetry errors impacting the AVISO GMSL trend uncertainty, with uncertainty level defined in a confidence interval of 1-sigma.	23
Table 5: Estimation of uncertainty envelopes from Jason-1 and Jason-2 GMSL time series for different applications.....	26
Table 6: Error budget of altimetry and tide gauge comparisons over a 10-year period (Prandi et al., 2016).	39
Table 7: Error modelling for the estimation of the altimetry GMSL drift from altimeter and tide gauge comparisons, using GLOSS/CLIVAR tide-gauge network.	41
Table 8: Error modelling for the estimation of the altimetry GMSL drift from altimeter and tide gauge comparisons, using PSMSL tide gauge network.	42
Table 9: Estimated uncertainties on trends for ~10-year time series.	62
Table 10 : SLA-DHA-mass trend uncertainty over the full serie and when considering a 1 year time period for comparison between the different products. Uncertainties are indicated at 90 % confidence level. Analyses performed with altimeter standards 2018, Argo DHA referenced to 1900 dbar corrected, and GRGS mass model.	65
Table 11: Trends uncertainties over a 1-year period for raw, 6-month and 1-year filtered out time series of GMSL differences between altimetry and tide gauges, and for different confidence intervals (68% and 90%).	86
Table 12: Minimal period needed to detect 1 mm/yr altimetry drift for raw, 6-month and 1-year filtered out time series of GMSL differences between altimetry and tide gauges, and for different confidence intervals (68% and 90%).	86
Table 13: Closure budget drift and associated uncertainty (90 % confidence level). Time-dependent uncertainties are shown as well as the total uncertainty which takes into account the non time-dependent uncertainties (related to GIA correction, 0-2000m thermosteric contribution, deep steric contribution, geocenter, land leakage). Analyses performed with CMEMS 2018, DHAs referenced to 1900 dbar and CSR mass model (Chambers et al.). GIA correction is applied to altimeter (+0.3 mm/yr).	94



Table 14: : Closure budget drift and associated uncertainty (90 % confidence level). Time-dependant uncertainties are shown as well as the total uncertainty which takes into account the non time-dependant uncertainties (related to GIA correction, 0-2000m thermosteric contribution, deep steric contribution, geocenter, land leakage). Analyses performed with CMEMS 2018, DHAs referenced to 1900 dbar and GRGS mass model. Total GIA corrections (altimetry + mass) of 0.9 mm/yr and 0.8 mm/yr is respectively applied to Jason missions on the one hand and Envisat, AltiKa and multimissions data on the other hand (this reflects the different extent in latitude) 95

List of figures:

- Figure 1: Evolution of GMSL global mean sea level time series from 6 different groups (AVISO/CNES, SL_cci/ESA, University of Colorado, CSIRO, NASA/GSFC, NOAA) products. Annual signals are removed and signals lower than 6- month smoothing applied s filtered out. All the GMSL time series are have been centered in 1993 with zero mean zero. A Glacial Isostatic Adjustment (GIA) correction of -0.3 mm/yr has been subtracted to each data set.17**
- Figure 2: Comparison of MEI index and the global mean sea level time series (from CNES/AVISO global MSL time series) after removing the global trend 18**
- Figure 3: Global MSL evolution observed independently from all the altimeter missions 18**
- Figure 4: Evolution of ensemble mean GMSL time series (average of the 6 GMSL products from AVISO/CNES, SL_cci/ESA, University of Colorado, CSIRO, NASA/GSFC, and NOAA). On the black curve, the TOPEX-A drift correction-based this report) is applied. Annual signal removed and 6-month smoothing applied; GIA correction also applied. Uncertainties (90% confidence interval) of individual measurements are superimposed (shaded area)..... 19**
- Figure 5: Regional mean sea level trends over the January-1993/May-2017 period from AVISO products (SLA grids) 20**
- Figure 6: GMSL trend uncertainties (mm/yr) estimated for any altimeter periods between 1993 and 2017. The confidence interval is 90 % (1.65-sigma). On the Y-axis is represented the length of the window (in year) and on the X-axis the central date of the window used (in year)..... 24**
- Figure 7: Map of regional MSL trend uncertainties due to altimeter errors over the [1993,2016] period. 27**
- Figure 8: Tide gauge geographical distribution for GLOSS/CLIVAR and PSMSL networks..... 29**
- Figure 9: Processing of the comparison altimetry/tide gauge. Rectangle and parallelogram shapes respectively set for process step and products..... 30**
- Figure 10: Drift dispersion (using $\sqrt{2} \times \text{Mean Absolute Deviation}$ as a robust substitute to the standard deviation) between altimeter data (DDT products containing altimeter data from 1993) and tide gauges (PSMSL network). Left to tight: Without VLM correction, VLM correction using GPS and VLM correction using Peltier's Ice-6G model GIA correction. 31**
- Figure 11: Altimeter / tide gauge (GLOSS/CLIVAR network) comparisons with long-period tide correction on tide gauges (blue) and without (red). Altimeter: full AVISO TOPEX-Poseidon,**



Jason-1, Jason-2 and Jason-3 concatenated time series on top and Jason-2 only below. Periodic signals are removed and resulting time series are 2-month (thin lines) and 6-month (thick lines) low-pass filtered. Dotted lines represent a linear regression fit of the time series; slope values are indicated in the legend..... 32

Figure 12: Evolution of GMSL differences between altimeter and tide gauges for reference missions used in the GMSL indicator calculation (TOPEX/Poseidon, Jason-1, Jason-2 and Jason-3) with the GLOSS/CLIVAR network (blue line) and the PSMSL network (red line). Signal lower than 2 months and annual signals have been removed. The blue dashed line is the trend obtained applying a generalized least square method..... 34

Figure 13: Evolution of GMSL differences between altimeter and tide gauges for 35 days repetitive missions (ERS-1, ERS-2, Envisat and SARAL-AltiKa) and the 27 days repetitive mission Sentinel-3A, with the GLOSS/CLIVAR network (blue line) and the PSMSL network (red line)..... 35

Figure 14: Evolution of global MSL differences from altimeter / tide gauges comparisons (GLOSS/CLIVAR and PSMSL network) from TOPEX/Poséidon, Jason-1, Jason-2 and Jason-3 L2P products linked together..... 36

Figure 15: Evolution of global MSL differences from altimeter / tide gauges comparisons (GLOSS/CLIVAR and PSMSL network) from CMEMS multi-mission grids (L4 sea level product). 37

Figure 16: Altimeter GMSL drift uncertainties (mm/yr) estimated from GLOSS/CLIVAR (on left) and PSMSL (on right) tide gauge network for any altimeter periods between 1993 and 2017. The confidence interval is 90 % (1.65-sigma). On the Y-axis is represented the length of the window (in year) and on the X-axis the central date of the window used (in year). 42

Figure 17: GMSL drift estimates per mission obtained through altimeter / tide gauge comparisons. Two tide gauge networks are used: GLOSS/CLIVAR and PSMSL. Each dot represents the drift estimate for the complete duration of the mission (even for drifting orbits) and its associated bar represents the drift uncertainty at 90% confidence level. From left to right: TOPEX/Poseidon, Jason-1, Jason-2, Envisat, ERS-2, ERS-1, SARAL-AltiKa, Jason-3 and Sentinel-3A. 43

Figure 18: Spatial distribution of temperature and salinity Argo profiles from 2004-2016 46

Figure 19: Monitoring of the percentage of the ocean covered by Argo profiling floats (+/- 60° and without inland seas) from 01/01/2002 to 05/31/2017. 47

Figure 20: Histogram of the difference of variance of the SLA-DHA differences for each Argo float using successively 1°x1° versus 3°x1° boxes - i.e. Variance(SLA_1x1-DHA) - Variance(SLA_3x1-DHA) - when averaging along-track Jason-1 altimeter SLA before collocating with Argo profiles. (figure from Legeais et al. 2016). 49

Figure 21: Map of the mean differences between AVISO SSALTO/DUACS and Argo data (900 dbar) over 2005-2015 without (left) and with (right) a common temporal reference period (2003-2014) for the estimation of the SLA and DHA anomalies (figure from 2015 Argo annual report)..... 50

Figure 22: Histogram of valid SLA - DHA differences on left, and map of the invalid SLA - DHA differences on right..... 51



Figure 23: Dispersion between DUACS merged maps of altimeter SLA and the steric DHA from Argo plus the mass contribution from GRACE.	52
Figure 24: Temporal evolution of the differences between Envisat (blue), Jason-1 (purple), Jason-2 (orange), SARAL/AltiKa (green) and Argo DHA referenced to 1900 dbar corrected by GRACE mass model. Analyses performed with CMEMS 2018 and GRGS mass model. Corresponding annual and semi-annual signals have been removed. All curves are 2-months filtered. GIA correction is applied to altimeter (+0.3 mm/yr) and ocean mass (-1.1 mm/yr using Jason-1 or Jason-2 and -1.2 mm/yr using Envisat or SARAL/AltiKa).	53
Figure 25: Residuals of the SLA (CMEMS DT with 2018 standards) - DHA - mass (GRGS RL03v3) for various TS reference integration depth and associated drifts.	54
Figure 26: Residuals of the SLA - DHA - mass for various mass solutions and associated drifts. ...	55
Figure 27: Taylor diagram of the comparison of the sum of steric ARGO DHA (different reference level) with altimeter sea level time series (CMEMS, 2018 standards) (grey reference circle).	57
Figure 28: Taylor diagram of the comparison of the sum of steric ARGO DHA (different reference level and latitude extension) with altimeter sea level time series (CMEMS, 2018 standards) (grey reference circle).	58
Figure 29: Global ocean mass evolution for various solutions of the SH decomposition of the GRACE dataset (seasonal sinusoids removed).	60
Figure 30: Empirical uncertainty on trend estimation associated with the various mass solutions (JPL, GFZ and CSR) as a function of the time series length.....	63
Figure 31: Formal uncertainty (90 % confidence level) on trend estimation as a function of the time series length (multi-missions CMEMS 2018 product, DHA referenced to 1900 dbar, GRGS mass model). Time series autocorrelation is accounted for in the analysis. The red dots represent the computed uncertainty and is compared to the black line representing the predicted analytical solution scaling as $t^{-3/2}$.....	64
Figure 32: Phase uncertainty variation (90 % confidence level) as a time function with multi-missions CMEMS 2018 product, DHA referenced to 1900 dbar, GRGS mass model.	66
Figure 33: Total uncertainty variation and its various component (90 % confidence level) as a time function with multi-missions CMEMS 2018 product, DHA referenced to 1900 dbar, GRGS mass model. In black line the total uncertainties variation, in blue the formal adjustment one, in green the mass solution one, in red the constant one and in yellow the annual and semi-annual cycle removals uncertainties on the trend.	67
Figure 34: Slope values of the SLA – DHA – mass closure budget and their 90% confidence level associated uncertainties. Altimetry data are the multimission CMEMS DT 2018 product (DDT label in dark), Jason-1 (red), Jason-2 (blue), Envisat (purple), SARAL/AltiKa (yellow), Jason-3 (green), Sentinel-3A (turquoise). Analyses performed with CMEMS 2018 altimetric standards, DHAs referenced to 1900 dbar and 2 different mass model (GRGS, -squares- and CSR – circles-).	68
Figure 35 : Evolution of the GMSL trend uncertainty (mm/yr) in a confidence interval of 95% considering only the GMSL bias uncertainties to link altimeter missions together for 2	



different satellite configurations : a) Jason-2+ Jason-3+ Jason-CS (solid line), b) Jason-2 (or Jason-2 + Jason-3)+ Sentinel-3A (dashed lines).....	70
Figure 36: Evolution of uncertainty (1-sigma) versus the period length for altimetry and tide-gauges comparisons over the TOPEX-A altimeter period (GLOSS/CLIVAR and PSMSL)	71
Figure 37: TOPEX-A correction derived from altimeter and tide-gauges comparisons for approach 1.....	74
Figure 38: TOPEX-A correction derived from altimeter and tide-gauges comparisons for approach 2.....	74
Figure 39: AVISO GMSL of reference uncorrected (blue curve) and corrected (red curve) with the empirical TOPEX-A correction for approach 1.	76
Figure 40: AVISO GMSL of reference uncorrected (blue curve) and corrected (red curve) with the empirical TOPEX-A correction for approach 2.	77
Figure 41: GMSL differences between altimetry and tide gauges for Jason-1 (on bottom) and Jason-2 (on top) using the network. Red dots are from raw data, blue curve after applying a low-pass filter (cut-off of 2 months), and green curve after removing in addition the residual periodic signals (annual).	81
Figure 42: Evolution of 1-year trends calculated from Jason-2 and tide-gauges comparisons over all the Jason-2 period from raw time series (red dots) and the 2-months filtered time series (blue curve)	82
Figure 43: Evolution of the standard deviation of trends estimated for several periods from 6 months to 8 years from Jason-2 and tide-gauges comparisons (raw data in blue and 2 months filtered data in green).....	83
Figure 44: Evolution of the standard deviation of trends estimated over a 1-year window size for several cutoff periods of the low-pass filter from Jason-2 and tide-gauges comparisons	84
Figure 45: Evolution of the trend uncertainties by varying at the same time the length of the period (sliding window size) and the cut-off period of the low pass-filter	85
Figure 46 : Trend uncertainties associated to annual and semi-annual residual signals.....	94

Applicable documents

AD 1 Plan d'assurance produit de CLS CLS-ED-NT-03-394

Reference documents

RD 1 Manuel du processus Documentation CLS-DOC



List of Contents

1. Executive summary	12
2. Mean Sea Level indicator	13
2.1. Method and data used	13
2.2. Altimeter missions.....	13
2.3. Altimeter standards	13
2.3.1. Intermission biases	14
2.3.2. Gridding process	15
2.4. Evolution of MSL indicator	16
2.4.1. Global evolution.....	16
2.4.1.1. Cross comparison between several groups	16
2.4.1.2. Cross comparisons between altimeter missions	18
2.4.1.3. GMSL evolution after correcting TOPEX-A drift	18
2.4.2. Regional (map of trends)	20
2.5. Uncertainties	20
2.5.1. At global scale	20
2.5.2. GMSL trend uncertainties for any periods within [1993,2016]	21
2.5.3. Estimation of an uncertainty envelope of GMSL time series.....	25
2.5.4. At regional scale	27
3. MSL comparisons between altimetry and tide gauge measurements	28
3.1. Method and data used	28
3.2. Comparison of MSL time series between altimetry and TG	32
3.2.1. By altimeter missions	32
3.2.2. From reference missions together (L2P sea level products)	36
3.2.3. From CMEMS multi-mission grids (L4 sea level products).....	37
3.3. Uncertainties	38
3.3.1. Description of errors in altimetry and tide gauge comparisons	38
3.3.2. Error budget	38
3.3.3. New estimate of altimeter GMSL drift uncertainties from tide gauges for any periods within [1993,2016].....	39
3.3.3.1. Method.....	39
3.3.3.2. Error modelling.....	39
3.3.3.3. GMSL drift uncertainties from tide gauges for any altimetry periods	42
3.3.3.4. GMSL drift uncertainties from tide gauges for each altimetry mission	43
4. MSL comparisons between altimetry and ARGO+GRACE data.....	45
4.1. Methods of comparison and datasets	45
4.1.1. Overview.....	45



4.1.2. Datasets	45
4.1.2.1. Altimeter measurement	45
4.1.2.2. Argo in-situ measurements.....	46
4.1.2.3. Grace measurements of the mass contribution	47
4.1.3. Method	48
4.1.3.1. Colocation of in-situ and altimeter data:	48
4.1.3.2. Reference of DHA and SLA	49
4.1.3.3. Validation of collocated measurements:	50
4.2. Description of MSL comparisons altimetry/(TS+GRACE)	51
4.2.1. by altimeter missions	52
4.2.2. From multi-mission products (SLA grids)	53
4.2.2.1. Temporal analyses	53
4.2.2.2. Taylor diagram analyses	56
4.2.2.3. Partial conclusions.....	58
4.3. Uncertainties	59
4.3.1. Description of errors	59
4.3.1.1. Formal uncertainty	59
4.3.1.2. Phase Uncertainty	59
4.3.1.3. Terms associated with the mass and steric contributions	59
4.3.1.3.1. Errors associated with the determination of the mass solution.....	59
4.3.1.3.2. GIA correction.....	60
4.3.1.3.3. Depth of Argo profilers	61
4.3.2. Uncertainty estimation over the trend	61
4.3.2.1. Time dependant mass solution related uncertainty estimation	62
4.3.2.2. Formal uncertainty associated to trend estimation	63
4.3.2.3. Phase uncertainty associated to trend estimation.....	65
4.3.2.4. Order of magnitude discussion	66
4.3.2.5. Application: Use of the budget uncertainty to assess the significativity of the closure budget drift for the different missions	67
5. Specific studies	69
5.1. Impact of error on the global MSL to link altimeter missions together 69	
5.1.1. Summary of (Zawadzki and Ablain, 2016) paper	69
5.1.2. Extension of the study in case of loss of the reference mission (e.g. J3)	69
5.2. Estimation of an empirical TOPEX-A correction derived from altimetry and tide-gauges measurements	71
5.2.1. Overview.....	71
5.2.1.1. Strategy to select data before filtering	72
5.2.1.2. TOPEX-A/TOPEX-B GMSL bias calculation	72
5.2.2. TOPEX-A Correction.....	73



5.2.3. Impact on the Aviso GMSL time series	75
5.2.4. Inconsistency of the TOPEX-A/TOPEX-B bias calculation	75
5.3. Determination of GMSL trend uncertainty over a 1-year period for Jason-CS requirement	77
5.3.1. Overview.....	77
5.3.1.1. Context and objectives of the study	77
5.3.1.2. OSTST report	77
5.3.2. Several approaches.....	78
5.3.3. Mathematical formalism.....	79
5.3.4. Altimetry GMSL drift uncertainties from tide gauge comparisons	80
5.3.4.1. Overview	80
5.3.4.2. Method.....	81
5.3.5. Results.....	82
5.3.5.1. <i>Impact of the window size</i>	82
5.3.5.2. Impact of the cut-off period of low-pass filter.....	83
5.3.5.3. Analyses	84
5.3.6. Conclusion, recommendation & discussions	85
5.3.6.1. Conclusion.....	85
5.3.6.2. Recommendation for the Jason-CS stability requirement.....	86
5.3.6.3. Discussions	86
6. References.....	88
7. Annexes	91
7.1. Comparing tide gauges and satellite altimetry: errors and uncertainties (Prandi et al., 2016)	91
7.2. Analytical function of the noise uncertainty	92
7.3. Phase uncertainty estimation	93
7.4. Closure budget trends and uncertainties	94
List of acronyms	96



1. Executive summary

This document is the 2017 annual report of the Mean Sea Level activities performed in the framework of the SALP project (Cal/Val activities, lot 1.6). This includes:

- The description of the Mean Sea Level indicator,
- The comparisons between altimetry and tide gauges measurements,
- The comparisons between altimetry and ARGO+GRACE measurements,
- Specific studies linked with MSL activities.

In previous years, we provided separate reports. This year, we will prefer to gather them in a unique report in order to enhance the link between these different activities.

The main progress performed in 2017 is a better description of uncertainties for MSL indicator as well as for in-situ and altimeter data comparisons. Indeed, uncertainties have been estimated for different period lengths within a confidence interval of 90%.

For MSL indicator, this is an update of the uncertainty trend estimation already performed by (Ablain et al, 2015). After updating the modelling of MSL altimetry errors, the new GMSL uncertainty trend is now 0.4 mm/yr over the [1993,2016] period instead of 0.5 mm/yr in (Ablain et al., 2015). GMSL trend uncertainties have also been provided for any periods between 1993 and 2016 included. It is interesting to observe that the GMSL trend uncertainties are about the same over the whole period [1993,2016] than over the last 15 years [2002,2016].

In the same way, uncertainties of altimetry and in situ comparison methods have been calculated for period lengths from 1 to 10 years. For tide-gauges, an uncertainty close to 0.6 mm/yr is obtained over a 10-year period whereas it is close to 1 mm/yr for ARGO+GRACE measurements. This kind of analyses is very relevant so as to be able to detect any drifts or jumps on altimetry GMSL time series.

Thanks to these uncertainty studies, the 1.7 mm/yr TOPEX-A GMSL drift detected by comparison with tide gauges can be considered as statically significant since the uncertainty is 0.9 mm/yr within a confidence interval of 90%. This means that this error could be empirically corrected with tide gauges with a very good confidence. Such an empirical correction impacts directly the GMSL evolution with an acceleration of 0.08 mm/yr² instead of 0.03 mm/yr² before the correction.

To conclude, some of the studies presented in this report should lead to peer-review papers in 2018. We planned to publish -at least- the update of GMSL trend uncertainty.



2. Mean Sea Level indicator

2.1. Method and data used

The processing to provide the Mean Sea Level (MSL) record mainly depends on the geophysical corrections applied to the Sea Surface Height (SSH) measurements (hereinafter called ‘altimeter standards’), on the global and regional relative biases applied to link accurately the altimeter missions together, and on the gridding process applied to average the along-track measurements.

2.2. Altimeter missions

All the MSL groups (University of Colorado, AVISO/CNES, CCI/ESA, CSIRO, NOAA, NASA) used 1-Hz altimetry measurements derived from TOPEX/Poseidon, Jason-1, Jason-2 and very recently Jason-3 as reference missions to compute the MSL records. On the first hand, these missions provide the most accurate long-term stability at global and regional scales (Ablain et al. 2009), and they are all on the same historical TOPEX ground track allowing to construct a seamless record of global MSL change from 1993 to the present. Besides, all the others complementary missions (ERS-1, ERS-2, Envisat, Geosat Follow-on, CryoSat, SARAL/AltiKa and Sentinel-3A/B) are also very useful to increase the spatial resolution of mean sea-level grids, and also to provide relevant cross-comparison of the MSL evolution (Ollivier et al. 2012).

2.3. Altimeter standards

Altimetry measures the distance between satellite and sea surface. The satellite altitude minus this distance gives the SSH. However, numerous perturbations have to be taken into account, and corrections need to be applied to take into account various physical phenomena: propagation corrections (the altimeter radar wave is delayed during atmosphere travel (ionospheric correction, wet tropospheric correction, dry tropospheric correction), ocean surface correction for the sea state which directly affects the radar wave (electromagnetic bias), geophysical corrections for the tides (ocean, solid earth and polar tides as well as loading effects), atmospheric corrections for the ocean's response to atmospheric dynamics (inverse barometer correction (low frequency), atmospheric dynamics correction (high frequency)). Furthermore, SSH is calculated for each altimetric measurement considered as valid according to criteria (e.g., threshold, spline, statistics on the ground track) applied either to the main altimetric parameters, the geophysical corrections or the SSH directly. These criteria may vary from one mission to another depending on the altimeter's instrumental characteristics. The precise references for the corrections and orbits used when calculating the MSL depends on each group (University of Colorado, CNES/AVISO, CSIRO, NOAA, NASA, ESA/SL_cci).

In the framework of SALP activities, the altimeter standards used are presented in the table below. It is worth noting that the choice of these corrections can change in time. It is also the main source of differences between different MSL groups. To calculate the global MSL Aviso indicator, only the reference missions are used (T/P, J1, J2, and J3). For the regional MSL indicator, all missions are used to benefit from better spatial sampling.



L2P 2018	ERS-1	ERS-2	EN	T/P	J1	J2	GFO	C2	AL	H2	J3	S3A
Orbit	Reaper	Reaper	GDR-D	GFSC STD12/15	GDR-E	GDR-E	GSFC	GDR-E	GDR-E	GDR-D	GDR-E	GDR-E
Major Instrumental correction			PTR FPAC							Correction Doppler		
Sea State Bias	BM3 (Gaspar, Ogor, 1994)	Non parametric Mertz et al., 2005	Tran 2015 (compatible new MWR et new SWH)	Non parametric SSB [N, Tran and al. 2010]	SSB GDR-E	Tran 2012	Non parametric SSB [N, Tran and S. Labroue]	Non parametric SSB de J1 (des GDR-C) avec sig0 débiaisé	SSB Peachi (2D)	Non parametric SSB [N, Tran] (vent Labroue)	Tran 2012	Non parametric SSB [N, Tran]
Ionosphere	NIC 09	NIC09(cycle 1-36), GIM from cycle 37	Iono filtre SLOOP/GIM (GDR2.1)	Iono filtre SLOOP	Iono filtre SLOOP	Iono filtre SLOOP recalculé apres update SSB band C	GIM	GIM	GIM	GIM	Iono filtre SLOOP	Iono filtre SLOOP
Wet troposphere	GPD+	GPD+	MWR repro v3	GPD+	JMR repro	correction NN a 3 entrée (3IB) a partir de simulation ET par classes de vent/tropo.	From GFO radiometer	From ECMWF model	correction NN a 5 entrées (2TB+sig0+SST Reynolds+Gamma climato)	From ECMWF model	From J3-AMR radiometer	From S3A-AMR radiometer
Dry troposphere	Era Interim based	ECMWF Gaussian grids based	Era Interim based	ECMWF rectangular grids based	ECMWF Gaussian grids based	ECMWF Gaussian grids based	ECMWF rectangular grids based	ECMWF Gaussian grids based	ECMWF Gaussian grids based	ECMWF Gaussian grids based	ECMWF Gaussian grids based	ECMWF Gaussian grids based
Combined atmospheric correction	Era Interim based	MOG2D High Resolution forced with ECMWF pressure and wing fields + IB	Era Interim based	MOG2D High Resolution forced with ECMWF pressure and wing fields + IB				MOG2D High Resolution forced with ECMWF pressure and wing fields + IB from rectangular grids	MOG2D High Resolution forced with ECMWF pressure and wing fields + IB	MOG2D High Resolution forced with ECMWF pressure and wing fields + IB	MOG2D High Resolution forced with ECMWF pressure and wing fields + IB	MOG2D High Resolution forced with ECMWF pressure and wing fields + IB
Ocean tide	FES2014											
Solid Earth tide	Elastic response to tidal potential [Cartwright and Tayler, 1971], [Cartwright and Edden, 1973]											
Pole tide	[DESAL 2015]											
MSS	CNES-CLS 2015											

Table 1: Altimeter standards selected for the sea level calculation for the MSL AVISO indicator: the choice of these corrections can change in time or from a MSL group to another.

2.3.1. Intermission biases

An important step for computing accurately the GMSL time series is the calculation of the MSL biases between the altimeter missions, both at global and regional scales. Thanks to the verification phases between two consecutive missions (TOPEX/Jason-1, Jason-1/Jason-2, Jason-2/Jason-3) when both satellites are on the same ground track following each other by few seconds, the global biases are estimated with a very good accuracy close to 0.5–1 mm in terms of MSL (Zawadzki and Ablain 2016). The absolute value of this bias depends on the altimeter standards selected in the SSH calculation. It is worth noting that the absolute global MSL bias is often arbitrarily set to 0 in 1993 by convention. Similar method is also applied to derive the regional MSL biases generated by systematic effects for instance due to the orbits solutions (Couhert et al. 2015).

The relative GMSL biases of reference missions are presented in Table 2, with several references: a) 0 in 1993, b) TOPEX, c) the previous missions.

The relative GMSL biases of complementary missions not used in the GMSL series have also been indicated in the same table for information.



		BIAIS RELATIFS du GMSL (en mètre)		
		à GMSL=0 en 1993	à TOPEX	à la mission N-1
Missions de référence	TP	-0,032		
	J1	-0,010	0,023	0,023
	J2	-0,048	-0,016	-0,039
	J3	-0,077	-0,045	-0,029
Missions complémentaires	E1	-0,011	0,021	
	E2	-0,024	0,008	
	EN	0,431	0,463	
	G2	0,007	0,039	
	AL	-0,065	-0,033	
	C2	0,007	0,039	
	H2	-0,148	-0,116	
	J1G	-0,007	0,025	
S3A	-0,094	-0,062		

Table 2: GMSL relative bias between all the reference missions and all the complementary missions with several references: a) 0 in 1993 in the first column, b) TOPEX in the second column, c) the previous missions in the last column (only for reference missions).

2.3.2. Gridding process

The second main step is to average the along-track altimeter data in order to provide mean-sea-level grids in order to derive regional and then global MSL time series. Two different approaches can be considered. The first one has been developed for the CMEMS (Segment Sol Multi-missions Altimétrie et Orbitographie, Data Unification and Altimeter Combination System) system (Dibarboure et al. 2011). It consists in using the reference missions (TOPEX/Poseidon, Jason-1, Jason-2) to provide the long-term evolution and the complementary missions (ERS-1, ERS-2, Envisat, Geosat Follow-on, CryoSat, SARAL/AltiKa) to increase the spatial resolution and also to better cover high latitudes (beyond 66 degrees north and south). Basically, after removing spurious along-track altimeter data (e.g., impacted by rain cells, sea ice, etc...) and applying MSL biases between all the missions, long wavelength errors (e.g. orbit errors) are removed between all the missions through a global minimization of the crossover differences observed for the reference mission and between reference and complementary missions (Dibarboure et al. 2011)., and then the calculation of MSL grids combining all the missions together by an objective analysis approach (Ducet, Le Traon, and Reverdin 2000; Mailly, Blayo, and Verron 1997; Le Traon et al. 2003) is performed. This method applied and recommended by the SL_cci project, allows monthly sea-level grids to be derived, with a spatial resolution of 0.25° degrees. The global MSL time-series is easily deduced from the sea level grids with a weighted averaging (taking into account the box surfaces versus latitude) over the oceanic domain observed by the altimetry data (82°S to 82°N).

The second approach, applied by the following groups - University of Colorado, CNES/AVISO, CSIRO, NOAA, NASA – consists in only using the reference missions (TOPEX/Poseidon, Jason-1 and Jason-2) to provide global MSL time series. In this case, the method is simpler since the altimetry data are not merged but just linked together. Then, a simple averaging on a cycle basis of each mission (e.g. 1° along the latitudinal axis, 3° along the longitudinal axis for CNES/AVISO) is applied. The main



advantage of this approach is the reduction of the computing time (less altimeter missions, no objective analysis). On the other hand, the global MSL time series is only estimated between 66°S and 66°N, and the regional sea-level variations are not as well represented. Furthermore, errors in altimetry measurements such as long wavelength orbit errors or oceanic tide errors are not removed and can impact the mean-sea level estimate up to 1-2 mm at each cycle. However, these limitations between these gridding process approaches only slightly impact the global MSL trend or inter-annual signals with respectively differences lower to 0.05 mm/yr over all the altimetry period and reaching 1-2 mm over shorter periods between 1 and 3 years (Henry et al, 2014).

2.4. Evolution of MSL indicator

2.4.1. Global evolution

2.4.1.1. Cross comparison between several groups

Several groups (AVISO/CNES, SL_cci/ESA, University of Colorado, CSIRO, NASA/GSFC, NOAA) provide altimetry-based GMSL time series. All of them use 1-Hz altimetry measurements derived from T/P, Jason-1, Jason-2 and very recently Jason-3 as reference missions. These missions provide the most accurate long-term stability at global and regional scales (Ablain et al., 2009, 2017a), and are all on the same historical T/P ground track, allowing to construct a seamless record of GMSL change from 1993 to present. In addition, complementary missions (ERS-1, ERS-2, Envisat, Geosat Follow-on, CryoSat, SARAL/AltiKa and Sentinel-3A) allow to increase the spatial resolution and cover high latitude ocean areas > 66°N/S latitude (e.g. the CCI sea level data set; Legeais et al., 2017).

Several processing differences exist between these groups. The most important concern the geophysical corrections needed to take into account various physical phenomena such as propagation delays, sea state bias, ocean tides, and the ocean's response to atmospheric dynamics. These corrections are not systematically the same adopted by the different groups. Other differences come from data editing, methods spatially average individual measurements during orbital cycles and link between successive missions (Master et al., 2012, Henry et al., 2013).

Overall, the quality of the different GMSL time series is equivalent: the global GMSL increases by 3.28 to 3.44 mm/yr over the 1993-2017 period, (Figure 1) according to the different groups. The largest differences are observed at interannual time scale. Using an ensemble mean GMSL based on averaging all available GMSL time series (black curve in Figure 1), the averaged GMSL trend obtained is 3.34 mm/yr.

Although the global evolution is nearly linear (linear error adjustment provided by least square method is about 0.02 mm/yr), inter-annual variations are also observed. Removing the trend from the global MSL time series highlights these variations over 1-year to 3-year period. Their magnitudes depend on the period (+3 mm in 1998-1999, -5 mm in 2011-2012, and +10 mm in 2015-2016) and are well correlated in time with El Niño and southern oscillations (ENSO) events. The comparison of the Multivariate ENSO Index (MEI) with the detrended global MSL time series highlights very well this temporal correlation (Figure 2).

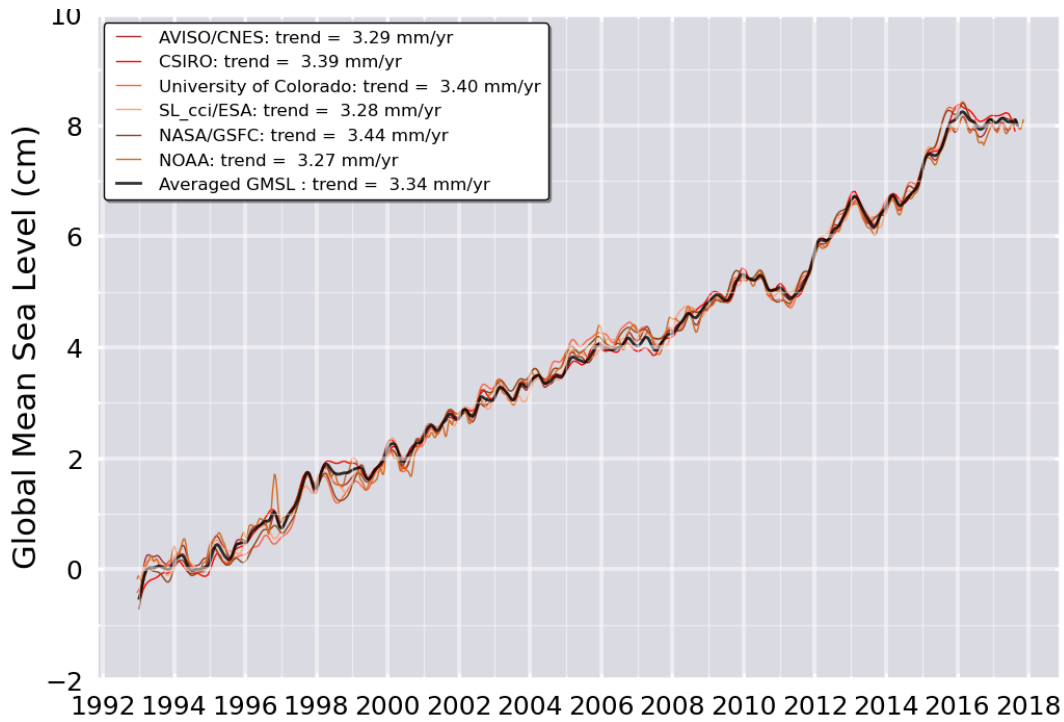


Figure 1: Evolution of GMSL global mean sea level time series from 6 different groups (AVISO/CNES, SL_cci/ESA, University of Colorado, CSIRO, NASA/GSFC, NOAA) products. Annual signals are removed and signals lower than 6- month smoothing applied s filtered out. All the GMSL time series are have been centered in 1993 with zero mean zero. A Glacial Isostatic Adjustment (GIA) correction of -0.3 mm/yr has been subtracted to each data set.

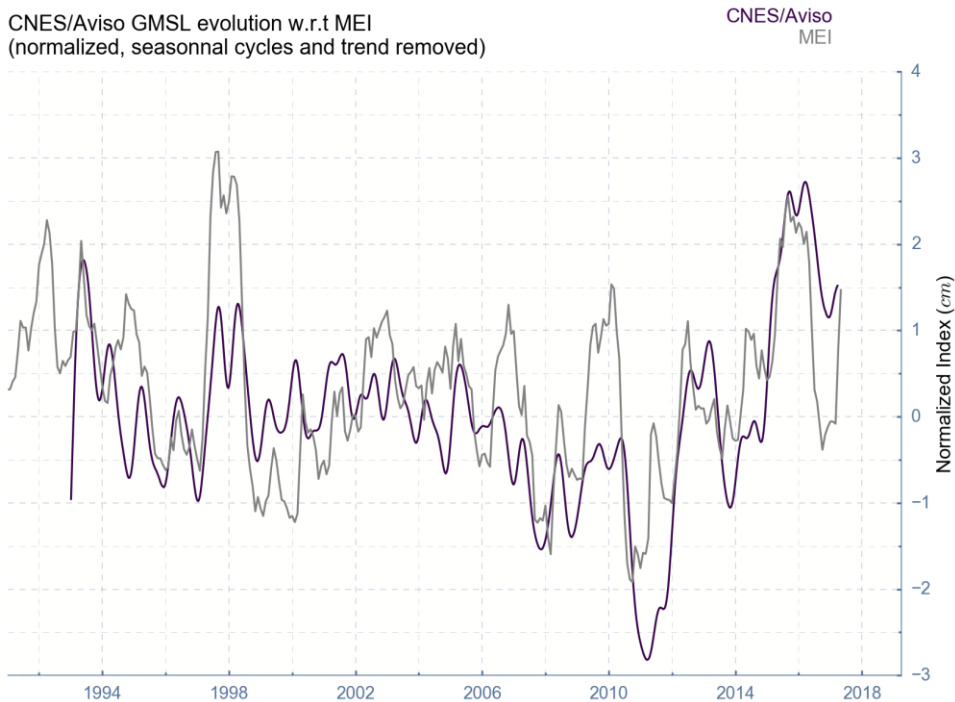




Figure 2: Comparison of MEI index and the global mean sea level time series (from CNES/AVISO global MSL time series) after removing the global trend

2.4.1.2. Cross comparisons between altimeter missions

The evolution of GMSL time series for almost all the altimetry missions is plotted in Figure 3 below. The interest of such comparisons is to highlight the relative good homogeneity of all the missions in terms of global MSL evolution. This comparison allows also to highlight some discrepancies reaching 1 cm for some missions (e.g. Envisat in 2003, ERS-1 in 1999, etc...). The GMSL trend obtained from all these missions is very close to the reference GMSL time series based on TOPEX/Poseidon, Jason-1, Jason-2 and Jason-3 measurements.

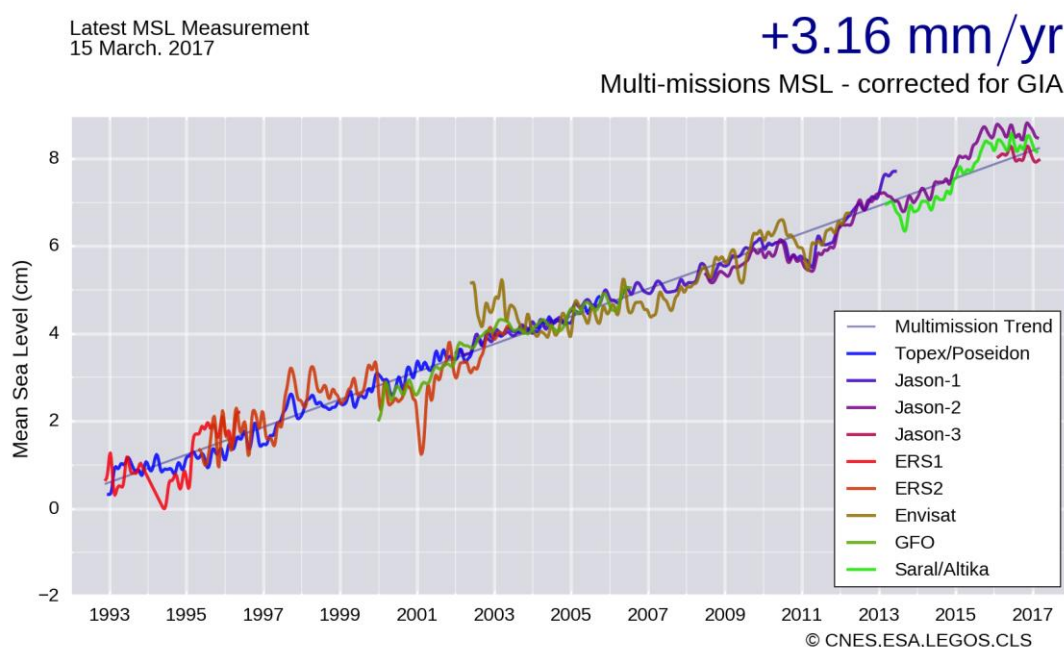


Figure 3: Global MSL evolution observed independently from all the altimeter missions

2.4.1.3. GMSL evolution after correcting TOPEX-A drift

As all system measurements, altimetry data are impacted by errors at different time scales. Most of the time, we are not able to correct these errors and they lead to an uncertainty estimate. In section 2.5, these errors and uncertainty estimations are largely described for the global and regional MSL.

However, among the altimetry error, one is particular important: it affects the first 6 years (1993-1998) of the T/P GMSL measurements due to a known instrumental drift of the TOPEX-A altimeter. This effect on the GMSL time series was recently highlighted via comparisons with tide gauges (G. Valladeau et al., 2012; Watson et al., 2015), via a sea level budget approach (i.e., comparison with the sum of mass and steric components) (Dieng et al., 2017) and by comparing with Poseidon-1 measurements (Zawadzki et al., 2016). Beckley et al. (2017) argued that the corresponding error on



the 1993-1998 GMSL resulted from wrong onboard calibration parameters. All approaches conclude that during the 1993-1998 time span the altimetry-based GMSL was overestimated.

Thanks to accurate comparisons with tide gauge measurements, we have detected a $-1.7 \text{ mm/yr} \pm 0.9 \text{ mm/yr}$ drift on TOPEX-A GMSL (see section 3.2) within a confidence interval of 90%. This drift breaks down into 2 drifts of about -1 mm/yr between January 1993 and July 1995 and 3 mm/yr between August 1995 and February 1999. The uncertainty level is higher over 4-year periods, close to 1.5 mm/yr within a confidence interval of 68%. However, an empirical correction can be proposed with a significant confidence (see section 5.2).

In the scientific literature, other TOPEX-A drift corrections proposed to subtract to the 1993-1998 GMSL time series are $1.5 \pm 0.5 \text{ mm/yr}$ (Watson et al., 2015 preferred value), $1.5 \pm 0.5 \text{ mm/yr}$ (Dieng et al., 2017) and on the order of 1.2 mm/yr when no onboard calibration correction is applied (Beckley et al., 2017).

Figure 2 shows the corrected GMSL time series (ensemble mean of the 6 processing groups), with the empirical correction proposed in this report (see section 5.2) applied over Jan-1993 to Feb-1999.

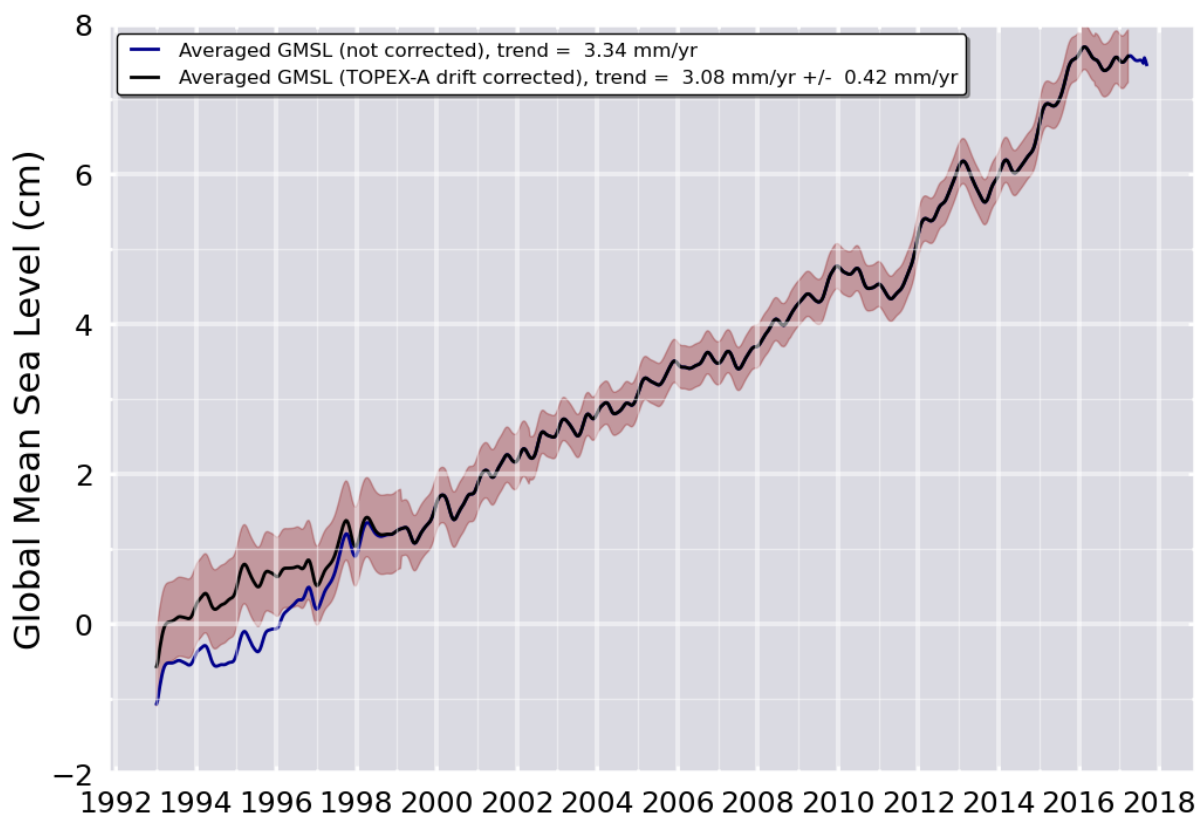


Figure 4: Evolution of ensemble mean GMSL time series (average of the 6 GMSL products from AVISO/CNES, SL_cci/ESA, University of Colorado, CSIRO, NASA/GSFC, and NOAA). On the black curve, the TOPEX-A drift correction-based this report) is applied. Annual signal removed and 6-month smoothing applied; GIA correction also applied. Uncertainties (90% confidence interval) of individual measurements are superimposed (shaded area).



2.4.2. Regional (map of trends)

The regional mean sea level variations are generally considerably larger than the global mean ones due to the large local variability generated by regional changes in winds, pressure, and ocean currents which average out at global scale (e.g. Stammer et al., 2013). The regional sea level trends (Figure 5) over 1993-2015 exhibit large scale variations with amplitudes ranging from -3 to 8 mm/yr in regions such as the western tropical Pacific Ocean, the boundary current systems, and the Southern Ocean. A part of these regional variations represents the inter-annual variations of the ocean (e.g. ENSO events). With a longer altimetry period, the regional sea level evolution will converge towards more homogenous MSL trends.

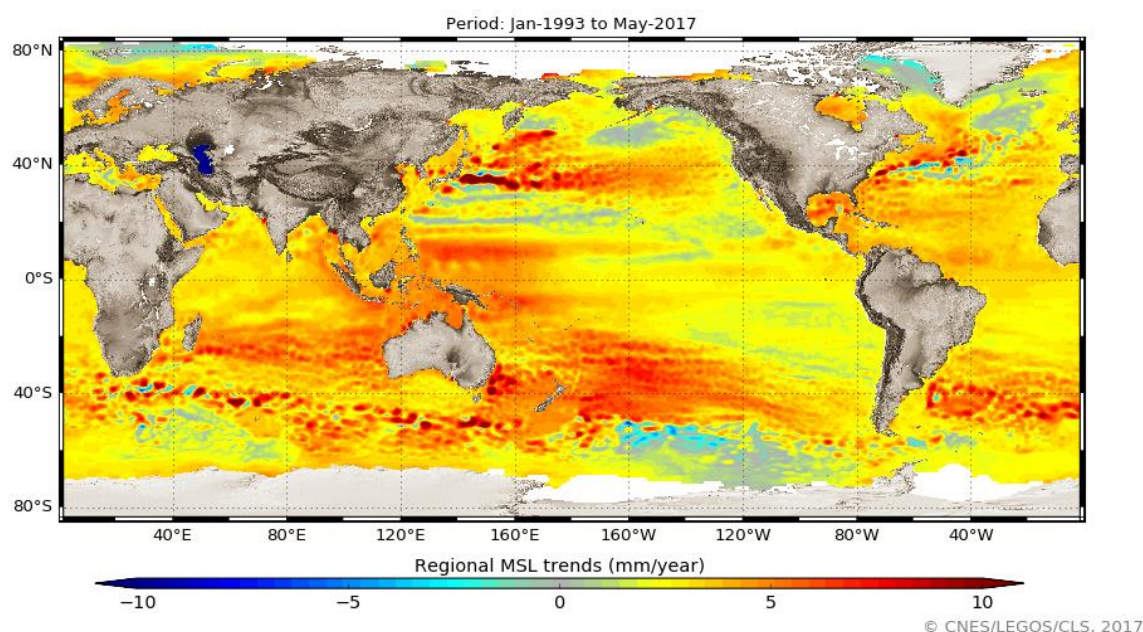


Figure 5: Regional mean sea level trends over the January-1993/May-2017 period from AVISO products (SLA grids)

2.5. Uncertainties

2.5.1. At global scale

The error budget dedicated to the main temporal (i.e. long-term - 5-10 years or more -, interannual - <5 years - and seasonal has been established by (Ablain et al., 2015) (see Table 3). Regarding the global MSL trend, an uncertainty of 0.5 mm/yr was estimated over the whole altimetry era (1993-2015) within a confidence interval of 90%. The *main* source of the error is the radiometer wet tropospheric correction with a drift uncertainty in the range of 0.2-0.3 mm/yr (J-F. Legeais et al., 2014). To a lesser extent, the orbit error (Couhert et al., 2014) and the altimeter parameters (range, sigma-0, SWH) instabilities (Ablain et al., 2012) also add additional uncertainty, of the order of 0.1



mm/yr. It is worth noting that for these two corrections, the uncertainties are higher in the first altimetry decade (1993-2002) where TOPEX/Poseidon, ERS-1 and ERS-2 measurements display stronger errors. Furthermore, imperfect links between TOPEX-A and TOPEX-B (February 1999), TOPEX-B and Jason-1 (April 2003), Jason-1 and Jason-2 (October 2008) lead to the errors of 2 mm, 1 mm and 0.5 mm respectively (Ablain et al., 2009, Zawadzki & Ablain, 2016). They explained a global MSL trend uncertainty of about 0.1 mm/yr over the 1993-2015 period. It is relevant to note that the remaining uncertainty of 0.5 mm/yr on the global MSL trend remains higher than the GCOS requirements (of 0.3 mm/yr over 10 years, see GCOS, 2011). All sources of errors described above and the gridding process (already described) have also an impact at the interannual time scale (< 5 years). The level of error is still 1.5 mm higher than the GCOS requirement of (0.5 mm). This may have consequences on the sea level closure budget studies at the interannual time scale. For the annual signal, the amplitude error was estimated lower than 1 mm. Knowing that the annual amplitude of the global MSL is of the order of 9 mm, the error can be considered low.

Spatial Scales	Temporal Scales	Altimetry Errors	User requirements
Global MSL	Long-term evolution (> 10 years)	< 0.5 mm/yr	0.3 mm/yr
	Interannual signals (< 5 years)	< 2 mm over 1 year	0.5 mm over 1 year
	Annual signals	< 1 mm	Not defined

Table 3: Global Mean sea level error budget for the main climate scales established by (Ablain et al, 2015)

2.5.2. GMSL trend uncertainties for any periods within [1993,2016]

The budget error presented in the previous section covers the [1993,2014] period. This year (in 2017), we have performed a new estimation of the GMSL trend uncertainties presented in this section. We have considered the whole altimeter period [1993,2016], updated the altimetry error modelling, and estimated GMSL trend uncertainties for any periods of the GMSL time series between 1993 et 2016.

First of all, we remind that the method used to estimate the GMSL trend uncertainties is the same as in (Ablain et al. 2009). It consists in applying an inverse method [Bretherton et al., 1976] to estimate a more realistic error from a statistical approach:

$$x_{est} = R_{xx} H^T (H R_{xx} H^T + R_{yy})^{-1} z, \quad (\text{Bretherton et al., 1976}) \quad \text{Eq. 1}$$



In this formula, \mathbf{x}_{est} is the estimated unknown vector (estimated trend here), \mathbf{z} is the observation vector and \mathbf{H} the observation operator, \mathbf{R}_{vv} the covariance matrix of observation errors and \mathbf{R}_{xx} the unknown covariance matrix. Thanks to this appropriate mathematic formalism, we are able to take into account each error after filling the covariance matrix of observation errors (\mathbf{R}_{vv}). This allows us to describe them differently according to the time period (TOPEX and Jason-1 can be separated) or their nature (jump or drift for instance). The formal error can then directly be estimated from the following formalism from the diagonal term in \mathbf{C}_{xx} (estimated unknown covariance matrix) corresponding to the slope:

$$\mathbf{C}_{xx} = \mathbf{R}_{xx} - \mathbf{R}_{xx} \mathbf{H}^T (\mathbf{H} \mathbf{R}_{xx} \mathbf{H}^T + \mathbf{R}_{vv})^{-1} \mathbf{H} \mathbf{R}_{xx}, \text{ (Bretherton et al., 1976)} \quad \text{Eq. 2}$$

A realistic error is then calculated after multiplying this formal error by the coefficient given by the student law for a dedicated confidence interval. Therefore, the difficulty of this formal approach consists in correctly defining the covariance matrix of observation errors \mathbf{R}_{vv} .

As mentioned in introduction, the modelization of altimetry errors was updated compare to (Ablain et al., 2009) to take into account a better knowledge of altimetry errors, and thus better estimate the covariance matrix of altimetry errors. Three families of errors were defined: a) correlated error with a given wavelength (λ) modeled by a gaussian function; b) error on the trends; c) error on GMSL bias to link altimetry missions together. Errors considering in our study are presented in the following Table 4:

Source of error	Family	Characteristic	Comment
High frequency errors (< 2 months):	Correlated error with $\lambda = 2$ months	$\sigma = 3$ mm for TOPEX period $\sigma = 2$ mm for Jason period.	All the high frequency errors lower than 2 months are included (geophysical corrections, SSB, etc ...) Errors is higher on TOPEX period to consider 59-days errors on TOPEX data (Zawadzki et al., 2017).
Medium frequency errors (between 2 months and 1 year):	Correlated error with $\lambda = 1$ year	$\sigma = 2$ mm for TOPEX/Poseidon $\sigma = 1.5$ mm for Jason period	All the errors between 2 months and 1 year are included (instrumental instabilities, geophysical corrections, etc ...). Uncertainty level is stronger on TOPEX altimeter due to additional altimeter calibration (range, sigma-0) errors, higher on TOPEX-A than on TOPEX-B.
Large frequency errors (between 1 year and 20 years):	Correlated error with a $\lambda = 20$ years	$\lambda = 20$ years $\sigma = 1.5$ mm over all the period	In (Ablain et al. 1999), wet troposphere by a trend uncertainty of about 0.2-0.25 mm/yr over all the period. This is likely true for periods until 20 years. But for



			longer periods, errors are progressively decorrelated. Therefore, it is more realistic to model these errors with a correlated error applying $\lambda=20$ years and an adapted σ .
TOPEX-A instabilities	Trend error	$\sigma = 0.6$ mm/yr Only on TOPEX-A period	Additional errors are added to characterize the TOPEX-A GMSL instabilities. The uncertainty level has been inferred from TOPEX-A and tide-gauge comparisons (see section 3). The -1.7 mm/yr TOPEX-A GMSL drift is assumed corrected (it's not an uncertainty but an error)
Long-term drift errors (orbit, GIA)	Trend error	$\sigma = 0.1$ mm/yr over all the period	Long-term drift error is lower is between 0.05 and 0.1 mm/yr (Couhert et al., 2015). GIA correction is -0.3 mm/yr +/- 0.05 mm/yr (G. Spada, 2017).
Error to link the altimetric mission GMSL time series together.	Bias error	$\sigma = 2$ mm for TOPEX-A/TOPEX-B and 0.5 mm for TOPEX-B/Jason-1, Jason-1/Jason-2, Jason-2/Jason-3.	Uncertainties to link altimetry missions were defined in (Ablain et al., 2009, Zawadzki and Ablain, 2016).

Table 4: Modelling of altimetry errors impacting the AVISO GMSL trend uncertainty, with uncertainty level defined in a confidence interval of 1-sigma.

The covariance matrix of altimetry errors can be easily inferred from Table 4. Then, the GMSL trend uncertainties are calculated for sliding windows from 1 year to 25 years and from 1993 to 2017 (Figure 6). It is worth noting that uncertainties are calculated in a confidence interval of 90%. This synthetic way to display GMSL trend uncertainties allows to provide them for any periods between 1993 and 2017.

The analysis of the plot highlights several interesting comments:

- As expected, the minimal uncertainty value is obtained for the longest period (24 years), close to 0.4 mm/yr (to be perfectly exact, the uncertainty obtained is -0.37 mm/yr over a 24.7-year period length). This means that the new GMSL trend uncertainty is now reduced by 0.1 mm/yr compared to (Ablain et al., 2015) over a shorter period [1993,2014].
- However, it is worth noting that this minimal uncertainty value is obtained for period length until about 15 years over the period but not taking into account TOPEX-A. For instance, considering the [2002,2016] period of 15 years, uncertainty is the same as for the total



period. This means that additional TOPEX GMSL measurements do not contribute to reduce the GMSL trend uncertainty.

- In a general view, considering a same period length, uncertainties are lower when TOPEX-A data are not considered. This result is of course expected, but we can now quantify it. For instance, if we focus on 10-year period lengths, uncertainties are reduced from about 1.5 mm/yr over the [1993,2002] period to 0.6 mm/yr over the [1993,2002].
- For small period length, uncertainties rise strongly to reach values higher than 10 mm/yr over a 1-year period which have no scientific interest. If we assume that the minimal uncertainty level needed to estimate the GMSL trend is 1 mm/yr, thus, a period length of 5 years is needed using recent data, and a little more is the selected period cover 2 altimeter missions (e.g Jason-1 and Jason-2 in 2008 for instance). On the TOPEX period, as already mentioned, the 1 mm/yr threshold is not reached.
- To finish, we can just mention that impact of uncertainty to link altimeter mission is clearly visible in 1999 (TOPEX-A/TOPEX-B), 2002 (TOPEX-B /Jason-1), 2008 (Jason-1/Jason-2). For Jason-2/Jason-3 (May 2016), it is not yet visible even if the error has been described. As expected, for a same date, the impact of these errors is reduced when the period is growing.

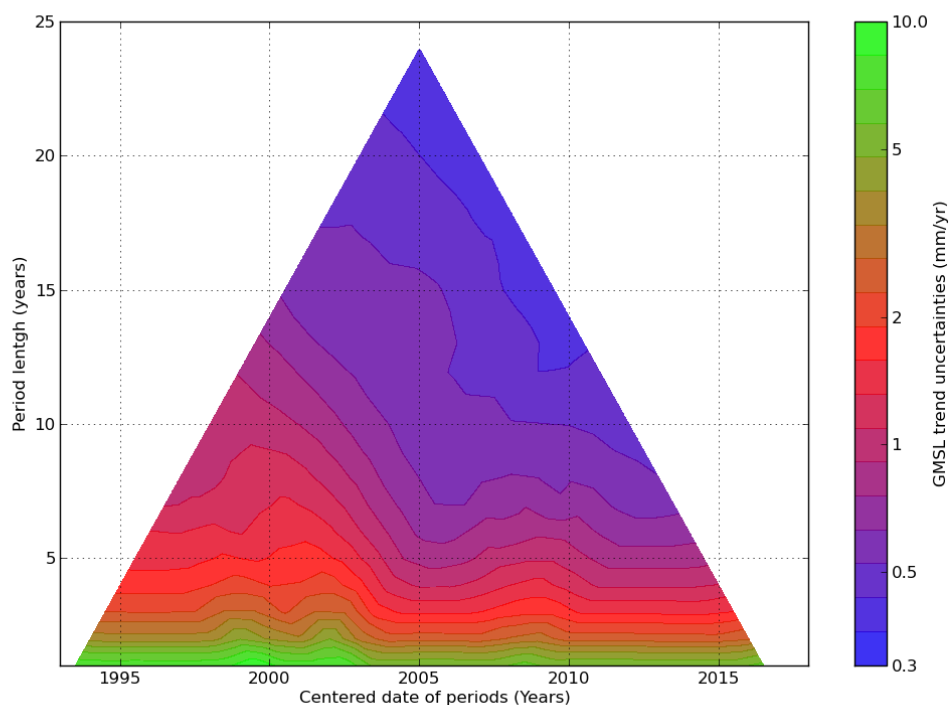


Figure 6: GMSL trend uncertainties (mm/yr) estimated for any altimeter periods between 1993 and 2017. The confidence interval is 90 % (1.65-sigma). On the Y-axis is represented the length of the window (in year) and on the X-axis the central date of the window used (in year).



2.5.3. Estimation of an uncertainty envelope of GMSL time series

For users, knowing as much as possible the errors impacting the MSL calculation is essential. This information allows rigorous analyses of the MSL variations and in fine the correct interpretation of the geophysical mechanisms underlying these variations. The characterization of these errors was performed over the whole altimetric period separating several time scales as the long-term evolution (mean sea level trend), but also the inter-annual and periodic signals (see section 2.5.1). However, providing a cycle-by-cycle estimation of the uncertainty is very challenging. In this section, we propose a methodology to estimate a confidence envelope based on a set operation.

The main principle is to generate a set of GMSL time-series that a priori have equivalent qualities by tuning different parameters. The dispersion of the set allows the estimation of confidence envelopes which can be adapted to a specific analysis. Choosing the parameters and their tuning requires exhaustive preliminary studies, that have been performed in the framework of Sea Level Climate Change Initiative.

In this study, we chose 4 different parameters to generate the set:

- **Altimetry standards:** probably the largest source of uncertainty. The improvement of altimeter standards has led to significant improvement in the MSL accuracy (ref). Yet, several solutions often exist, and it is not always possible to determine which one is the best. Thus, whenever possible, several high-quality solutions have been used for the standards (MSS, tiduals models, orbits...etc). However, consistent standards have been used between the records: if a tidal model has been used for Jason-1, the same is used for Jason-2.
- **Data Selection:** the quality of coastal measurements is lesser than in open ocean because of the land contamination in the altimeter and radiometer footprints. Thus, we tried 3 different solutions for the data selection: i) all available measurements, ii) bathymetry > 100m, iii) bathymetry > 200m.
- **Average Mesh Grids:** resolution of the mesh grids before global average (2°x2°, 3°x1°...etc)
- **Relative bias Estimation:** the estimation of the inter-mission relative biases is performed over a sub-period of the 20-cycle tandem phases. However, the length and the position of the sub-period within the tandem phase is subjective. Thus, we tried here several combinations of length and positions to estimate the inter-mission relative biases.

This methodology lead to the computation of about 18000 GMSL records with Jason-1 and Jason-2 only. Now, based on the application, there are several possibilities to derive uncertainty envelopes based on the dispersion of this GMSL set:

Application	Methodology	Uncertainty envelope
-------------	-------------	----------------------

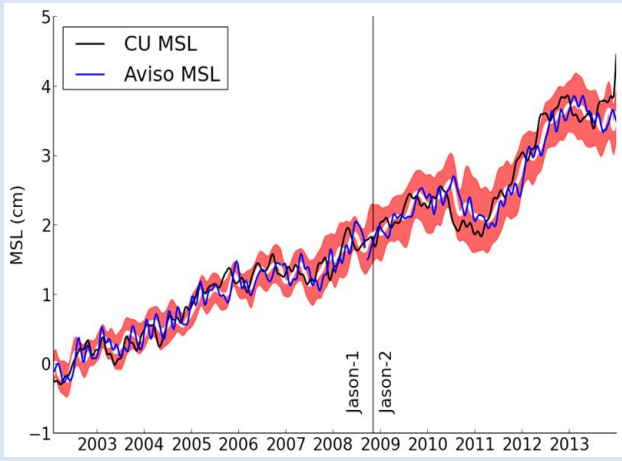
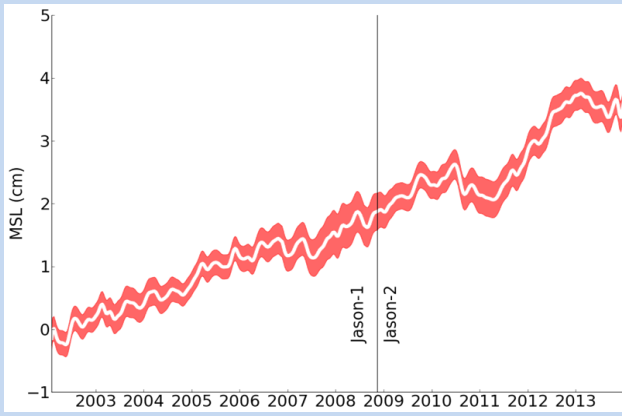

<p>Long-term evolutions</p>	<p>All GMSL continuous records are unbiased with respect to the first year (the average GMSL over the first year is the bias). Then, the cycle-by-cycle mean is computed (white curve), as well as the 2-standard deviation uncertainty envelope (95% confidence level, red envelope)).</p> <p>In this case, the long-term evolutions of the uncertainty are visible. From 2009 onwards, the confidence envelope cumulates the uncertainty from Jason-1, the relative bias and Jason-2 and thus becomes larger and larger.</p> <p>In the example on the right, the Colorado University and the Aviso MSL have been added, fitting perfectly in the envelope.</p>	
<p>short-term evolutions with trend</p>	<p>Jason-1 and Jason-2 GMSL records are processed separately at first. The cycle-by-cycle mean, and 2-standard deviation envelope are estimated separately and then linked back taking into account the uncertainty due to the relative bias.</p> <p>In this case, the uncertainty of Jason-1 and the relative bias are not propagated onwards. This way, the uncertainty envelope does not show the long-term uncertainties.</p>	
<p>short-term evolutions without trend</p>	<p>All GMSL continuous records are de-trended. The cycle-by-cycle mean and 2-standard deviation envelope are estimated.</p> <p>In this case, the focus is on the instantaneous uncertainty and allows a better analysis of the short-term evolutions, regardless of the trend. This envelope allows comparisons, for instance, to Multivariate ENSO Index.</p>	

Table 5: Estimation of uncertainty envelopes from Jason-1 and Jason-2 GMSL time series for different applications.



2.5.4. At regional scale

The regional trend uncertainty due to altimetry errors is of the order of 2 to 3 mm/yr depending on the regions (Prandi et al., 2016): see table 2. The orbit solutions are the main source of errors the range of 1-2 mm/yr (Couhert et al., 2014) with large spatial patterns at hemispheric scale. The Earth gravity field model errors explain an important part of these uncertainties (Rudenko et al., 2014). Furthermore, errors are higher in the first decade (1993-2002) where the Earth gravity field models are less accurate due to the unavailability of the Gravity Recovery and Climate Experiment (GRACE) data before 2002. Additional errors are still observed, e.g., for the radiometer-based wet tropospheric correction in tropical areas, other atmospheric corrections in high latitudes, and high frequency corrections in coastal areas. The combined errors give rise to an uncertainty of 0.5-1.5 mm/yr. Finally, the 2-3 mm/yr uncertainty on regional sea level trends remains a significant error compared to the 1 mm/yr GCOS requirement.

A similar mathematical approach as for the calculation of GMSL trend uncertainty was applied in (Prandi et al., 2018) to estimate of map of regional MSL trend uncertainties (Figure 7). The signature of natural ocean variability (e.g. inter-annual variability as ENSO oscillation) is visible because of the formal error adjustment of trends.

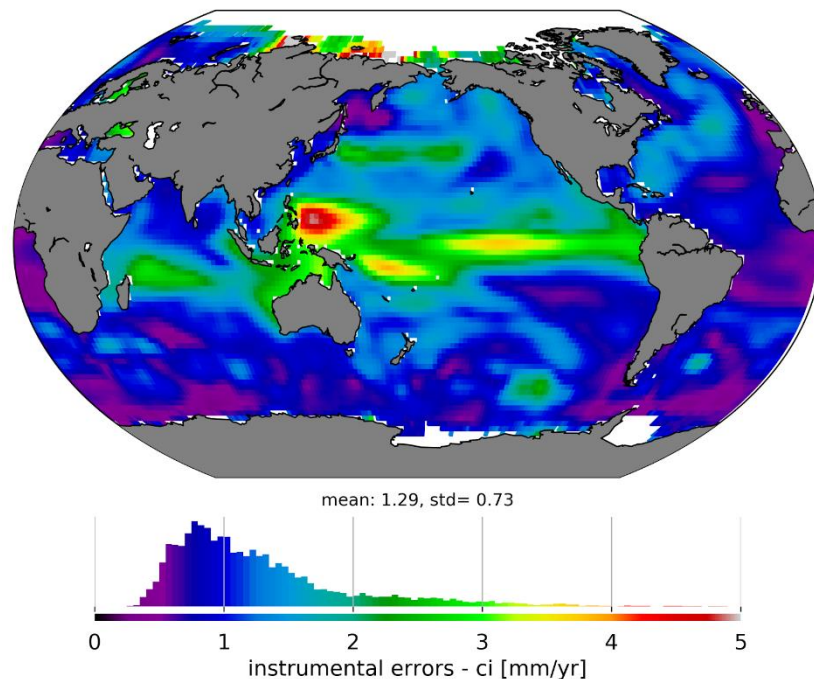


Figure 7: Map of regional MSL trend uncertainties due to altimeter errors over the [1993,2016] period.



3. MSL comparisons between altimetry and tide gauge measurements

3.1. Method and data used

One of the main objectives of comparing altimeter and tide gauge measurements is to ensure that the altimeter record is not drifting over time using independent data. Simply put, the approach consists in using a wide network of tide gauges, which are accurate enough and providing a large enough ensemble to build regional or global biases between an altimetry mission and tide gauges.

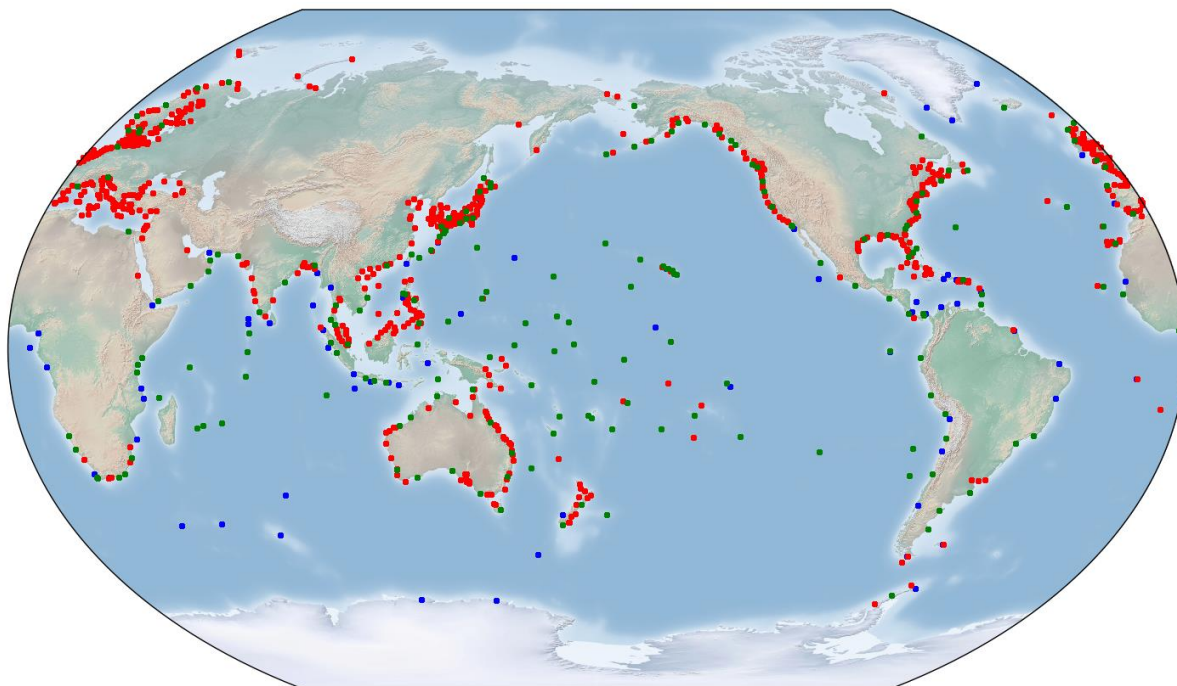
Two tide gauge networks are used:

- GLOSS/CLIVAR: 279 hourly records distributed by UHLSL which are selected for their “as far as possible” homogeneous coastline coverage. The data control of UHLSL guarantees a robust data quality and a constant hourly sampling of the SSH time series.
- PSMSL: 982 monthly records.

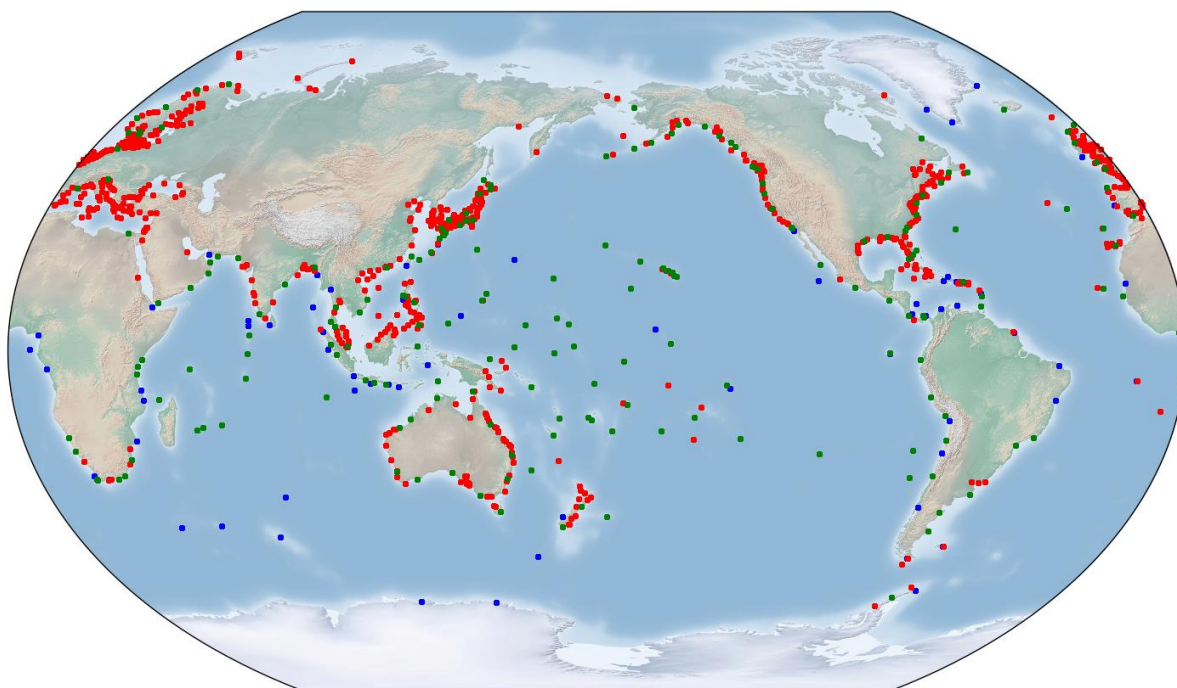
For altimetry data, the L2P altimetry products are used with CMEMS-2018 standards. It is worth noting that CMEMS 2014 standards were used in “*Calval Alti-TG annual report 2016* “. However, the impact of using either of these two altimeter standard versions has a low impact.

Concerning the method, altimetry and tide gauge data are first projected to a common spatio-temporal reference using a process chain described thoroughly in *Calval Alti-TG annual report 2016* and showed on Figure 9.

One should note that as the in-situ datum is station-dependent, altimetry to tide gauge comparison is limited to relative variations and may only be used to detect eventual jump or drift between the two records. A global difference between altimetry and tide gauge series is estimated by averaging all the stations SLA difference. By considering this global time series, one should be able to detect an eventual anomaly (drift or jump) between in-situ and remote sensing.



- Gloss-Clivar: 279 tide gauges
- PSMSL: 982 tide gauges
- 196 common tide gauges



- Gloss-Clivar: 279 tide gauges
- PSMSL: 982 tide gauges
- 196 common tide gauges

Figure 8: Tide gauge geographical distribution for GLOSS/CLIVAR and PSMSL networks.

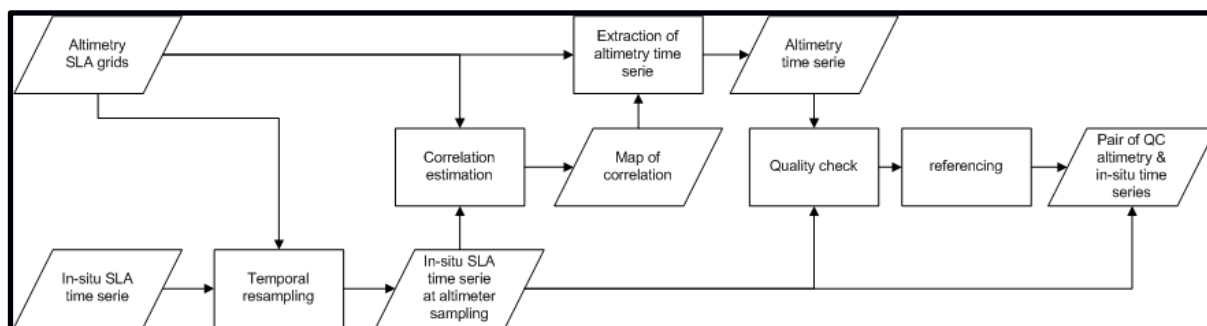


Figure 9: Processing of the comparison altimetry/tide gauge. Rectangle and parallelogram shapes respectively set for process step and products.

Tide gauge relative SSH measurements are corrected as much as possible for various effects so that the physical content is comparable to absolute SSH measurements from altimetry:

- **Tidal effects:**
 - High-frequency variations are removed with a Demerliac low-pass filter (see Bessero, 1985).
 - Long period tides are removed using FES2014 tide model.
- **High-frequency atmospheric effects:** corrected with Mog2d Dynamical Atmospheric Correction (DAC) (Dorandeu and Le Traon, 1999; Carrere and Lyard, 2003).
- **Vertical land motion (VLM):** VLM contains a Glacial Isostatic Adjustment (GIA) component for which accurate values are provided by Peltier's Ice-6G model. However, other VLM effects occur on a small spatial scale which can only be evaluated by using GPS or DORIS measurements close to the tide gauge location. Figure 10 shows spatial variations of VLM of the order of 1 cm/yr near a tide gauge. The GPS receiver is located 1.7 km away, but it proves too far to measure the tide gauge VLM (a distance under 100m seems to be needed). Unfortunately, the nearest GPS receiver is too far from the tide gauge in most cases, rendering VLM correction impossible for the time being. Figure 10 shows altimeter / tide gauge (PSMSL network) comparisons' drift distribution for 3 cases: without any VLM correction, with closest GPS data correction and with Peltier's Ice-6G model GIA correction. We observe no significant difference between the 3 cases: drift values continue to be of the order of 1 cm/yr while satellite GMSL drifts are expected to be of the order of 1 mm/yr. This confirms the inability to correct VLM at tide gauge locations for such studies at global scale. Therefore, to date, **no VLM correction is applied**. However, as it is an important source of errors, further investigations will be needed to use better VLM datasets or to improve the data processing.

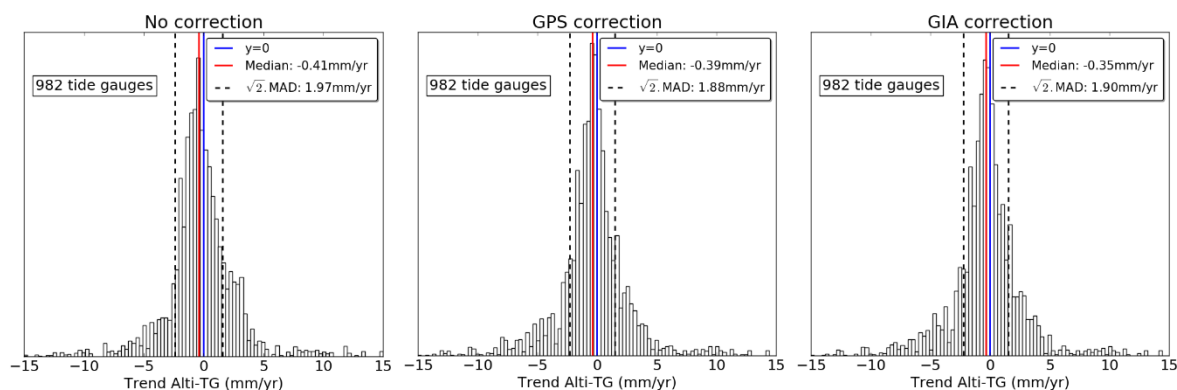


Figure 10: Drift dispersion (using $\sqrt{2} \times$ Mean Absolute Deviation as a robust substitute to the standard deviation) between altimeter data (DDT products containing altimeter data from 1993) and tide gauges (PSMSL network). Left to right: Without VLM correction, VLM correction using GPS and VLM correction using Peltier's Ice-6G model GIA correction.

Calval Alti-TG annual report 2016 contained two small-impact errors in the data processing that have been corrected in 2017:

- Long-period tide corrections** for tide gauge data were not taken into account in the 2016 report due to an error in the software implementation. Figure 11 shows global MSL differences from altimeter / tide gauge comparisons with and without these corrections using GLOSS/CLIVAR tide gauge data. The top figure representing the full AVISO TOPEX/Poseidon, Jason-1, Jason-2 and Jason-3 time series shows that the impact on the drift estimate is very low for the full time series and for most periods within this time series. However, for specific cases like the Jason-2 time period which lies exactly between two long-period tide extrema, not correcting for long-period tides on tide gauges can lead to approx. 0.3 mm/yr errors on altimetry drift estimates, therefore reaching significant values.
- GIA correction:** A 0.3 mm/yr (Peltier et al., 2004) value used to be added to all estimated drifts through altimeter / tide gauge comparisons to remove GIA-induced sea level rise on altimetry. However, while this operation is justified to calculate the GMSL indicator from altimetry data, in the case of a comparison between altimeter and tide gauge data, no drift correction must be applied since altimeter and tide gauges are impacted by the same physical effect, and thus observe the same sea level variation due to GIA. It is worth noting that the mean value of GIA drift is not the same in coastal areas (-0.8 mm/yr at TG locations) than in open ocean (-0.27 mm/yr) (G. Spada, 2017). The only vertical movement between the two coordinate systems is the tide gauge's vertical land motion (VLM).

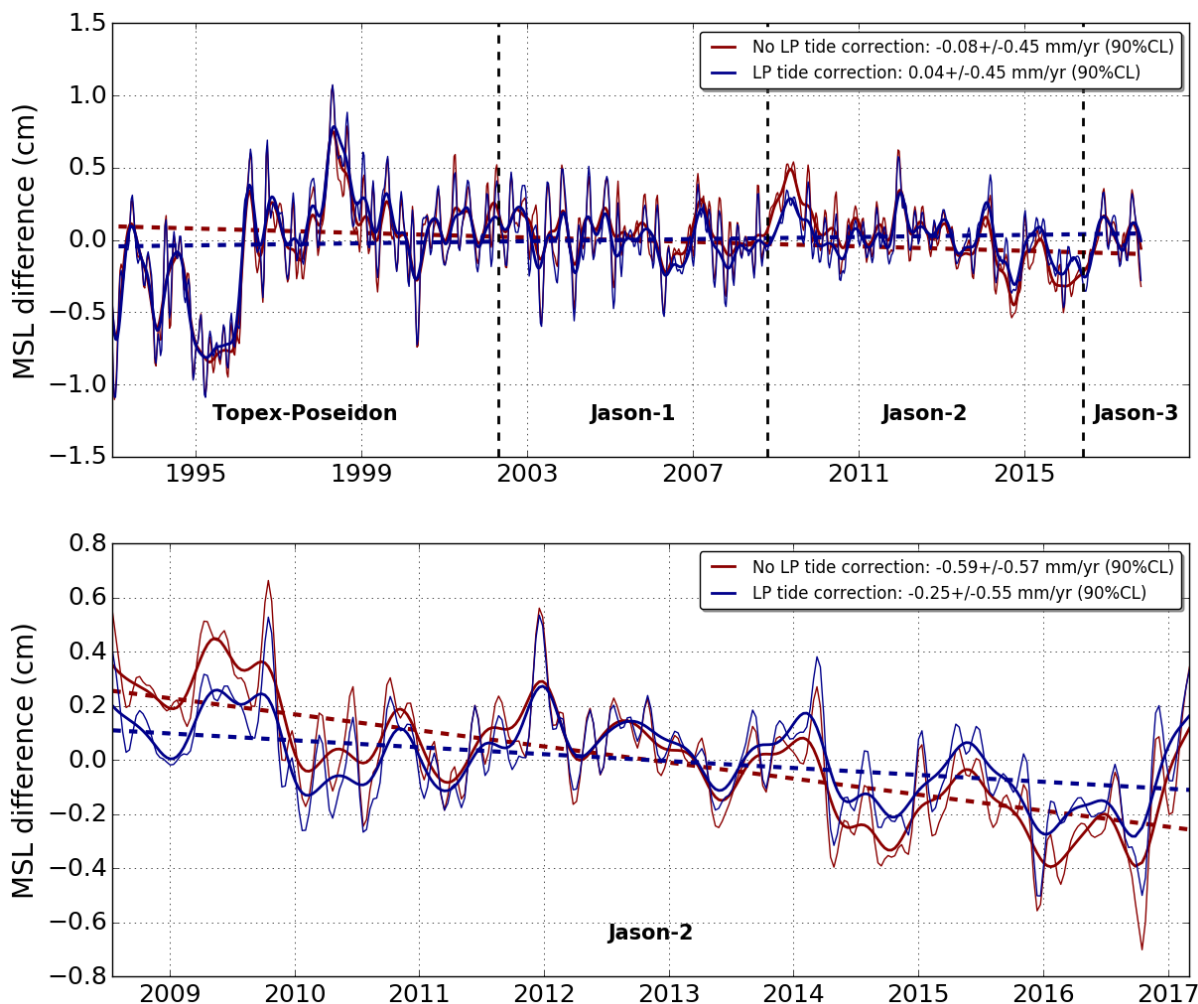


Figure 11: Altimeter / tide gauge (GLOSS/CLIVAR network) comparisons with long-period tide correction on tide gauges (blue) and without (red). Altimeter: full AVISO TOPEX-Poseidon, Jason-1, Jason-2 and Jason-3 concatenated time series on top and Jason-2 only below. Periodic signals are removed and resulting time series are 2-month (thin lines) and 6-month (thick lines) low-pass filtered. Dotted lines represent a linear regression fit of the time series; slope values are indicated in the legend.

3.2. Comparison of MSL time series between altimetry and TG

3.2.1. By altimeter missions

In this section, altimetry and tide gauge MSL time series are described for each altimetry missions (from L2P products with CMEMS 2018 standards) from missions TOPEX/Poseidon, Jason-1, Jason-2, Jason-3, ERS-1, ERS-2, Envisat, SARAL/AltiKa and Sentinel-3A.

The curves obtained are presented in Figure 12 for the reference missions (TOPEX/Poseidon, Jason-1, Jason-2, Jason-3) used for the GMSL calculation and in Figure 13 for the complementary missions (ERS-1, ERS-2, Envisat, SARAL/AltiKa and Sentinel-3A). For all the analyses, both GLOSS/CLIVAR and PSMSL tide gauges network have been used.



Uncertainties on the GMSL trend estimates are also reported in each figure. They are explained in detail in following section 3.3 .

The analysis of these comparisons is presented for each mission individually. Drifts are presented for GLOSS/CLIVAR and PSMSL network, noted (GC/PS mm/yr) in the text below:

- **TOPEX-Poseidon:** A strong and significant (1.7/1.2) mm/yr drift is detected on TOPEX-A period, no significant drift on TOPEX-B period. The TOPEX-A drift is well-known by the altimeter science community and a specific study is conducted in section 5.2 of this report. The TOPEX-A drift is composed into two drifts of about -1 mm/yr over the [1993,1995.5] period and +3 mm/yr over the [1995.5,1999.1].
- **Jason-1:** A small and non-significant negative drift of (-0.2/-0.4) mm/yr is observed on the main Jason-1 period (this means before the orbit change).
- **Jason-2:** As for Jason-1, a small and non-significant negative drift of (-0.4/-0.2) mm/yr is observed on the main Jason-2 period (this means before the orbit change).
- **Jason-3:** A positive drift of about +0.8 mm/yr is detected but not reliable due to the short time period used (1.3 years). Uncertainty is higher than 3 mm/yr over such a short period.
- **ERS-1:** No significant drift detected but a very unstable GMSL yielding large uncertainties when compared with both tide gauge networks.
- **ERS-2:** A large and significant (-1.1/-1.2) mm/yr drift is detected with significant inter-annual variations.
- **Envisat:** Non-significant drift detected, but significant inter-annual variations with a negative drift in 2003 already mentioned in the literature (Ollivier et al., 2012)
- **SARAL-AltiKa:** Non-significant drift detected.
- **Sentinel-3A:** A large positive drift (+2.0 mm/yr) is detected, but not reliable due to the short time period used (1 year).

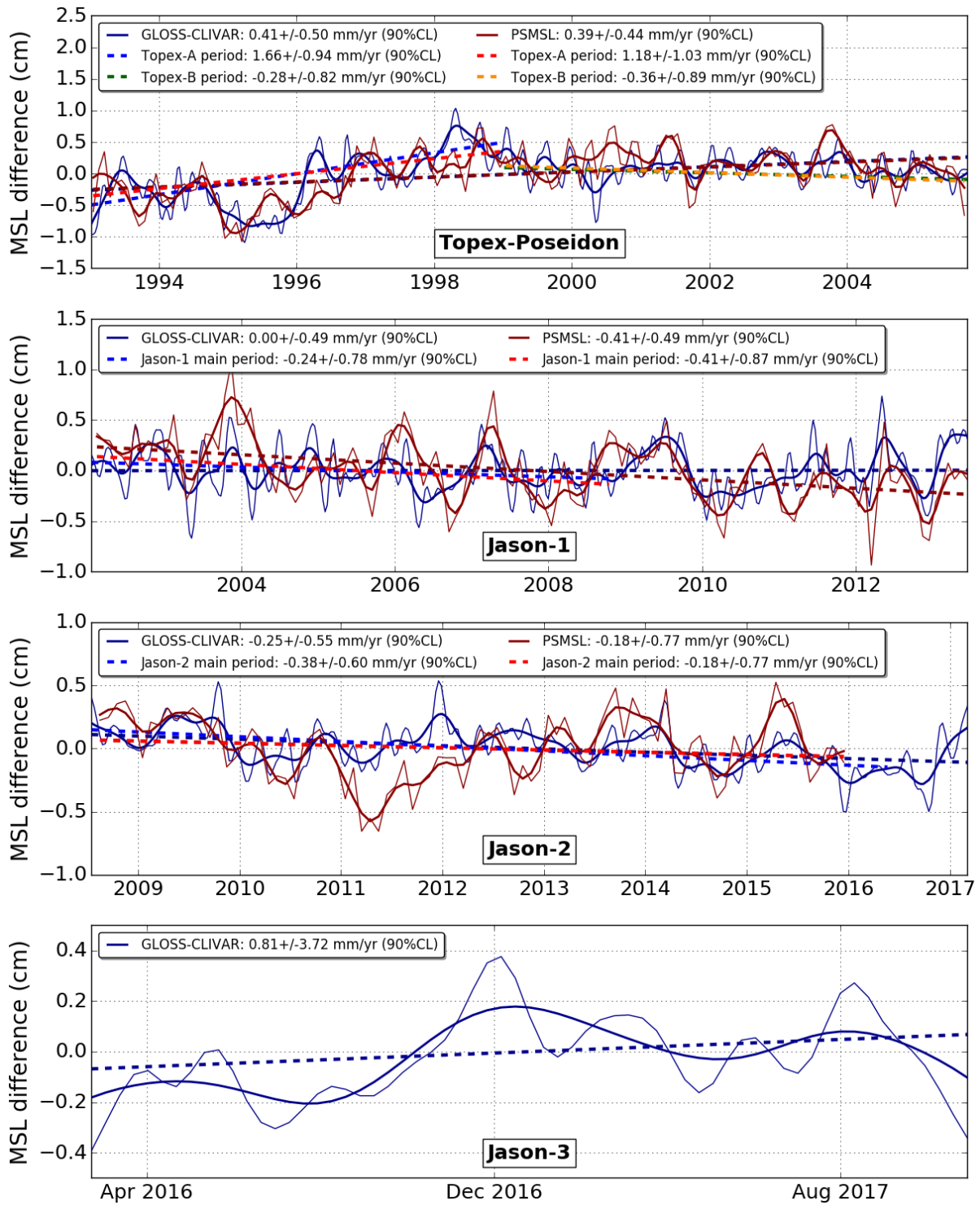


Figure 12: Evolution of GMSL differences between altimeter and tide gauges for reference missions used in the GMSL indicator calculation (TOPEX/Poseidon, Jason-1, Jason-2 and Jason-3) with the GLOSS/CLIVAR network (blue line) and the PSMSL network (red line). Signal lower than 2 months and annual signals have been removed. The blue dashed line is the trend obtained applying a generalized least square method.

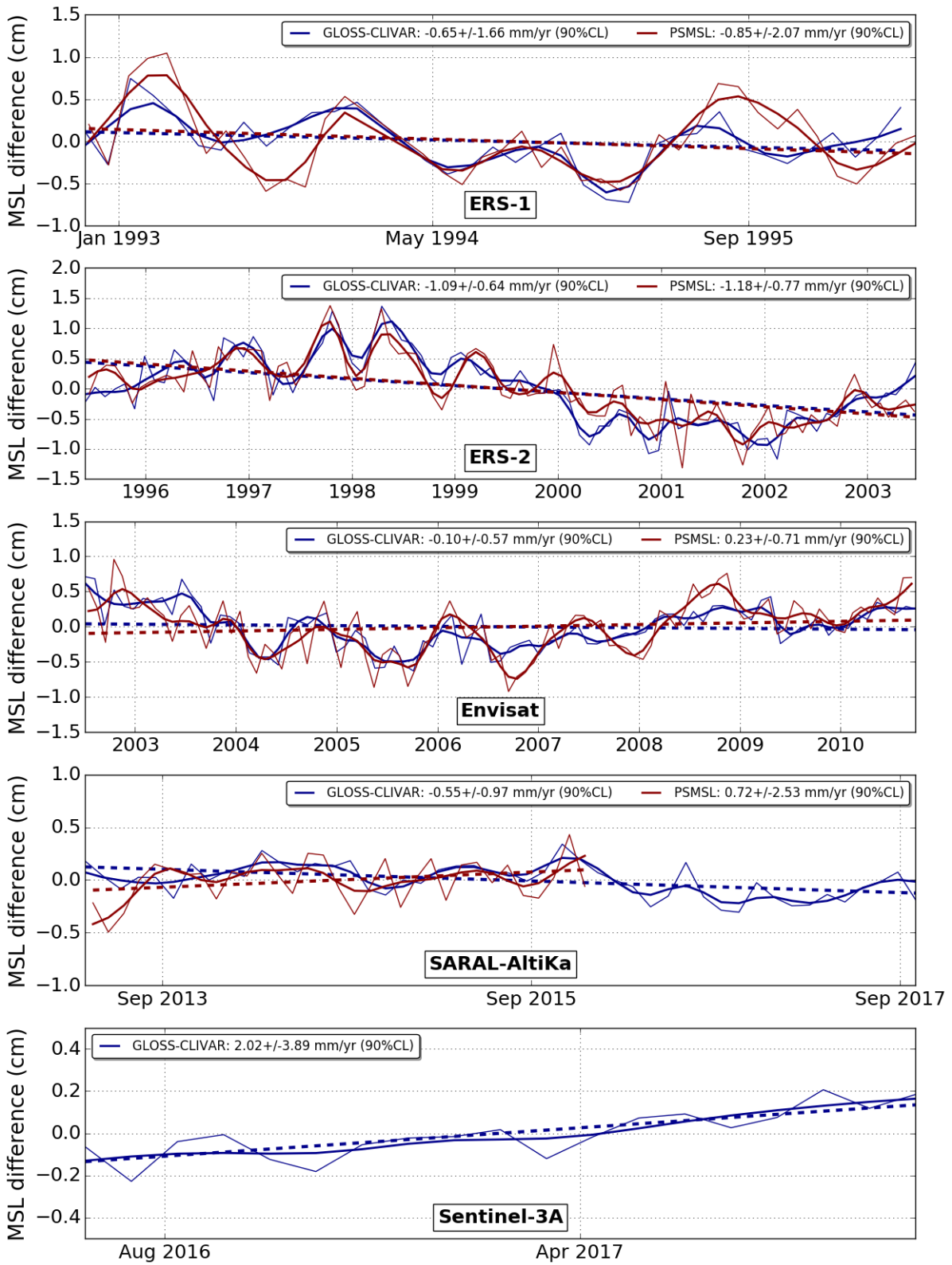


Figure 13: Evolution of GMSL differences between altimeter and tide gauges for 35 days repetitive missions (ERS-1, ERS-2, Envisat and SARAL-AltiKa) and the 27 days repetitive mission Sentinel-3A, with the GLOSS/CLIVAR network (blue line) and the PSMSL network (red line).



3.2.2. From reference missions together (L2P sea level products)

In this section, we performed altimetry and tide gauges comparison from reference missions linked together in the same way as the AVISO GMSL indicator. This allows us to directly determine potential drifts or jumps in the GMSL time series. The MSL differences using GLOSS/CLIVAR and PSMSL networks are presented in Figure 14 from 1993 to 2016 included (2015 with PSMSL network).

The global drift is very slightly positive (<0.1 mm/yr) over the full period with an uncertainty of 0.45 mm/yr with GLOSS/CLIVAR and 0.38 mm/yr with PSMSL. On TOPEX-A period, as already mentioned, a strong signal is visible composed with a 1.7 mm/yr drift composed into two drifts of about -1 mm/yr over the [1993,1995.5] period and +3 mm/yr over the [1995.5,1999.1] period. These drifts are statistically significant and highlight a strong error of the GMSL evolution over this period. Thus, in the future this error on TOPEX-A should be corrected to better estimate the MSL evolution (for more detail, see the specific study in section in 5.2 of this report).

In addition to the TOPEX-A drift, we can observe that the high frequency content (lower than 6 months) of altimetry and tide gauges comparisons is higher on TOPEX-B and Jason-1 data than in Jason-2 and Jason-3. This could be due to stronger errors on altimetry measurements (e.g. 59-days error signal on TOPEX-B (Zawadzki et al., 2017)) but also to the tide gauge network with more numerous and more accurate tide gauges towards the end of the altimetry era. These causes are considered as error sources of the altimetry/TG method and therefore contribute to the trend uncertainty (see next section).

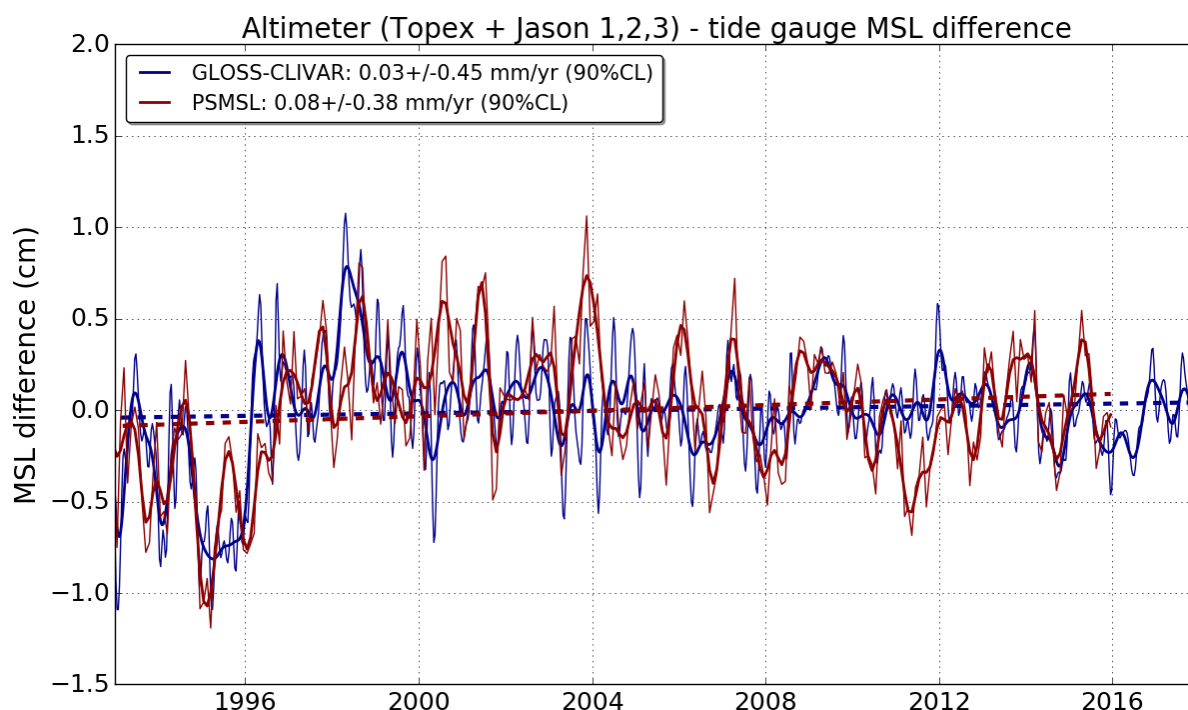


Figure 14: Evolution of global MSL differences from altimeter / tide gauges comparisons (GLOSS/CLIVAR and PSMSL network) from TOPEX/Poséidon, Jason-1, Jason-2 and Jason-3 L2P products linked together.



3.2.3. From CMEMS multi-mission grids (L4 sea level products)

The comparisons with tide-gauge networks have also been performed using CMEMS multi-mission grids called L4 sea-level products. Evolution of MSL differences from these products with tide gauges are plotted in Figure 15.

In theory, very similar results to those presented in Figure 15 should be obtained with L2P sea-level products, since L4 products are built from L2P products. Thus, the same altimeter data and standards are used. In practice however, after comparing the two figures, we observe some notable differences. Although the GMSL drift over all the and the TOPEX-A drift are observed similarly, a large signal of a few millimeters amplitude is detected on the Jason periods from 2002 onwards on L4 products.

Several investigations are ongoing to explain these differences between L2P and L4 products:

- Evaluate the impact that differences in L2P/L4 sea level content in coastal areas (due to L3/L4 processing) have on global altimeter / tide gauge comparisons
- Evaluate the impact of differences in tide gauge selections on altimeter / tide gauge comparison results. At present time, for instance, MSL differences between L2P products and tide gauges are obtained by concatenating results from different missions, and thereby contain greater tide gauge variability than MSL differences from L4 products.

This investigation will be led in priority in 2018, and will lead to a complete analysis in next annual report.

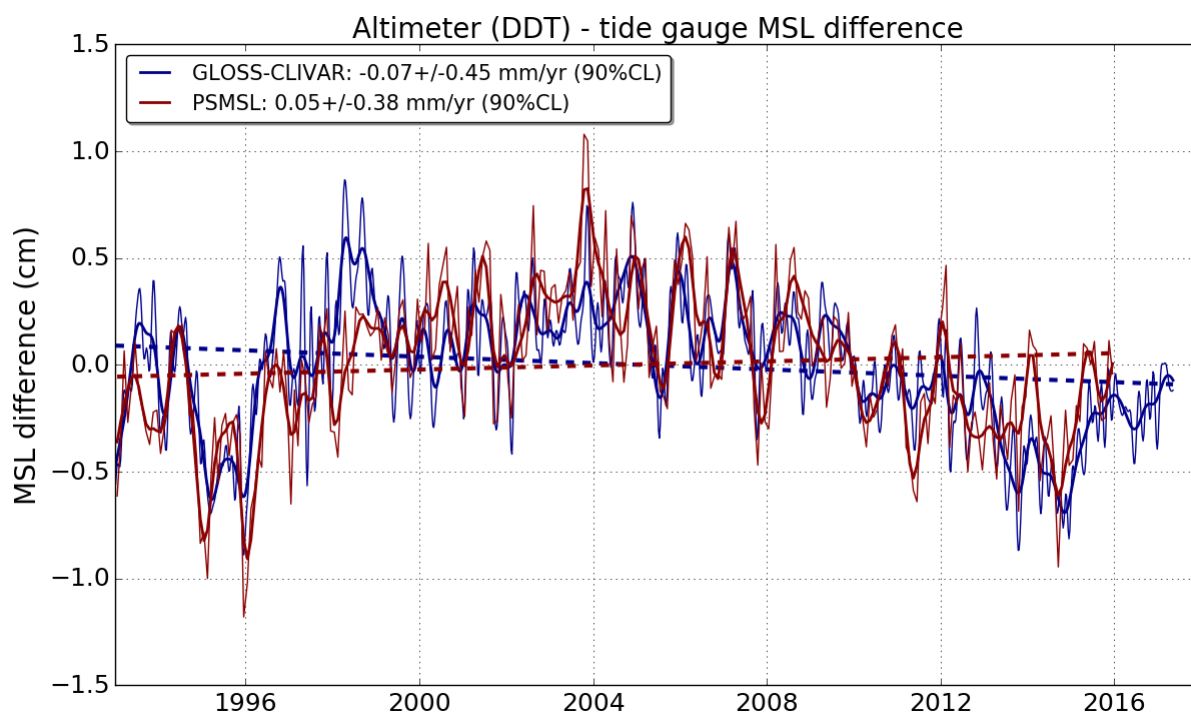


Figure 15: Evolution of global MSL differences from altimeter / tide gauges comparisons (GLOSS/CLIVAR and PSMSL network) from CMEMS multi-mission grids (L4 sea level product).



3.3. Uncertainties

3.3.1. Description of errors in altimetry and tide gauge comparisons

Different error sources impact the altimetry and tide gauge comparisons with the objective to detect drift or jump in altimetry MSL. These errors come from tide gauge networks which contain internal errors as any measurement system and from the method to compare altimetry and tide gauge data. (Valladeau et al., 2014) listed and described these errors, which are listed hereafter:

- Altimetry and tide gauge measurements colocation
- Absolute geo-referencing of tide gauges
- Time-varying geo-referencing of tide gauges: vertical land motion
- Global number of tide gauges considered within the process
- Tide gauges spatial sampling
- Temporal coverage of tide gauges

In addition to these errors, we take into account small time scale altimetry errors as high-frequency (< 2months) noise in the time series obtained from altimeter/tide gauge comparisons. Those errors are mission-dependent.

3.3.2. Error budget

(Prandi et al., 2016) established a preliminary error budget of altimeter and tide gauges comparison to estimate the uncertainty of the altimeter GMSL drift estimate. It is presented in Table 6. Four sources of errors were considered over periods close to 10 years:

- **Vertical Land Motion:**
 - o tide gauges relative sea level measurements are directly affected by local vertical land motion,
 - o without precise monitoring (GPS, DORIS) we cannot correct for such movements,
 - o even when GPS velocities are available, it is very difficult to demonstrate an improvement (spread of trend differences unchanged)
 - o uncertainty is evaluated to **0.3 mm/yr** (lower bound)
- **In-situ geographical distribution and ensemble mean (called "averaging"):**
 - o Tide gauge data availability is limited in space and time,
 - o Basic quality control results in large unobserved areas,
 - o Increasing the number of stations helps reduce uncorrelated errors,
 - o Homogeneous coverage will increase the robustness of global altimeter drift estimations
 - o Different averaging schemes (correcting for station density or not) might introduce artefacts
 - o uncertainty is evaluated to **0.15 mm/yr**
- **Network sensitivity:**
 - o Test small random changes in the in-situ network used,
 - o Represents random unavailability of stations,
 - o Even small changes can lead to large impacts,
 - o Uncertainty estimated to **0.4 mm/yr**,



- **High frequency errors:**
 - Uncorrelated high frequency errors mainly due to tide gauge and altimeter measurement errors, but also error collocation of both datasets.
 - Uncertainty estimated to **0.2 mm/yr**

Error	Uncertainty
Vertical Land Motion	0.3 mm/yr
High frequency errors	0.2 mm/yr
Averaging	0.15 mm/yr
Network	0.4 mm/yr
TOTAL (RSS)	0.7 mm/yr

Table 6: Error budget of altimetry and tide gauge comparisons over a 10-year period (Prandi et al., 2016).

3.3.3. New estimate of altimeter GMSL drift uncertainties from tide gauges for any periods within [1993,2016]

3.3.3.1. Method

The error budget proposed by Prandi et al., 2016 describes the average. Therefore, drift uncertainties are not accurately evaluated for each specific case. For instance, the error from Vertical Land Motion will decrease with the number of tide gauges available on the mission's time period, each mission will have specific altimeter high-frequency errors, and more importantly, uncertainties will decrease with the length of the time period considered.

In this study, we evaluate the different error components specific to each case. The mathematical formalism then involves constructing a covariance matrix from those error estimations, which describes error evolutions for the MSL time series obtained through altimeter / tide gauge comparison, and using the Generalized Least Squares method to compute the time series' linear component i.e. the mission's altimetry drift from tide gauges. The approach is similar to the error modelling described in chapter 2.5.

3.3.3.2. Error modelling

In the case of comparison of altimeter and tide gauge data, the first step consists in modelling errors to calculate the covariance matrix of error observation (e.g. R_{vv} in Eq. 2). However, to date, we are not able to describe the covariance of errors which impact altimeter and tide gauge comparison (described in the previous section). So, we propose an approximation of these errors modeling them in several categories:

- High frequency errors (< 2 months): these errors correspond to correlated errors lower than 2 months coming from tide gauges and altimetry errors. Indeed, for all scales lower than 2



months, altimetry errors are considered as a limitation in altimeter and tide gauges comparison to estimate the altimetry GMSL drift. Furthermore, these errors could depend on the tide gauge network (e.g. temporal sampling) and the altimeter missions (e.g. high frequency errors as higher for TOPEX/Poseidon than for Jason-2 and Jason-1 due to the 59-day error signal stronger on TOPEX/Poseidon). Therefore, they are evaluated separately for each mission and tide gauge network.

- Medium frequency errors (between 2 months and 1 year): these errors correspond to correlated errors between 2 months and 1 year. They also integrate all the errors coming from tide gauge and from altimetry measurements for the same reason as previously.
- Large frequency errors (between 1 year and 3 years / between 3 years and 10 years): these errors correspond to the correlated errors between 1 year and 3 years, and between 3 years and 10 years. They only include errors from tide gauge data, since those are the scales at which we would like to characterize any potential altimeter drifts. The origin of these error is unknown. The impact of tide gauge MSL biases or the method to collocate data is suspected. The analysis of altimetry/tide gauges MSL time series (see Figure 12 for instance) exhibits large scale differences between PSMSL and GLOSS/CLIVAR network, indicating that such errors must be modelled.
- Drift errors: these errors correspond to a linear error over all the altimetry period. These errors are mainly due to the VLM errors of tide-gauge networks since the main component of this error is linear. As these errors are decorrelated between each tide gauge, the global trend uncertainty is σ/\sqrt{N} where σ is average VLM uncertainty for each tide-gauge and N is the number of tide gauges.
- Bias errors: these correspond to errors due to the method to link altimetry mission together (eg. TP and J1, J1 and J2, ...) when using only L2P products. To date, altimeter and tide gauge comparisons are performed processing each altimetry mission separately. Then, the time series are linked together after correcting the potential inter-mission relative bias. This bias estimation is associated with an uncertainty that we estimate close to 1 mm. It is worth noting that this error is currently a limitation of our method which could be easily improved in 2018.

The standard deviation of filtered altimeter/TG time series in the adequate range of frequencies ($\lambda < 2m$ or $2m < \lambda < 1yr$, ...) are used as correlated error estimates. Large and medium frequency errors are supposed to come solely from tide gauges; we thereby use the Jason-2 mission, which is known to be very stable, to evaluate those errors and then use those values for all other missions.

The 2 following tables show the different source and characteristic of errors impacting altimetry and tide-gauges comparisons, for the reference missions and for GLOSS/CLIVAR (Table 7) and PSMSL (Table 8) networks.

Source of Error	Family	Characteristic		
		T/P	J1	J2+J3



High frequency errors (< 2 months):	Correlated error with a given wavelength: $\lambda = 2$ months	$\sigma = 4.0$ mm	$\sigma = 3.5$ mm	$\sigma = 2.4$ mm
Medium frequency errors (between 2 months and 1 year):	Correlated error with a given wavelength: $\lambda = 1$ year	$\sigma = 1.6$ mm		
Large frequency errors (between 1 year and 3 year):	Correlated error with a given wavelength: $\lambda = 3$ years	$\sigma = 0.7$ mm		
VLM error	Drift error	$\sigma = 0.25$ mm/yr	$\sigma = 0.23$ mm/yr	$\sigma = 0.22$ mm/yr
Error to link the altimeter/TG time series together.	Bias error	$\sigma = 1$ mm to link TP/J1, J1/ J2 and J2/J3		

Table 7: Error modelling for the estimation of the altimetry GMSL drift from altimeter and tide gauge comparisons, using GLOSS/CLIVAR tide-gauge network.

Source of Error	Family	Characteristic		
		T/P	J1	J2+J3
High frequency errors (< 2 months):	Correlated error with a given wavelength: $\lambda = 2$ months	$\sigma = 3.0$ mm	$\sigma = 2.8$ mm	$\sigma = 2.3$ mm
Medium frequency errors (between 2 months and 1 year):	Correlated error with a given wavelength: $\lambda = 1$ year	$\sigma = 1.7$ mm		
Large frequency errors (between 1 year and 3 year):	Correlated error with a given wavelength: $\lambda = 3$ years	$\sigma = 1.3$ mm		
Very large frequency errors (between 3 year and 10 years):	Correlated error with a given wavelength: $\lambda = 10$ years	$\sigma = 1.0$ mm		
VLM error	Drift error	$\sigma = 0.25$ mm/yr	$\sigma = 0.23$ mm/yr	$\sigma = 0.22$ mm/yr



Error to link the altimeter/TG time series together.	Bias error	$\sigma = 1 \text{ mm}$ to link TP/J1, J1/ J2 and J2/J3
--	------------	---

Table 8: Error modelling for the estimation of the altimetry GMSL drift from altimeter and tide gauge comparisons, using PSMSL tide gauge network.

3.3.3.3. GMSL drift uncertainties from tide gauges for any altimetry periods

As for the global MSL trend uncertainties, we have estimated the uncertainties of the altimeter GMSL drift with tide gauge networks for any altimeter periods between 1993 and 2017. In Figure 16 are plotted these uncertainties for GLOSS/CLIVAR network on left and PSMSL on right within a confidence interval of 90%. They are directly inferred from the error modeling presenting in the previous section. The analysis of uncertainties shows:

- A minimal uncertainty close to 0.4 mm/yr over the longest period (24 years)
- At 10 years, uncertainty are respectively about 0.6-0.7 mm/yr and 0.9-1.0 mm/yr with GLOSS/CLIVAR and PSMSL networks
- For periods lower than 4-5 years, uncertainties are systematically higher than 1.0 mm/yr with GLOSS/CLIVAR network (1.5 with PSMSL one)
- Uncertainty level increases at altimeter mission change (2002, 2008) highlighted by a “bump”: this is an artefact of our current method that should be improved in 2018.

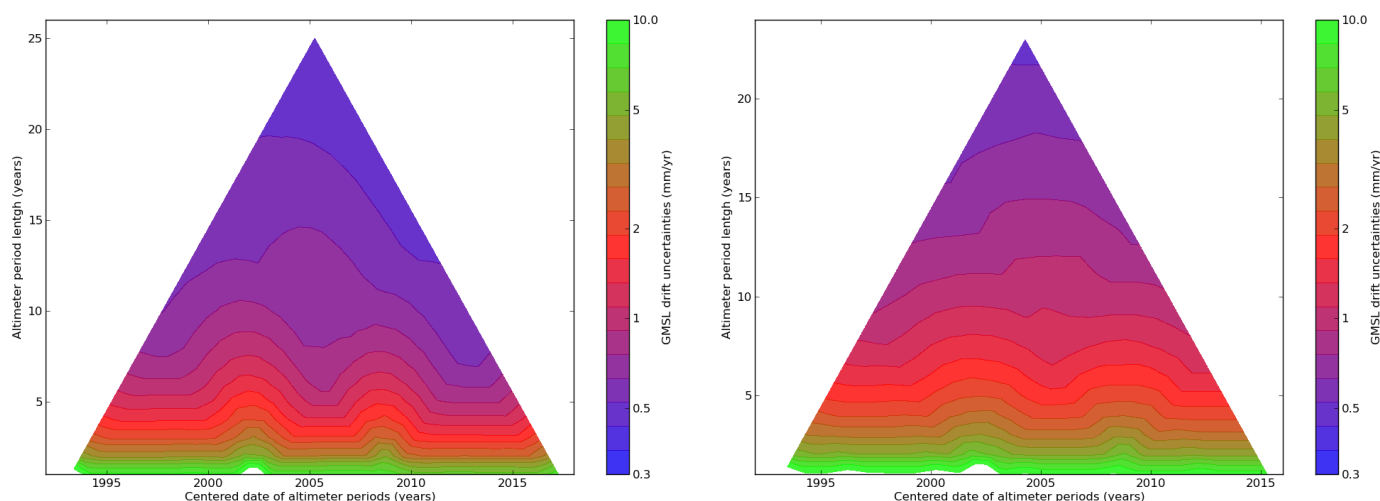


Figure 16: Altimeter GMSL drift uncertainties (mm/yr) estimated from GLOSS/CLIVAR (on left) and PSMSL (on right) tide gauge network for any altimeter periods between 1993 and 2017. The confidence interval is 90 % (1.65-sigma). On the Y-axis is represented the length of the window (in year) and on the X-axis the central date of the window used (in year).



3.3.3.4. GMSL drift uncertainties from tide gauges for each altimetry mission

Figure 17 shows GMSL drift and associated uncertainty estimates for each mission obtained through altimeter / tide gauge comparisons using GLOSS/CLIVAR and PSMSL networks. In most cases, missions' full-time periods are used (e.g. for the 1993-2005 period for T/P). However, PSMSL data for years 2016 and 2017 is incomplete and therefore unused for altimeter / tide gauge comparisons, and GLOSS/CLIVAR data is not available from March 2017 onwards. Consequently, no Jason-3 and Sentinel-3A comparisons with PSMSL data are provided, and the Jason-2 and SARAL/AltiKa time periods used for altimeter / tide gauge comparisons with PSMSL are shorter than with GLOSS/CLIVAR. The time periods used for each comparison are apparent in Figure 12 and Figure 13 where all global MSL altimeter / tide gauge time series are provided. Estimated drift and uncertainty values for more specific time periods (TOPEX-A period for instance) are also provided in same figures.

Several interesting results can be mentioned:

- Uncertainties are larger with PSMSL network than GLOSS/CLIVAR for short period ($< \sim 5$ years) and equivalent or slightly lower for larger periods.
- The drifts obtained are not statistically significant within a confidence interval of 90% for all the missions except for TOPEX-A ($-1.7 \text{ mm/yr} \pm 0.9 \text{ mm/yr}$ with GLOSS/CLIVAR and $-1.2 \pm 1.0 \text{ mm/yr}$ with PSMSL) and for ERS-2 ($-1.1 \pm 0.7 \text{ mm/yr}$ with GLOSS/CLIVAR and $-1.2 \pm 0.8 \text{ mm/yr}$ with PSMSL)

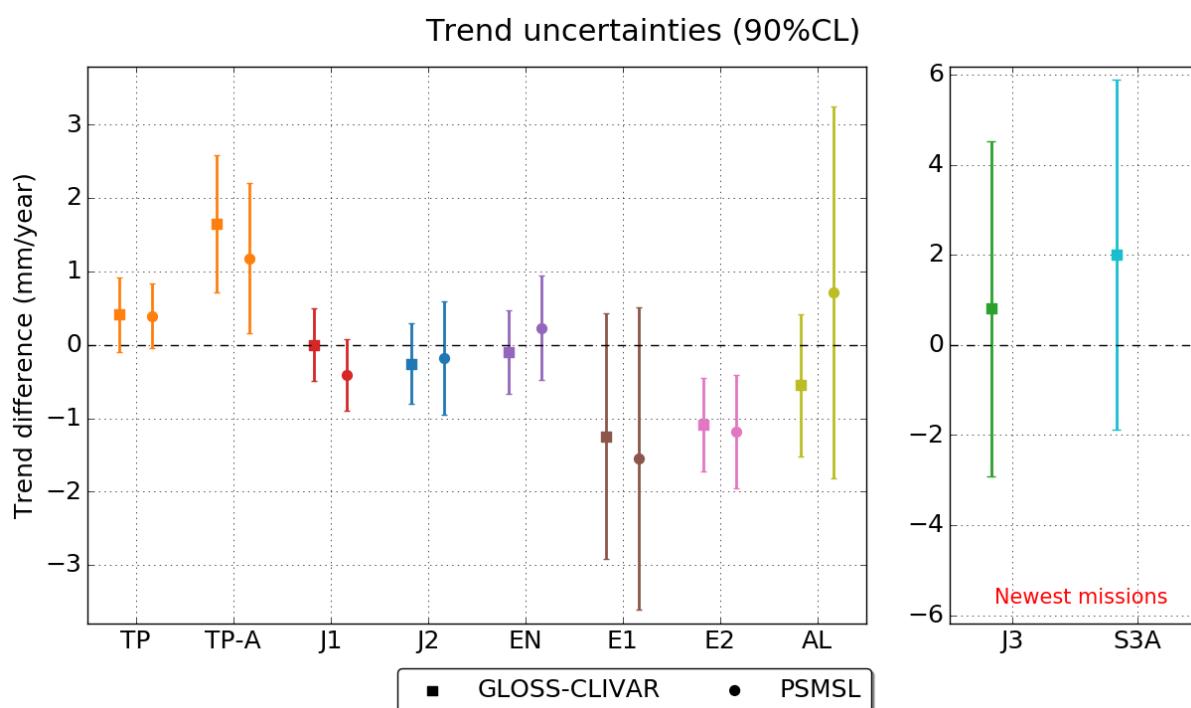


Figure 17: GMSL drift estimates per mission obtained through altimeter / tide gauge comparisons. Two tide gauge networks are used: GLOSS/CLIVAR and PSMSL. Each dot represents the drift estimate for the complete duration of the mission (even for drifting orbits) and its associated bar represents the drift uncertainty at 90% confidence level. From left to right: TOPEX/Poseidon, Jason-1, Jason-2, Envisat, ERS-2, ERS-1, SARAL-Altika, Jason-3 and Sentinel-3A.





4. MSL comparisons between altimetry and ARGO+GRACE data

4.1. Methods of comparison and datasets

4.1.1. Overview

Comparison of the altimeter sea level data with in-situ measurements is a complementary and independent tool from internal and cross comparison of altimeter products. Temperature and salinity profiles obtained from profiling floats such as these of the ARGO network provide such independent data. The spatial distribution over the open ocean of the TS profilers as well as their large number provide a complementary approach of the tide gauges measurements for altimeter product validation. This section details means of comparing sea level anomalies (SLA) derived from altimeters with dynamic height anomalies (DHA) obtained from the TS profiles.

Since the temperature and salinity profiles derived from the TS floats only probe the steric elevation of the ocean, DHA data can be combined with complementary ones providing an estimate of the sea level variation due to water mass contribution (e.g. from the Greenland and Antarctica ice sheets, land water contribution...). The combination of TS and mass measurements therefore allows to estimate the total height variation of the water column that can be compared with the one provided by altimetry. Mass contributions are measured by gravimetry missions such as GRACE and different research groups have developed solutions to infer the associated sea level variation (e.g. GRGS, CSR, GFZ ...).

TS + mass data allow to detect the absolute altimeter drift. To that purpose a precise error budget has to be built accounting for TS as well as GRACE data associated uncertainties. This budget and its impact on the analysis are detailed in section 4.3. The quality of the altimeter SLA for both single mission (along track level 2 products) and multi-missions (gridded merged level 4 products) are then estimated in sections 4.2.1 and 4.2.2 respectively. Details on the datasets are provided into section 4.1.2.

Mass contribution is not systematically used since relative comparison of altimetry with ARGO data can be sufficient to assess the performance of one mission with respect to another one or to detect the impact of new altimeter standards (Legeais et al. 2016).

4.1.2. Datasets

4.1.2.1. Altimeter measurement

In this study, along-track (level 2) altimeter SSH are used from several satellite altimeters, where standards are updated with the Geophysical Data Record (GDR) altimeter products. Details of the SSH computation and time period for each altimeter are presented on the Aviso website. We conducted analyses based on two sets of altimeter standards. Each set is described in appendix. As the comparison with in-situ data is performed since 2004, date from which the Argo network covers a large enough oceanic surface, we focus the analyses on the Envisat, Jason-1, Jason-2, SARAL/AltiKa and Jason-3 space missions.



4.1.2.2. Argo in-situ measurements

In this study, we use delayed mode and real-time quality-controlled T/S profiles (Guinehut et al. 2009) from the Coriolis Global Data Assembly Center (www.coriolis.eu.org; CORIOLIS). As described in (Legeais et al. 2016), DHAs are computed as follows: dynamic heights are first computed from the integration of the Argo pressure, temperature and salinity vertical profiles using a reference depth. In order to calculate anomalies of dynamic heights consistent with altimeter SLAs, a mean dynamic height is used as a reference (see 4.1.3.2). Figure 18 shows spatial distribution of SLA-DHA measurements over the period 2004-2016.

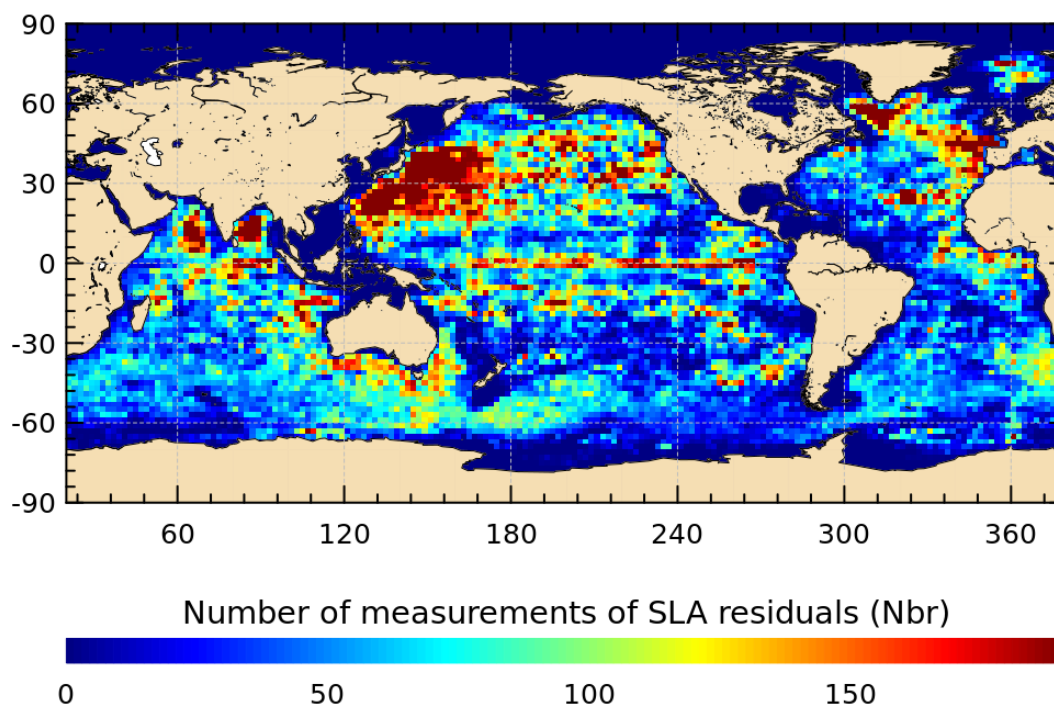


Figure 18: Spatial distribution of temperature and salinity Argo profiles from 2004-2016

The vast amount of T/S profiles are available over almost the global open ocean (Figure 18). Best sampled areas (Kurushio current, parts of the North Indian, North Atlantic and North Pacific oceans) have more than 1000 profiles per box of $3^\circ \times 5^\circ$. About 500 profiles per box are found in large parts of the global ocean, except in the South West Atlantic Ocean and in the southern part of the Antarctic Circumpolar current where about 200 profiles per box are found. The number of available profiles has regularly increased since 2002 (Figure 19). Nevertheless, spatial distribution has not always been high enough in some areas to produce statistically valid analyses. As discussed by Roemmich and Gilson (2009), Figure 19 indicates that considering a threshold of two thirds of the open ocean surface covered by Argo floats ($\pm 60^\circ$), analyses should be performed with in-situ data from about mid 2004 onwards, which is done in this report. This constitutes a great asset for latest altimeter missions (Jason-1, Envisat, Jason-2, SARAL/AltiKa, Sentinel-3a and Jason-3). It leads to a global in-situ dataset of more than 900000 T/S profiles distributed over almost the global open ocean.

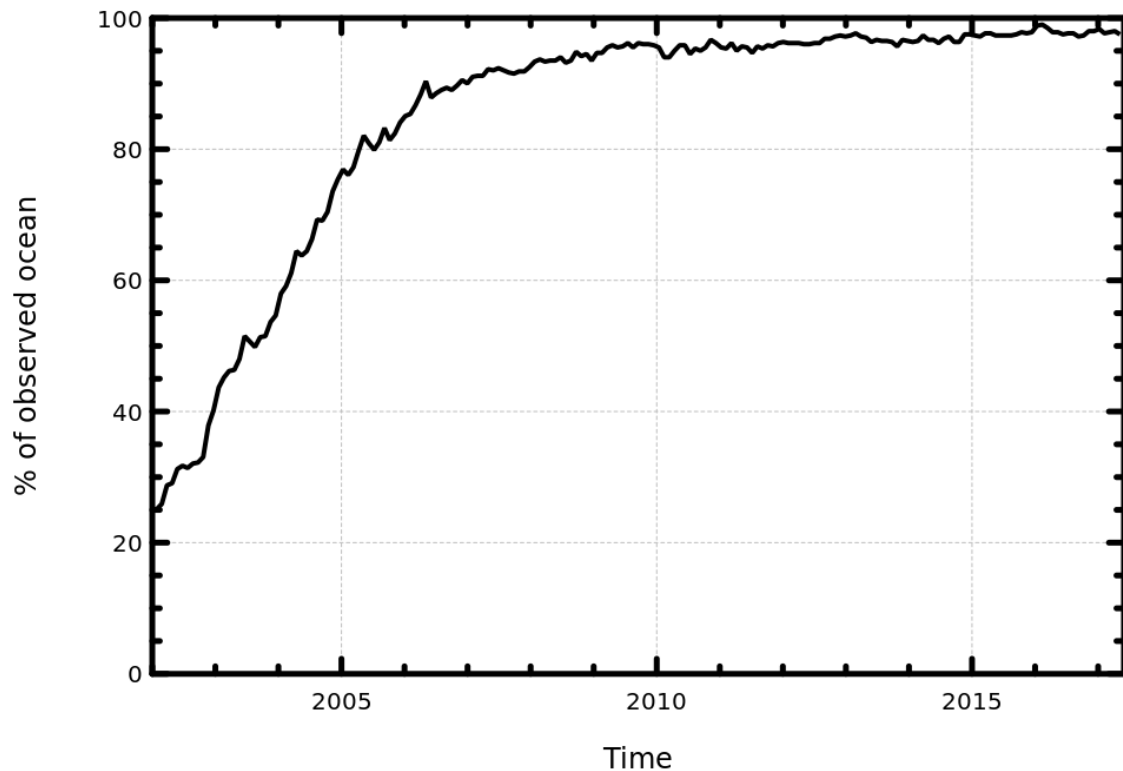


Figure 19: Monitoring of the percentage of the ocean covered by Argo profiling floats ($\pm 60^\circ$ and without inland seas) from 01/01/2002 to 05/31/2017.

4.1.2.3. Grace measurements of the mass contribution

The physical contents of the altimeter and steric in-situ dynamic heights are different and, in particular, a phase offset is observed between the two global averages due to the seasonal distribution of the mass contribution which is missing in the Argo dataset (Chen et al. 1998). This mass contribution can be derived from GRACE data in order to compare with altimetry. Different research groups produce different mass solutions using the GRACE datasets (CSR, GFZ, JPL, GRGS). These products present some heterogeneities: for example, the GRGS GRACE data are not filtered and are not corrected from the post glacial rebound (Glacial Isostatic Adjustment) correction, the gridded GRC ocean maps are optimized to examine regional ocean bottom pressure variations, but are not intended to be spatially averaged to determine global mean ocean mass. To solve this later difficulty, a dataset of the ocean mass variations in mm of sea level is provided (<http://xena.marine.usf.edu/~chambers/SatLab/Home.html>). It consists in monthly global mean of the equivalent sea level (Johnson and Chambers 2013) and can thus only be used for analyses of the global altimeter sea level drift. This dataset is corrected from the GIA and a 300 km coastal mask is applied in order to reduce land leakage. The fact that it consists in a time series prevents us from regional analyses and can thus not be systematically used in the scope of our activities. In addition, this makes the technical aspect of the comparison more difficult since the processing chain is not



adapted for direct comparison of global time-series. The GRGS dataset used in our analyses is the RL03v3, released in October 2016 and that includes data until May 2016.

4.1.3. Method

In order to perform alti/TS comparisons a processing sequence has been developed in the context of the SALP project. It aims at being regularly operated to validate all altimeter missions. Altimetry as well as TS and mass data are firstly pre-processed as hereafter detailed:

- Colocation with altimeter data
- References of DHA and SLA
- Validation of collocated measurements in order to exclude bad data

4.1.3.1. Colocation of in-situ and altimeter data:

As the altimeter sampling is better than the in-situ coverage (a global altimeter coverage of the ocean every 9.91 days for Jason missions versus a single T/S profile), grids of 10-day averaged along-track SLA are computed in order to have a sufficient spatial coverage. The grid is chosen to be $3^{\circ} \times 1^{\circ}$ in the longitudinal and latitudinal dimensions respectively in order to account for zonal ocean coverage of the altimeters over a tan day period. (Legeais et al. 2016) compared such a $3^{\circ} \times 1^{\circ}$ against a $1^{\circ} \times 1^{\circ}$ gridding, they showed that neither the amplitude and phase of the annual signal nor the trend of the SLA-DHA differences are affected by changes in box sizes of this magnitude. When comparing the differences in the variances of SLA-DHA computed over $1^{\circ} \times 1^{\circ}$ versus $3^{\circ} \times 1^{\circ}$ the histogram provides a mean of $+1.3 \text{ cm}^2$ which indicates that averaging along track altimeter data over $3^{\circ} \times 1^{\circ}$ makes them more consistent with in situ Argo observations (Figure 20).

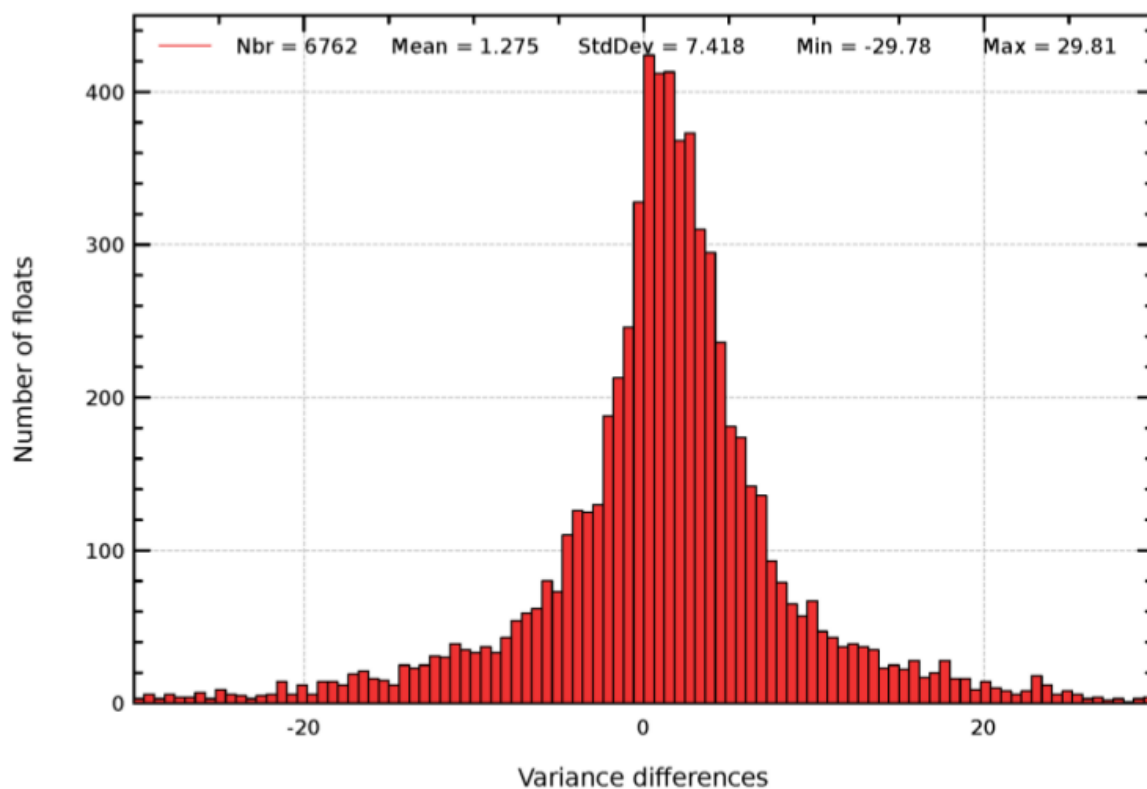


Figure 20: Histogram of the difference of variance of the SLA-DHA differences for each Argo float using successively $1^\circ \times 1^\circ$ versus $3^\circ \times 1^\circ$ boxes - i.e. $\text{Variance}(\text{SLA}_{1 \times 1} - \text{DHA}) - \text{Variance}(\text{SLA}_{3 \times 1} - \text{DHA})$ - when averaging along-track Jason-1 altimeter SLA before collocating with Argo profiles. (figure from Legeais et al. 2016).

As already detailed in the 2016 Argo annual report, the same 10-day temporal averaging period was chosen for missions on a 35-day repetitive orbit (Envisat, SARAL/AltiKa). The arguments in favor of this choice are that the ocean state does not significantly change within less than 10 days and that it allows a better comparison with Jason missions. The cons are that ocean temporal and spatial sampling are therefore different from one cycle to another for non-10-day repetitive missions. The collocation of Argo and altimeter data is then made by interpolating the SLA grids (bi-linearly in space and linearly in time) at the location and time of each in-situ profile. Similarly, the grids of ocean mass data are also collocated with each Argo profile.

4.1.3.2. Reference of DHA and SLA

Anomalies are computed with respect to a reference level, as shown in it is critical that both SLA and DHA data have the same interannual temporal reference. The in-situ DHA are referenced to a mean of the Argo dynamic heights over the 2003-2014 time period. This is different from the 20-year reference period of the SLA (1993-2013). The temporal reference of the altimeter SLA is therefore adapted to match the period used for DHA calculations: the mean of the AVISO SSALTO/DUACS maps over 2003-2014 is removed from the along-track L2 altimeter SSH. Although the global statistics of



the SLA-DHA differences are not significantly affected by the choice of a common reference period, the trend differences at regional scales are directly impacted (Figure 21 see section 3.2 of 2015 Argo annual report for further details).

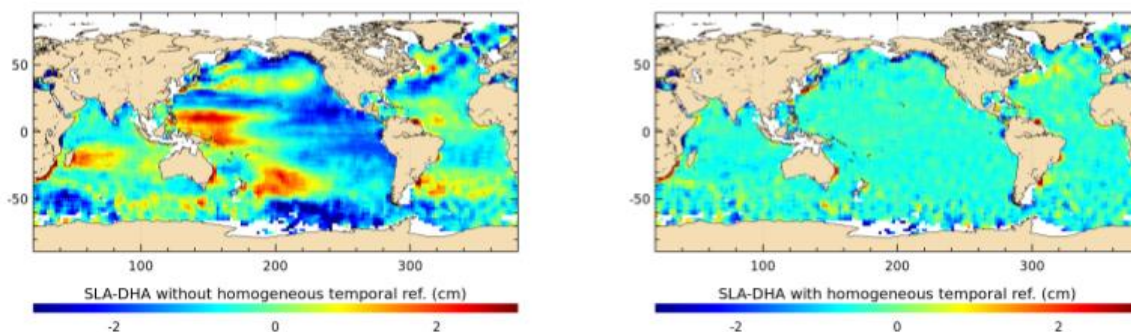


Figure 21: Map of the mean differences between AVISO SSALTO/DUACS and Argo data (900 dbar) over 2005-2015 without (left) and with (right) a common temporal reference period (2003-2014) for the estimation of the SLA and DHA anomalies (figure from 2015 Argo annual report).

4.1.3.3. Validation of collocated measurements:

SLA and DHA data are used according to the validity flags present in these products (see respectively AVISO and CORIOLIS databases for more details). Additionally, two selection criteria are added in order to exclude potential remaining spurious data:

- The difference between altimeter SLA and in-situ DHA has to be lower than 20 cm. Such a choice is based on the histogram of SLA-DHA residuals (Figure 22, left).
- In situ DHA data larger than 1.5 m are not taken into account

Such a selection excludes about 0.4 % of the total collocated measurements for the CMEMS DT 2018 product. As presented in Figure 22 (right) the excluded measurements are mainly located in regions of high ocean variability. These excluded data are not associated with erroneous data but their rejection is due to the collocation method itself. We nevertheless point out an anomaly in the Bay of Bengal. This feature occurs both for mono-mission (Jason-1 and Altika) and multi-mission altimetry products analyses. This could therefore be associated with a single profiler bias. Such analysis is beyond the purpose of this study.

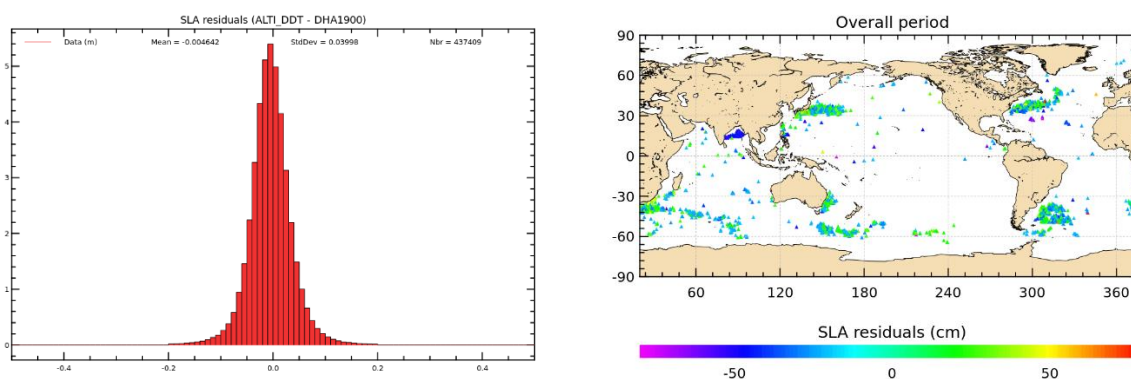


Figure 22: Histogram of valid SLA - DHA differences on left, and map of the invalid SLA - DHA differences on right.

4.2. Description of MSL comparisons altimetry/(TS+GRACE)

The processing sequence uses the database of collocated altimetry and Argo profiles to generate statistics of the altimeter sea level differences compared with in-situ measurements for each altimeter mission. Then, various diagnoses are produced from these statistics in order to detect potential anomalies in altimeter data. The global dispersion of the datasets (e.g. Figure 23) provides information on the correlation and coherence between both types of data and then, deeper analyses can be performed such as temporal and spatial evolution of the statistics of the differences, histograms, Taylor diagrams, uncertainties estimations...

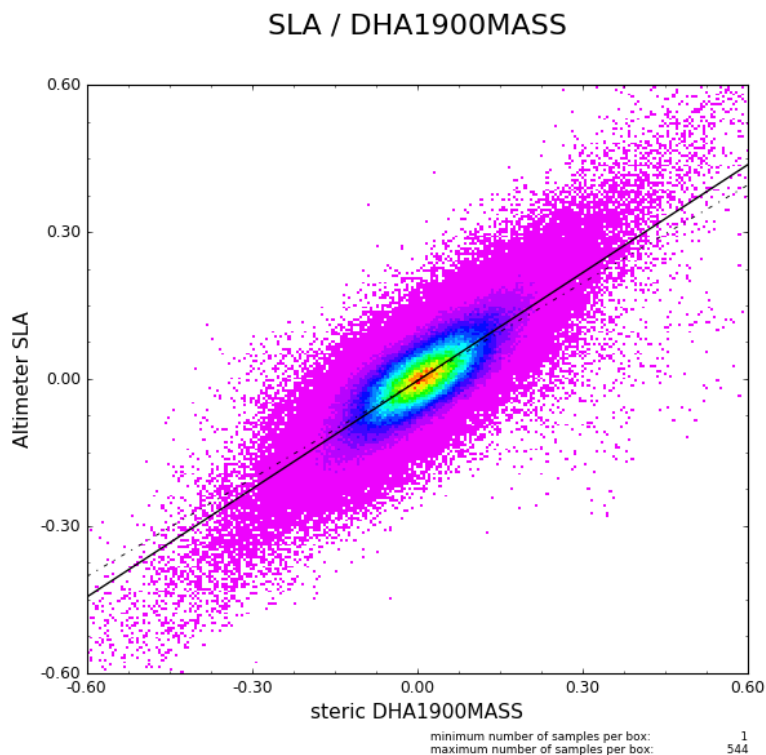


Figure 23: Dispersion between DUACS merged maps of altimeter SLA and the steric DHA from Argo plus the mass contribution from GRACE.

4.2.1. by altimeter missions

In 2015 and 2016, studies have been conducted in the framework of Sea Level Climate Change Initiative and SALP project, in order to select the best altimeter standards at climate time scale, mesoscale, etc. The results lead to different standards selection choices in the two projects (since the objectives are different). In this section, the CMEMS 2018 standards are used. The old set of standards (so-called CMEMS 2014) and the new one (so-called CMEMS 2018) have been compared. However, as for tide gauge comparisons, very small differences have been observed (not included in this report).

To perform closure budget analysis (Altimetric data - steric - mass) various mass solutions are available, different reference pressure can also be considered for the DHA. Section 4.3.1 presents these differences, their impact in term of uncertainty on the closure budget analysis is then estimated. In this current section, mono-mission results are presented using the GRGS mass solution and the Argo dataset referenced to 1900 dbar.

The GRGS mass solution and altimetric data are not corrected from the GIA. Thus, a slope of +0.3 mm/yr has to be removed to correct altimetric data and -1.2 mm/yr or -1.1 mm/yr for the GRGS mass model respectively if the high latitudes are taken into account or not (Chambers et al 2010).

Figure 24 shows the closure budget temporal evolution using CMEMS 2018, ARGO DHA referenced to 1900 dbar and GRGS mass model.



Envisat : +0.78 mm/yr

Jason-1 : -0.23 mm/yr

Jason-2 : +0.65 mm/yr

SARAL/AltiKa : +2.97 mm/yr

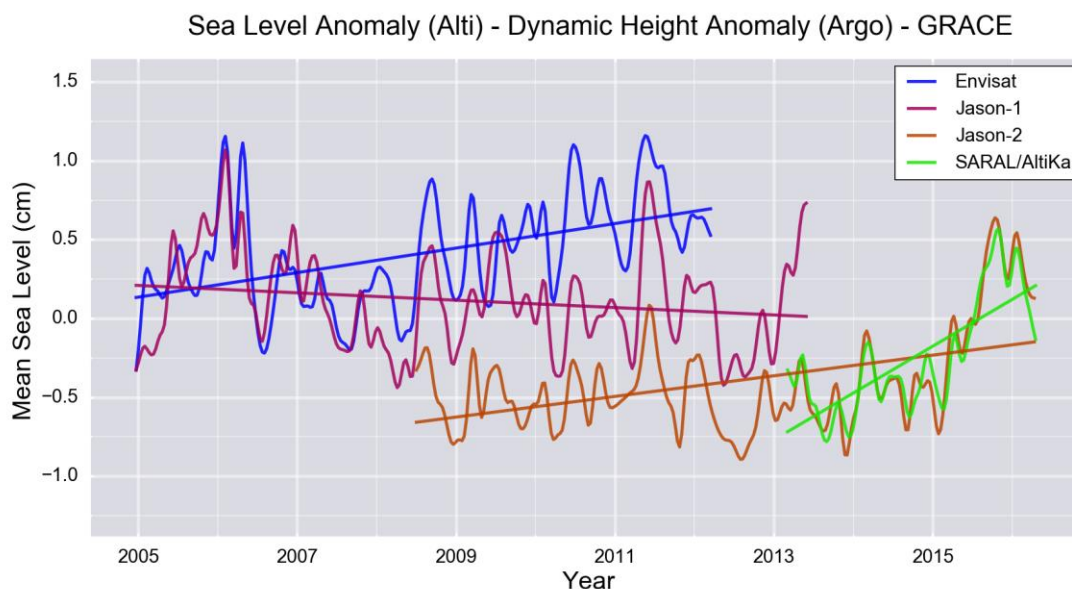


Figure 24: Temporal evolution of the differences between Envisat (blue), Jason-1 (purple), Jason-2 (orange), SARAL/AltiKa (green) and Argo DHA referenced to 1900 dbar corrected by GRACE mass model. Analyses performed with CMEMS 2018 and GRGS mass model. Corresponding annual and semi-annual signals have been removed. All curves are 2-months filtered. GIA correction is applied to altimeter (+0.3 mm/yr) and ocean mass (-1.1 mm/yr using Jason-1 or Jason-2 and -1.2 mm/yr using Envisat or SARAL/AltiKa).

One can remark the large positive slope value using SARAL/AltiKa. It can be explained by the small temporal series and the resulting uncertainty for this mission; this is further detailed in section 4.3.2. However, this temporal time series are largely affected by the pattern over 2015/2016. A significant increase of the residual signal is visible over this period by these two missions. The good agreement between the Jason-2 and AltiKa measurements over this period could suggest that the anomaly is mainly due to the mass solution + steric contribution. We point out that the 2015 -2016 period is affected by gaps of 2 months of unavailable data or low reliability data. To that respect the processing chain that consists in interpolating the GRGS GRACE maps and collocate them with the ARGO and altimetry data at a 10-day time step is likely to presents its limitations. This is discussed in this report and an alternative method has been implemented. It consists in using a water equivalent heights time series derived from the GRACE data (e.g. such as these provided by Chambers et al.) and subtracting it from the SLA-DHA global time series and is further detailed in section 4.2.2.1.

4.2.2. From multi-mission products (SLA grids)

4.2.2.1. Temporal analyses

Studying the temporal evolution of the closure budget at a global scale is a useful and complementary method to intermission altimetric comparisons when searching for potential altimeter drifts. The residuals of the SLA – DHA – mass difference are presented in Figure 25 for the



multi-mission product computed with the CMEMS 2018 standards. The blue curve represents the temporal evolution of the closure budget and its associated drift when referencing the ARGO DHA to 1900 dbar. The results with a 900 dbar reference are represented (red curve) for comparison. The difference between the two curves emphasizes the improvement on the closure budget analysis allowed by a profiler network probing deeper steric content. This point is further discussed in section 4.2.2.2.

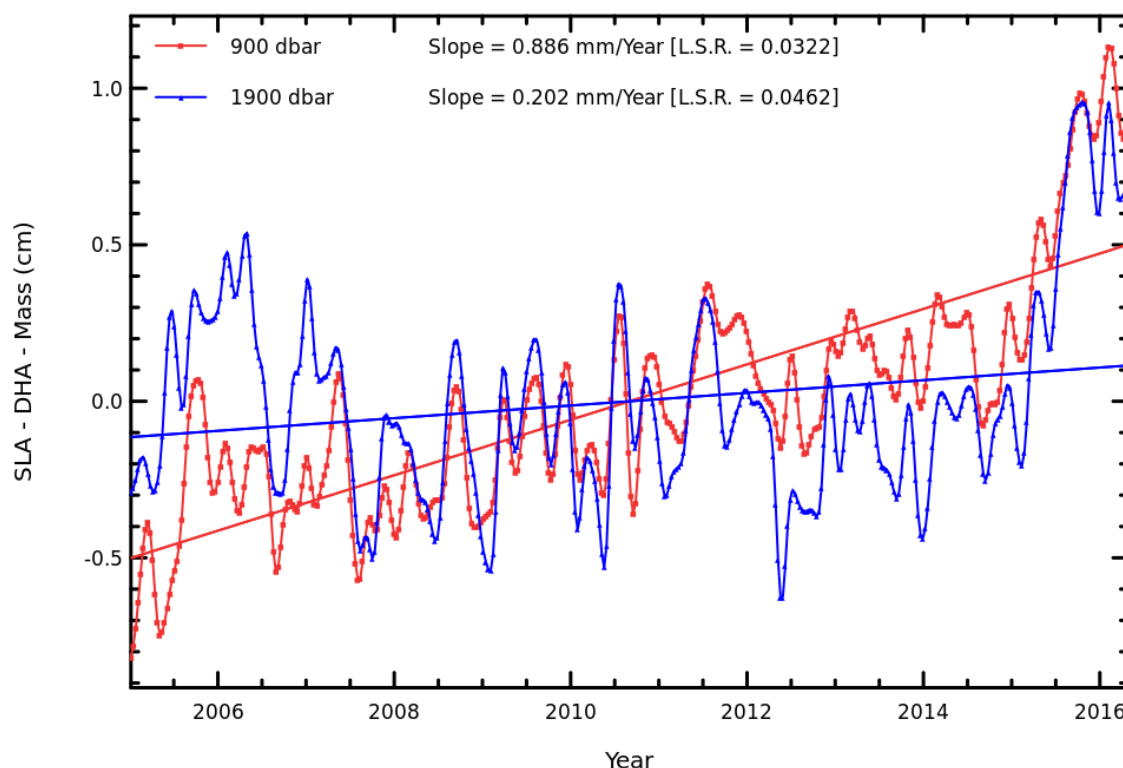


Figure 25: Residuals of the SLA (CMEMS DT with 2018 standards) - DHA - mass (GRGS RL03v3) for various TS reference integration depth and associated drifts.

As mentioned earlier on, various datasets of the mass contribution to the sea level are provided by different groups using different treatment of the GRACE data to compute the equivalent water height. As a comparison to the analysis performed with the GRGS mass solution, datasets of the mass contribution provided by Chambers et al.

(<http://xena.marine.usf.edu/~chambers/SatLab/Home.html>) were also considered. They consist in a monthly global mean of the EWH over the 2003-2016 period for the CSR, GFZ and JPL solutions. Corrections from the GIA and a 300-km coastal mask in order to reduce land leakage are included. These data allow for a comparison with the GRGS dataset and therefore an estimation of the uncertainty arising from the mass solution on the closure budget. This is discussed in further details in sections 4.3.1 and 4.3.2.



Figure 26 presents the residual term defined as $\text{Alti} - \text{TS} - \text{Mass}$ for various mass solutions using the GRACE data. While altimetry, Argo and mass data are 10 day collocated when using the GRGS mass maps and then globally averaged, for the three other solutions the global equivalent water height time series provided by Chambers et al is directly subtracted to the mean global SLA-DHA time series. The residuals slope for the CSR, GFZ and JPL solutions are coherent within a 0.15 mm/yr while the slope when using the GRGS solution differs from 0.79 mm/yr. These differences are explained by the spherical harmonics treatment difference between the mass solutions as well as in the removal process of the GIA: a similar treatment was performed on the solutions provided by Chambers but differs from the one applied on GRGS data (see section 4.3.1 for further details). Considering the uncertainty budget on the residuals drift estimate (section 4.3) all four values are in agreement.

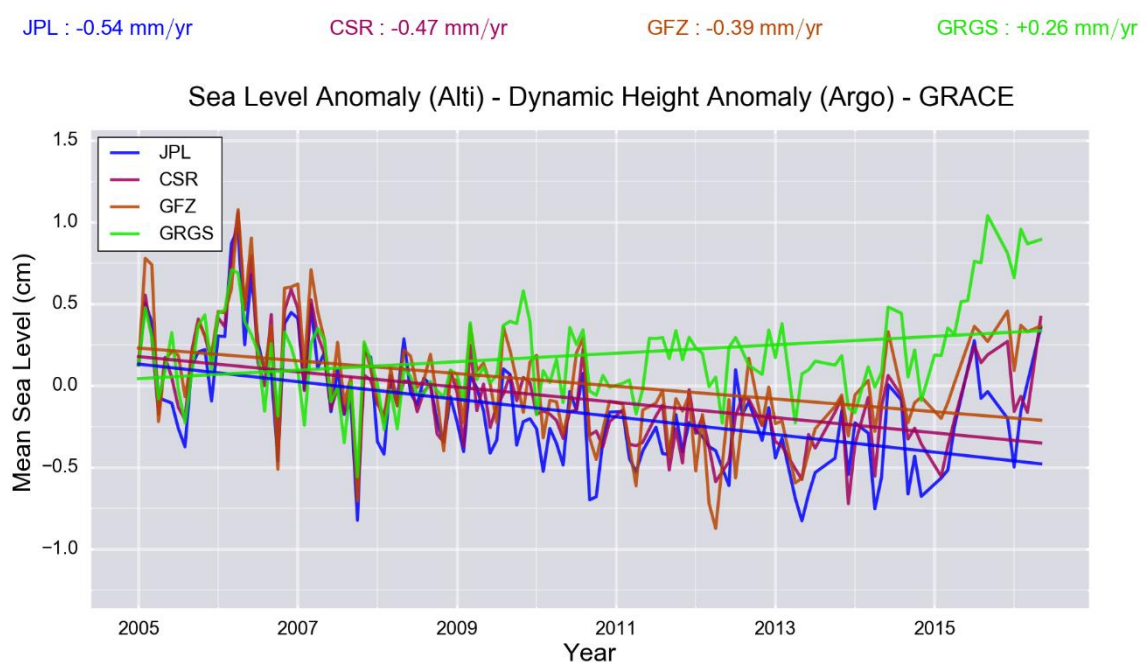


Figure 26: Residuals of the SLA - DHA - mass for various mass solutions and associated drifts.

When focusing on interannual timescales, one can notice, in the residuals, negative values in 2007-2008 and positive values in 2015-2016 that correspond to La Niña and El Niño events. Such residuals could be associated with one of the probe (alti, TS, mass) missing this event. Dieng et al (2015) proposed a method based on computing the correlation between the detrended residuals and each of the detrended components in order to possibly diagnosis a relation between short term fluctuations and either the altimeter, steric or mass serie. They showed that the residual anomalies from seasonal to inter-annual timescales are mainly correlated with ocean mass and steric sea level anomalies. This suggests that the annual anomalies in the SLA-DHA-mass residuals are likely to be mainly explained by in both GRACE-based ocean mass and Argo-based steric data. The undersampling of the Indonesian region by the Argo fleet can therefore be of significant importance during La Niña and El Niño events that particularly affect this area. This could explain the similar



anomalies in 2006-2008 presented in Figure 26 whatever mass solution is considered. As for the 2015-2016 anomalies, the differences seen with the different mass solutions suggests that their different treatments are affected by the gaps occurring in the GRACE data availability since 2015.

It is worth mentioning that the 1900 dbar curve in Figure 25 presents a slightly different drift than the red curve in Figure 26 (+0.202 mm:yr vs +0.259 mm/yr). In Figure 25, the equivalent water height derived from the mass was collocated with the altimeter and TS measurements whereas in Figure 26 the global mass correction was applied afterwards to reproduce the method applied to the deal with the CSR, GFZ and JPL data that are only provided at a global scale. This comparison emphasizes the weak difference between those drifts, compared to the overall accuracy. This difference is of the order of 0.06 mm/yr, it represents the impact of collocating the mass data or applying its correction at a global scale and is small compared to the other uncertainty sources present in closure budget analyses.

4.2.2.2. Taylor diagram analyses

The CMEMS DT 2018 products are compared with the steric and mass components. Figure 27 presents the Taylor diagram of the comparison of the sum of the Argo (at 900 and 1900 dbar, red and blue dots respectively) and GRACE measurements with altimetry measurements. The blue dot (1900 dbar profilers) shows that the correlation between the CMEMS DT altimetry measurements and the steric plus mass data is higher than 0.8. Such a value is obtained before application of the GIA correction on altimetry as well as GRACE data, this correction is detailed a bit further on. The comparison between the red and blue dots in Figure 27 emphasizes that both centered RMS difference and correlation between the altimetry and TS+Mass data are better (smaller RMSD and strengthened correlation) when using profilers that probe deeper steric contribution. This result is in agreement with Legeais et al 2016.

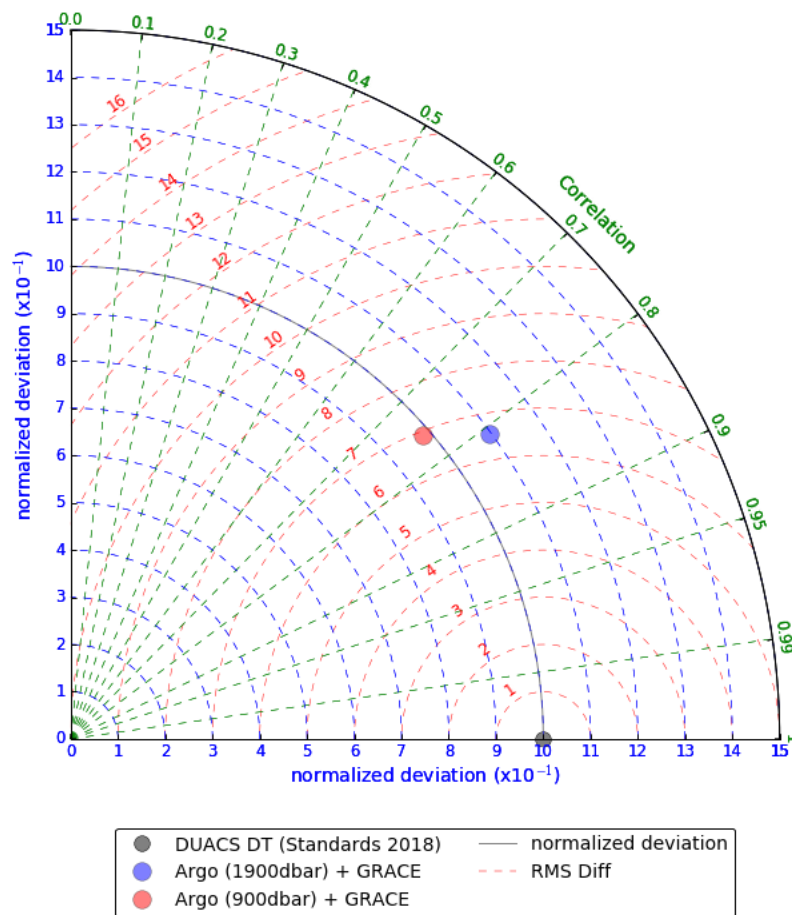


Figure 27: Taylor diagram of the comparison of the sum of steric ARGO DHA (different reference level) with altimeter sea level time series (CMEMS, 2018 standards) (grey reference circle).

The previous diagnosis is based on the collocation of altimeter and Argo measurements as well as on the use of monthly maps (GRGS RL03v3 in this study) representing the equivalent water height (EWH) derived from the mass GRACE solutions. Such an approach allows to perform regional analysis. In Figure 28, we further detail the discussion about water column integration to derive the steric contribution. The red symbols represent a selection in the tropical band while the blue ones correspond to higher latitudes. Diamonds represent a selection of the profilers reaching 1900 dbar while circles represent a larger selection including all profilers reaching 900 dbar and more. As presented in (Legeais et al. 2016), although restraining the analysis to profilers reaching at least 1900 dbar reduces the number of available ARGO-Altimeter collocations, the temporal sampling of the Argo float is not significantly affected. Therefore, the differences between a 900 and a 1900 dbar analysis are not drawn by spatial selection effects and are representative of the integration depth.

As shown by the diamonds correlations and RMS are improved when considering the deep contribution. This effect is nevertheless much stronger at high latitudes where the water column is not as stratified as in the tropics. Therefore, Figure 28 illustrates that the contribution from the deep ocean to the steric signal is more important at high latitudes.

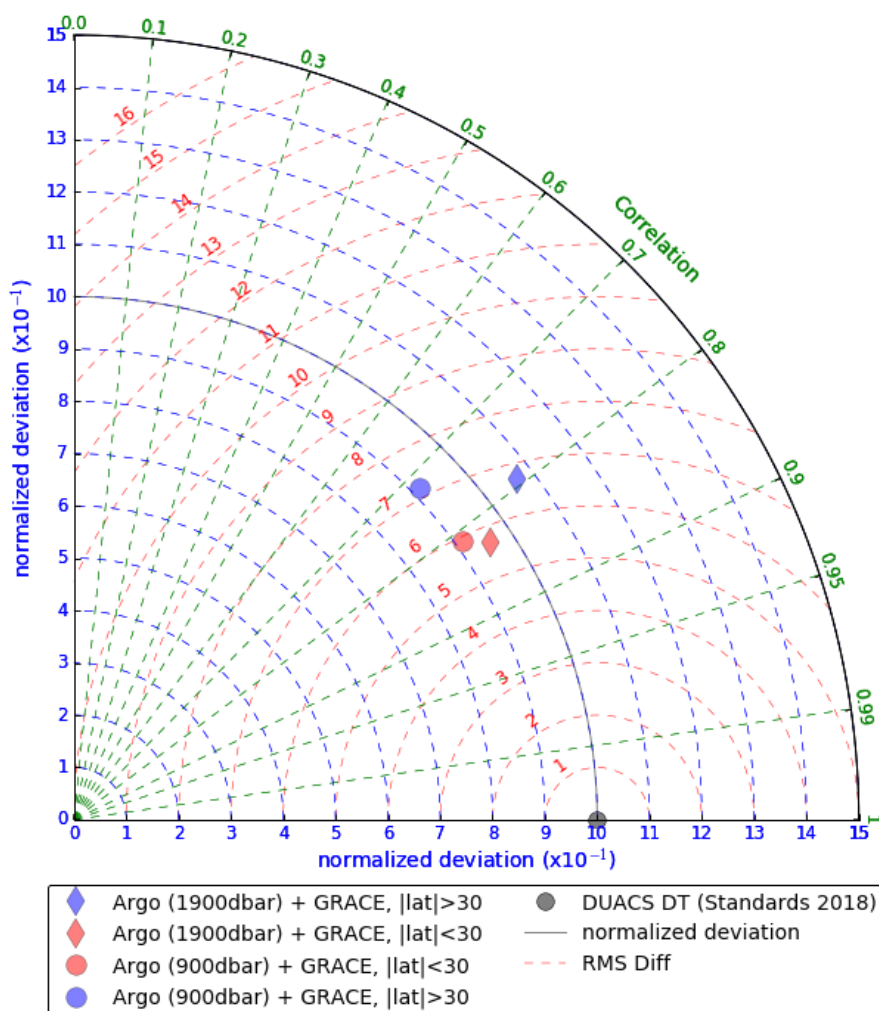


Figure 28: Taylor diagram of the comparison of the sum of steric ARGO DHA (different reference level and latitude extension) with altimeter sea level time series (CMEMS, 2018 standards) (grey reference circle).

4.2.2.3. Partial conclusions

- 1) The differences in the processing of the GRACE datasets mainly induces differences of several millimeters observed in the curves of Alti - TS - Mass at an interannual time scale. The absolute drift values, on the contrary, are in good agreement and cannot be distinguished, given the uncertainty budget, from a null drift as will be detailed in section 4.3. The CMEMS DT multi-mission products therefore does not present any detectable altimetry drift with respect to the steric and mass data over the 2004-2016 period.
- 2) Diagnoses can also be performed at a regional scale. The deep steric contribution (lower than 900 dbar) is shown to improve both correlation and RMS difference between the altimetry and steric + mass measurements. The present study emphasize that such



improvement is larger at high latitude than in the tropical band. Such a result is in agreement with the more stratified distribution of the water column in the tropics making the steric signal mainly arise from the upper layer.

4.3. Uncertainties

In order to confirm the presence or not of an altimeter drift with respect to the dynamic heights and equivalent water height derived from the profilers and mass measurements, the method uncertainty budget has to be precisely quantified. The different components are described in section 4.3.1 and their associated estimates are quantified into section 4.3.2.

4.3.1. Description of errors

The error on the closure budget is constituted of a noise term, a phase uncertainty and terms associated with the mass and steric contributions.

4.3.1.1. Formal uncertainty

The formal uncertainty is due to the impact of the noise present in the time series on the slope estimation. Such uncertainty depends on the time series length and altimeter. The main sources of this noise term arise from the noise in the altimeter time series, the noise associated with the InSitu and mass measurements and the collocation of all these components.

4.3.1.2. Phase Uncertainty

The phase uncertainty is related to possible annual and semiannual residual signal within the SLA-DHA-mass residuals. It can generate an apparent drift as a function of the phase and the time series length. Details about this uncertainty calculation are given in the appendix 7.3.

4.3.1.3. Terms associated with the mass and steric contributions

4.3.1.3.1. Errors associated with the determination of the mass solution

GRACE data are decomposed on spherical harmonics (SH) so as to provide an equivalent water height solution. The global ocean mass evolution is affected by this decomposition of the GRACE data as well as some land to ocean mass signal leakage. CSR, GFZ and JPL provide EWH solution, each center using slightly different processing and analysis strategies. The different datasets were compiled by Chambers et al. at a global scale and they applied a similar mask and GIA correction to all three datasets. Consequently, comparing them provide a reasonable estimate of the uncertainties associated to SH decomposition methods. Figure 29 represents the equivalent water height after removing the 0.5 and 1-year periodic signals and applying a 6-month filter. Considering this range of solutions, the uncertainty on the slope estimation is of the order of 0.1 mm/yr.

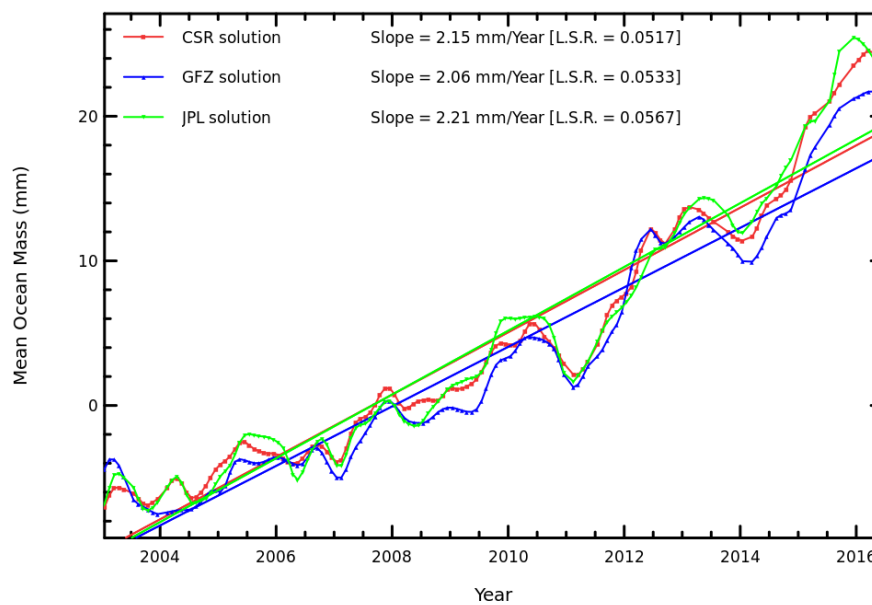


Figure 29: Global ocean mass evolution for various solutions of the SH decomposition of the GRACE dataset (seasonal sinusoids removed).

Satellites orbit the Earth mass center but this geocentre moves relatively to the crust. This motion induces an uncertainty of the order of 0.59 mm/yr on the equivalent sea level trend (Blazquez et al.).

4.3.1.3.2. GIA correction

The glacial isostatic adjustment (GIA) is a rebound of the terrestrial and oceanic crust in response to the melting of the ice caps. Since GRACE measures all gravity variations, one must remove the effect of the post glacial rebound. Since the GIA correction is of the same order as the expected mass trend (1-2 mm/yr equivalent sea level rise) its uncertainties lead to significant differences in trend estimates. (Chambers et al. 2010) estimated those latter to be of the order of 0.3 mm/yr.

In this report, closure budget analyses using the GFZ, JPL and CSR mass solutions already contain the GIA correction included in these product, therefore only the +0.3 mm/yr GIA correction on altimetry was applied. In the analysis using the GRGS mass solution we included a GIA correction of -1.2 mm/yr (+0.3 mm/yr GIA correction on altimetry (Peltier 2004), i.e. an overall -0.9 mm/yr correction) for the multi-missions analyses as well as mono mission analyses on Envisat and Saral/AltiKa missions. A GIA correction of -1.1 mm/yr (+0.3 mm/yr GIA correction on altimetry, i.e. an overall -0.8 mm/yr correction) was applied for closure budget analysis on the Jason missions due to their latitude extension being limited to 66° degree. These global GIA corrections were computed using the Geruo et al (2013) GIA correction map.



4.3.1.3.3. Depth of Argo profilers

The steric signal is sampled through the height of the water column accessed by the profiler. The large majority of the profilers reach a depth of 900 m whereas only about half probe the ocean down to 1900 m. Comparing the altimeter drift estimate with GRACE + Argo (900 and 1900 dbar reference level) data (Figure 25) provides an estimate of the average contribution of steric in the 900m - 1900m range. A 1.7 mm/yr and 0.3 mm/yr trend correction were applied to account for the GIA in the mass and altimetric data respectively. Such correction, applied on both curves, nevertheless does not change the 0.38 mm/yr difference between the two drifts. This value provides an assessment of the 900m - 1900m steric contribution when regarding closure budget analyses. It is nevertheless difficult to disentangle which of this 0.38 mm/yr drift is deep physical signal and which is errors. The deep thermosteric contributions (lower than 2000m) were estimated to be 0.11 ± 0.10 mm year⁻¹ with 95% confidence level (Purkey and Johnson 2010). In the future, should uncertainties on ocean mass estimated from gravimetry measurements and GMSL be reduced, such a contribution from deep ocean could rather be estimated (Dieng et al. 2015) from Alti -Argo-Mass analyses.

4.3.2. Uncertainty estimation over the trend

Various studies have provided estimates of the uncertainties associated with the mass and steric data. The formal and phase uncertainties, which are time series length dependent, were usually not accounted for. This section quantifies them, emphasizing they are negligible for long time series (~10 years) but dominant when considering short series, which is relevant when assessing the performances of recent missions.

Table 9 summarizes the uncertainties sources over the thermosteric and the mass contribution compiled from the literature. The uncertainty value associated to geocenter motion is of the order of 0.59 mm/yr (90% confidence level) as pointed out by Blasquez et al. (article under rev., see also "CAVE MSL meeting").

Source	Uncertainty [mm/yr]	Comments
SH decomposition of GRACE data	0.1 ^a	Depend on Mass analysis method
Land leakage (after 300 km coastal band mask application)	0.1 ^a	Depend on Mass analysis method
Geocenter motion	0.59 ^b [90% CL]	Depend on Mass analysis method
GIA correction on global ocean mass	0.3 (90% CL) ^c [0.36 (95%CL)]	Time independent term
0-2000m thermosteric contribution	0.21 (90% CL) ^c [0.25 (95%CL)]	
Deep steric contribution	0.1 (95% confidence level) ^{c,d}	



^a : from (Legeais et al. 2016), confidence level not specified

^b : from (Blasquez et al. - submitted)

^c : from (Chambers et al. 2017)

^d : from (Purkey and Johnson 2010)

Table 9: Estimated uncertainties on trends for ~10-year time series.

These uncertainties provided in the literature were estimated over 10-year time series. The GIA correction applied on the mass time series in closure budget analyses is independent of the study's length, therefore the uncertainty associated to this particular correction can be considered as time independent. On the contrary, the uncertainties associated with the mass solution and the steric contribution strongly depend on the length of the considered time series. This should be accounted for in the context of discussing the potential significance of an altimetry product drift, especially for the Jason-3 and Sentinel-3a missions for which the Altimetry/TS-Mass time series only spans a year. In this case the 0.1 mm/yr uncertainty estimation computed over a 10-year period strongly underestimates the uncertainty associated to the mass solution as detailed in the following section.

4.3.2.1. Time dependant mass solution related uncertainty estimation

Although various studies have already estimated the uncertainty associated with the mass solution (representative of the spherical harmonic decomposition method, land leakage and accounting of the geocenter motion) for long time series (10 years) in the context of multi-mission analysis, its impact on short time series has not been estimated. It is nevertheless of particular interest for closure budget analysis performed to assess the quality of recent altimetry missions.

In this study, different mass solutions were considered over various time period in order to estimate the uncertainty associated with the spherical harmonic treatment of the GRACE data.

Figure 30 shows empirical values of the mass solutions' uncertainty as a function of the time series length (hereafter L) using the multi-mission dataset as altimetric data. For each L value, several segments are extracted from the altimetry (multi-mission dataset) - steric (referenced to 1900 dbar) - mass (various mass solutions: JPL, CSR, GFZ). The mass solutions' uncertainty for a given L is then estimated as the mean of the standard deviations (90 % confidence level) of the slope values on each segment. Given that this uncertainty is estimated from standard deviations of 3 mass solutions a multiplier coefficient of 3/2 is applied to obtain a better estimation (standard deviation is a biased estimator for a small sample size).

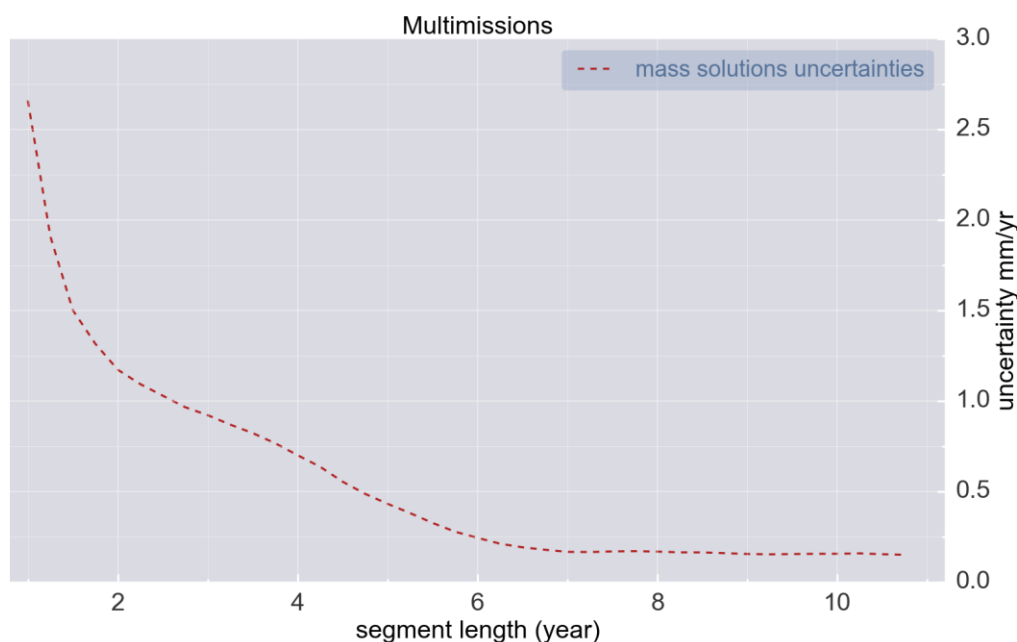


Figure 30: Empirical uncertainty on trend estimation associated with the various mass solutions (JPL, GFZ and CSR) as a function of the time series length.

Over a 10-year period the uncertainty on the slope value due to the different mass solutions is about 0.15 mm/yr which appears to be consistent with the SH decomposition uncertainty presented in Table 9. In the context of short study periods (Alti-Ts-Mass using Jason-3, Sentinel-3A or even SARAL/AltiKA) it goes up to about 0.9 mm/yr and 2.66 mm/yr in the case of a three and one year time series length respectively. This result has to be taken into account when a potential altimetry product drift is discussed as it is largely affected by the duration of time series.

4.3.2.2. Formal uncertainty associated to trend estimation

The formal uncertainty on slope estimation is estimated using the following method: considering the SLA-DHA-mass time series, for each duration, segments of this time length are drawn from the altimetry-steric-mass time series. The slope uncertainty is then computed as the mean of the individual uncertainties derived from the least square fit on each single segment. Results are presented in Figure 31 in the case of the residuals obtained between the multi-missions CMEMS 2018 product and DHA referenced to 1900 dbar plus GRGS mass model. The curve follows the $t^{-3/2}$ analytically predicted shape (see appendix 7.2 **Erreur ! Source du renvoi introuvable.**).

Autocorrelation in time series has an impact on this uncertainty estimation and must be accounted for. Thus, the series autocorrelation value is used to compute an effective sample size (Cazenave et al. 2016) from a maximum time lag of 3 months. The following ratio is then used as a multiplier factor to obtain a better estimation:

$$\sqrt{\frac{n_{s\text{amp}}}{n_{\text{eff } s\text{amp}}}} \text{ with } \left\{ \begin{array}{l} n_{s\text{amp}}: \text{samples size} \\ n_{\text{eff } s\text{amp}}: \text{effective samples size (estimated)} \end{array} \right\}$$

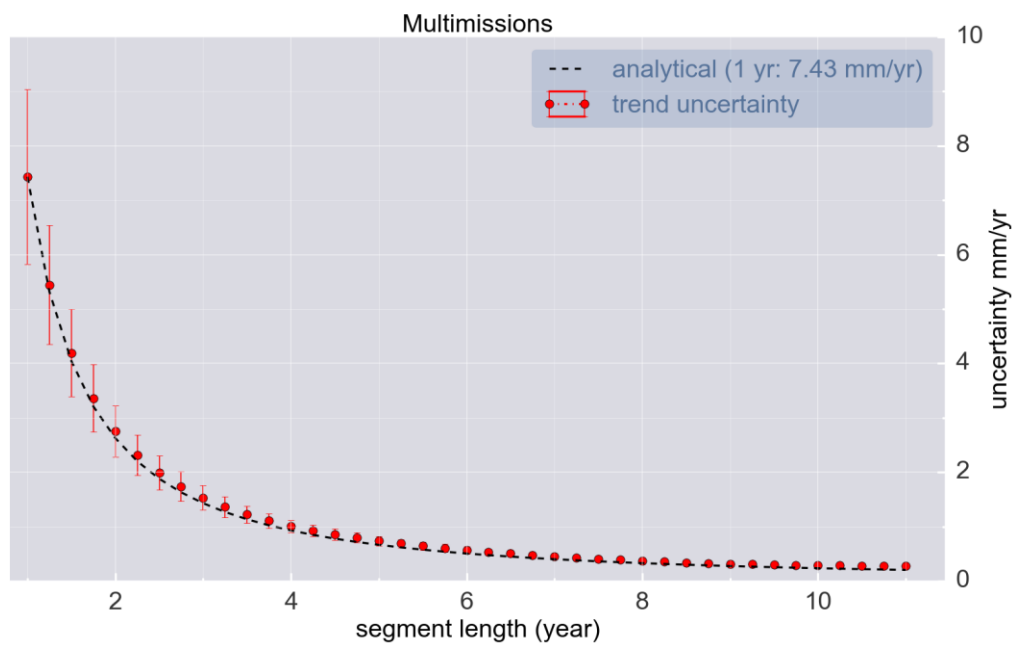


Figure 31: Formal uncertainty (90 % confidence level) on trend estimation as a function of the time series length (multi-missions CMEMS 2018 product, DHA referenced to 1900 dbar, GRGS mass model). Time series autocorrelation is accounted for in the analysis. The red dots represent the computed uncertainty and is compared to the black line representing the predicted analytical solution scaling as $t^{-3/2}$.

In this example in which the altimetric dataset is the CMEMS DT 2018 product, when considering a 11-year long time series, the associated trend uncertainty value is of the order of 0.3 mm/yr and reaches an asymptotic value. This curve emphasizes that performing a closure budget analysis over a shorter time period would yield an increase of the error budget do to the increase of the trend uncertainty. In particular Figure 31 shows that analysis on shorter than 4 years series would more than triple the trend uncertainty with respect to its optimal asymptotic value.

We point out that, since the trend uncertainty represents the noise contribution to the total error budget on the drift, and the noise theoretically depends on the input altimetric data, the curve providing the trend uncertainty as a function of the series length has to be recomputed for each altimetry product. This was performed as a validation exercise of the method: these trend uncertainty curves were computed for various mono-mission altimetric datasets and results are summarized into Table 10. The trend uncertainty column provides the uncertainty computed when considering the full dataset time extent. For comparison purposes the 1-year uncertainty value is



also provided. As expected, the uncertainty value is larger for dataset whose length is shorter. To that respect, the trend uncertainty on the closure budget is up to 1.83 mm/yr for AltiKa CMEMS 2018 product (DHA referenced to 1900 dbar and GRGS mass model) due to the short time period yet covered by the mission. It nevertheless worth noting that most recent missions present a smaller 1-year uncertainty (e.g. 7.13 mm/yr for AltiKa), as expected given their smaller noise level. This conclusion is in agreement with the one obtained with altimetry – tide gauges.

Mission	trend uncert. (mm/yr)	time series length (year)	1 year uncert. (mm/yr)
Jason-1	0.37	8.43	7.87
Jason-2	0.46	7.77	7.89
Envisat	0.54	7.23	8.95
AltiKa	1.83	3.12	7.13
Multi-missions	0.3	11.33	7.5

Table 10 : SLA-DHA-mass trend uncertainty over the full serie and when considering a 1 year time period for comparison between the different products. Uncertainties are indicated at 90 % confidence level. Analyses performed with altimeter standards 2018, Argo DHA referenced to 1900 dbar corrected, and GRGS mass model.

4.3.2.3. Phase uncertainty associated to trend estimation

When computing the Altimetry - steric - Mass difference, an annual cycle may still be present in the residual part due to the non-perfect cancellation of those three terms in the centimetric range. In the analysis, annual and semiannual cosines are therefore fitted to account for this effect and correct it. The residual cyclic component nevertheless generates an uncertainty on the trend estimation. This term is a function of the duration of the time series and the phase (see appendix 7.3 for details). Although this uncertainty is not significant for time series longer than 4 years, it has to be addressed once the potential drift of a mission with a short time series is discussed. Figure 32 represents the phase uncertainty variation (90 % confidence level) as a function of time on the closure budget using the multi-mission CMEMS 2018 product, DHA referenced to 1900 dbar and GRGS mass model.

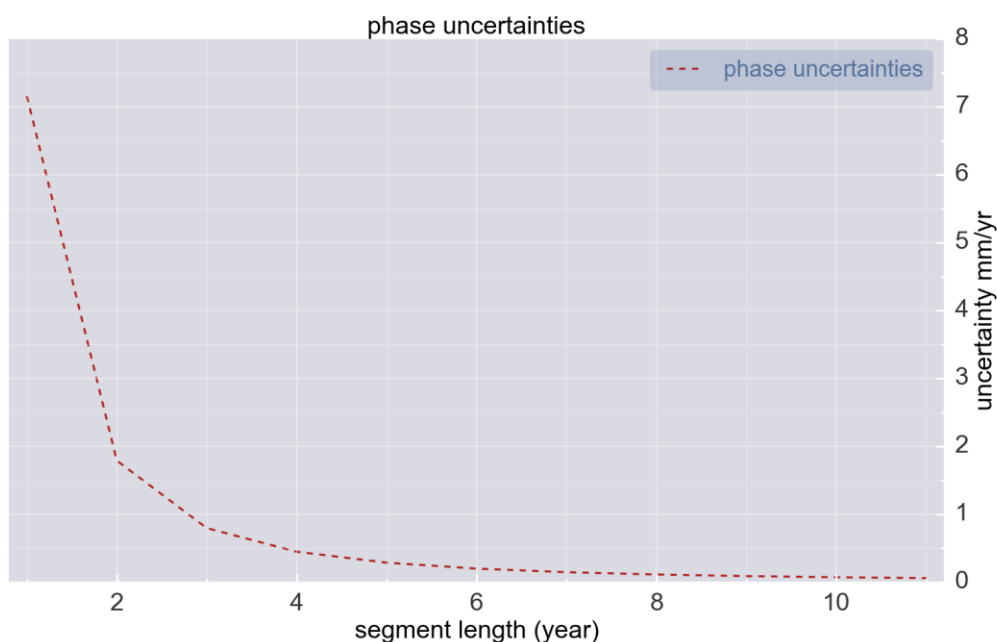


Figure 32: Phase uncertainty variation (90 % confidence level) as a time function with multi-missions CMEMS 2018 product, DHA referenced to 1900 dbar, GRGS mass model.

Phase uncertainty quickly decreases with time series length and is therefore negligible for analysis over 10 years periods. On the contrary its contribution can be significant when considering recent missions for which only short time series are available. Tables in 7.4 presents the phase uncertainty for the different products.

4.3.2.4. Order of magnitude discussion

The budget uncertainty is dominated by constant uncertainties for long (i.e. 10 years) time series, this uncertainty is of the order of 0.75 mm/yr (90% confidence level). The time dependency of other contributions was investigated. They consist in the formal and phase uncertainties (Figure 31 and Figure 32) as well as the one associated with the mass solutions (Figure 30). These time-dependent contributions are the main components in the error budget for time series lower than 4 years at a level of several mm/yr. Accounting for these terms is therefore of particular importance when assessing the Jason-3 and Sentinel-3A potential drifts.

The global budget uncertainty on drift estimation and its various components as a function of time series length are represented in Figure 33. The total uncertainty is computed as the quadratic sum of the uncertainty components. Regarding the trends, the longer the available time series period, the more reliable the data. The asymptotic value is reached from about 7 years of data.

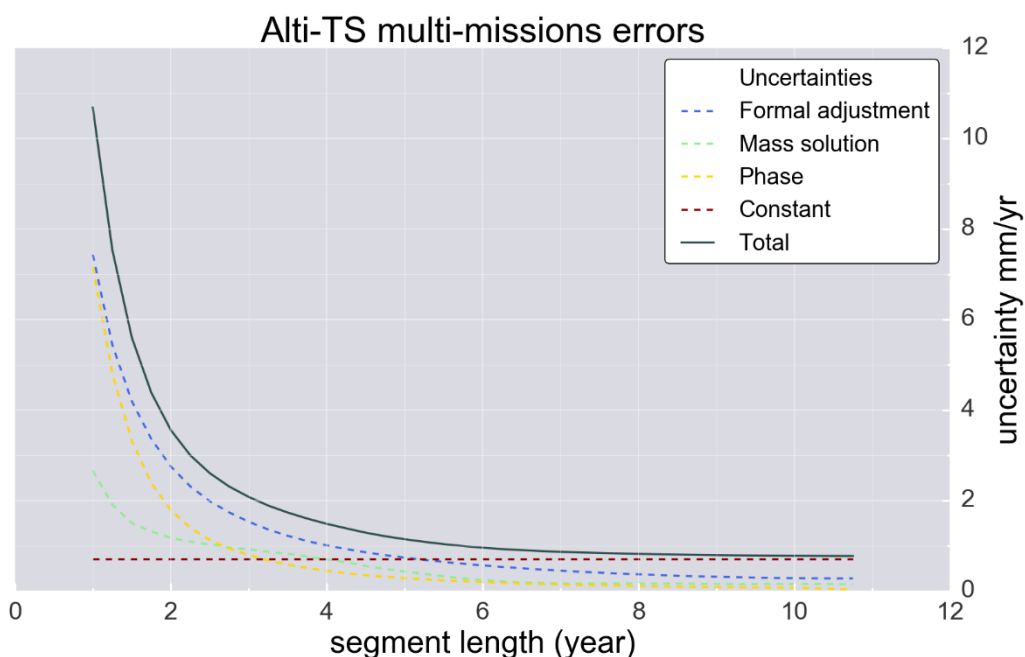


Figure 33: Total uncertainty variation and its various component (90 % confidence level) as a time function with multi-missions CMEMS 2018 product, DHA referenced to 1900 dbar, GRGS mass model. In black line the total uncertainties variation, in blue the formal adjustment one, in green the mass solution one, in red the constant one and in yellow the annual and semi-annual cycle removals uncertainties on the trend.

4.3.2.5. Application: Use of the budget uncertainty to assess the significativity of the closure budget drift for the different missions

Drift values of the closure budget are summarized in Figure 34. Uncertainties corresponding to a 90% confidence level are represented as error bars, computed according to the previous section. Both GRGS and CSR mass solutions are considered, except for the Jason-3 and Sentinel-3A analyses for which the period covered by the GRGS data is not large enough. All drift values and associated uncertainties are summarized into the tables present in appendix 7.4.

One can notice a systematic bias of about 0.6 mm/yr between the analyses performed with the two different mass solutions. It may be explained by some differences in the mass data processing (geocenter, GIA removal ...). Consequently, more investigations are needed to understand this point. They could consist in using a sum of geophysical quantities to estimate the ocean mass term (e.g. Dieng et al. 2017 : temporal changes in mass of glaciers, Greenland and Antarctica ice sheets, liquid water storage on land...) and potentially avoid the additional unknown uncertainties present into GRACE data due to their periodic unavailability over the 2015-2016 period. Such study would nevertheless require to build the uncertainty model associated with the different components of the mass estimate.

Given the trends' uncertainty, no mono-mission nor CMEMS drift are confirmed with both mass solution analyses at a 90% confidence level. Thus, two problematic issues appear in Figure 34. Firstly,



a non-compatible to zero (90% confidence level) drift can be noticed in the closure budget performed with AltiKa data with CMEMS 2018 standards, DHA referenced to 1800 dbar and GRGS mass model. Time series duration in this case is short (~ 3 years) and largely affected by the pattern at the end of the closure budget (also visible with Jason-2 and multi-missions data). During this period one can observe several lack of data in GRACE data, these are filled by interpolations process in the Alti-TS-Mass data collocation algorithm. Such lack of data and their induced errors is not accounted for in the presented uncertainty model, which is therefore likely to underestimate the closure budget associated uncertainties when including the 2015-2016 datasets in the analysis. The alternative method we developed (collocation of the altimetric and steric data, global averaging and then removal of the globally averaged mass contribution) does not perform such interpolations. This can be clearly seen in Figure 26 where the residuals computed with the GRGS dataset significantly differ from these using the Chambers et al. solutions.

The second anomaly is the negative drift appearing on the Jason-1 closure budget, when using the CSR mass model. It could be explained by statistical reasons since all uncertainties are given with 90 % confidence level (this drift would be compatible with a superior confidence level) but more investigations would be needed to solve this point.

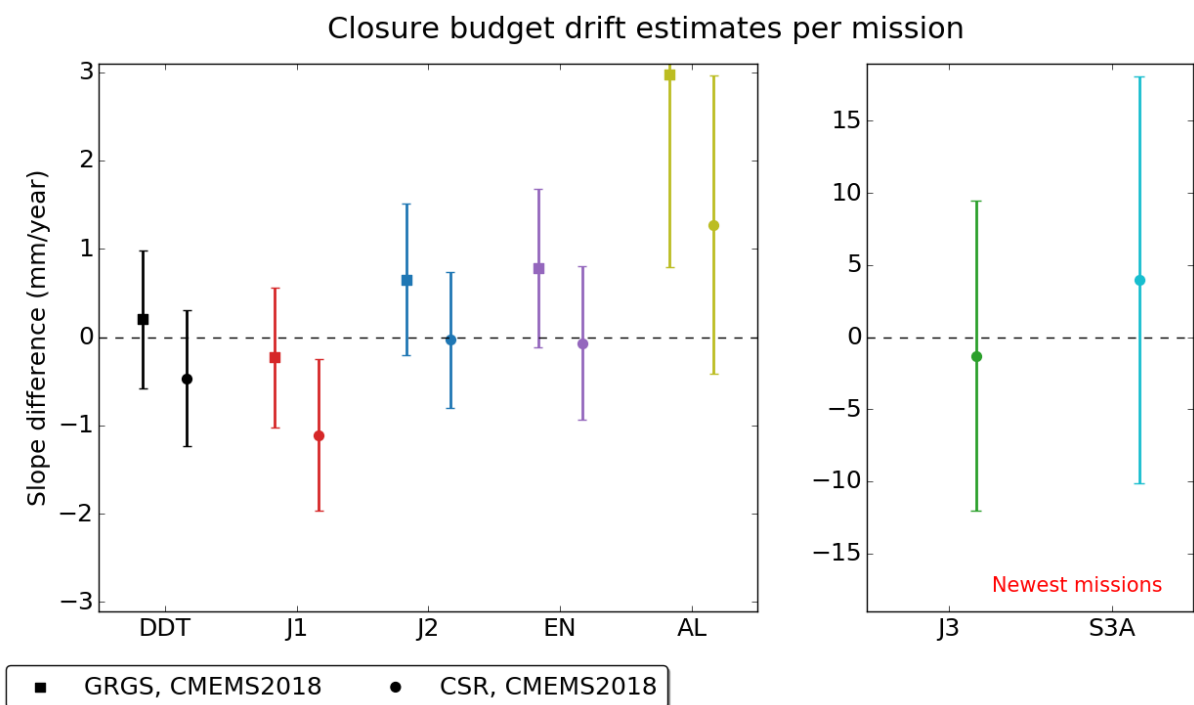


Figure 34: Slope values of the SLA – DHA – mass closure budget and their 90% confidence level associated uncertainties. Altimetry data are the multimission CMEMS DT 2018 product (DDT label in dark), Jason-1 (red), Jason-2 (blue), Envisat (purple), SARAL/AltiKa (yellow), Jason-3 (green), Sentinel-3A (turquoise). Analyses performed with CMEMS 2018 altimetric standards, DHAs referenced to 1900 dbar and 2 different mass model (GRGS, -squares- and CSR – circles-).



5. Specific studies

5.1. Impact of error on the global MSL to link altimeter missions together

5.1.1. Summary of (Zawadzki and Ablain, 2016) paper

The current mean sea level (MSL) continuous record, essential to understanding the climate evolution, is computed with the altimetric measurements of the TOPEX/Poseidon mission, succeeded by Jason-1 and later Jason-2. The accurate continuity of the record is ensured by the conservation of the "historical" TOPEX orbit as well as by calibration phases between the successive missions which enable a rigorous computation of their relative biases.

Jason-3 is the natural successor of Jason-2: on the same orbit with a calibration phase. Shortly after Jason-3, another altimetric climate-oriented mission, Sentinel-3a, has been launched on a different orbit. In this paper, (Zawadzki and Ablain, 2016), simulated altimetric sea level data are used to estimate the uncertainty on the intermission relative bias depending on whether Jason-3 or Sentinel-3a is linked up to Jason-2. Then, the corresponding impact on the GMSL continuous record over a 25-year or 10-year period is estimated.

The study shows that the calibration phases between Jason-1/Jason-2 or Jason-2/Jason-3 enable a rigorous estimation of the inter-mission relative biases with a 1 mm uncertainty. It corresponds to a 0.15mm/yr uncertainty on a 10-year MSL record. In the absence of calibration phase, the relative bias uncertainty rises up to 2.5mm, corresponding to a 0.4mm/yr uncertainty. Compared to the 0.3mm/yr GCOS requirement, these uncertainties are very significant.

However, these relative bias uncertainty estimations are linked with the methodology to estimate the bias.

5.1.2. Extension of the study in case of loss of the reference mission (e.g. J3)

In order to extend the current MSL record, Jason-CS (Sentinel-6) will be the natural successor of Jason-3 in 2020: on the same orbit with a calibration phase.

In the previous section, we demonstrated that the accurate continuity of the record is ensured by the conservation of the "historical" TOPEX orbit as well as by calibration phases between the successive missions. However, these uncertainties are obviously correlated with the method used to estimate the inter-mission relative bias.

The objective of this section is to develop a work plan in preparation to Jason-CS (Sentinel-6) launch. The altimeter constellation currently provides an unprecedented number of altimeters in addition to the main reference mission. Can we improve the accuracy of the methods to estimate the relative biases using a multi-mission approach to strengthen the link between Climate missions? Would—using Jason-3, Sentinel-3A and 3B, Jason-2 GM be more accurate? What would be the MSL trend uncertainty induced by the premature loss of Jason-3 ?



First of all, based on the relative bias uncertainties estimated in the previous section (i.e consistent with the current intermission relative bias estimation method), we estimated the uncertainty on the GMSL trend, from 1993 onwards, induced by:

- linking up Jason-CS to Jason-3 in 2020
- or linking up Sentinel-3a to Jason-3 and Jason-CS to Sentinel-3a in case of premature loss of Jason-3

With the current methodology, linking Jason-CS to Jason-3 in 2020 would have a low impact on the trend uncertainty. This is the combination of an accurate estimation of the relative bias thanks to the calibration phases and the length of the MSL record. over 1993-2023, the corresponding uncertainty on the MSL trend would reach 0.18 mm/yr at 95% confidence level.

However, in case of Jason-3 failure, switching temporarily to Sentinel-3a and then to Jason-CS would have a significant impact on the trend. Subsequent to the duration of the Sentinel-3a transition between Jason-3 and Jason-CS, the corresponding uncertainty on the MSL trend would be between 0.27 mm/yr and 0.33 mm/yr at 95% confidence level.

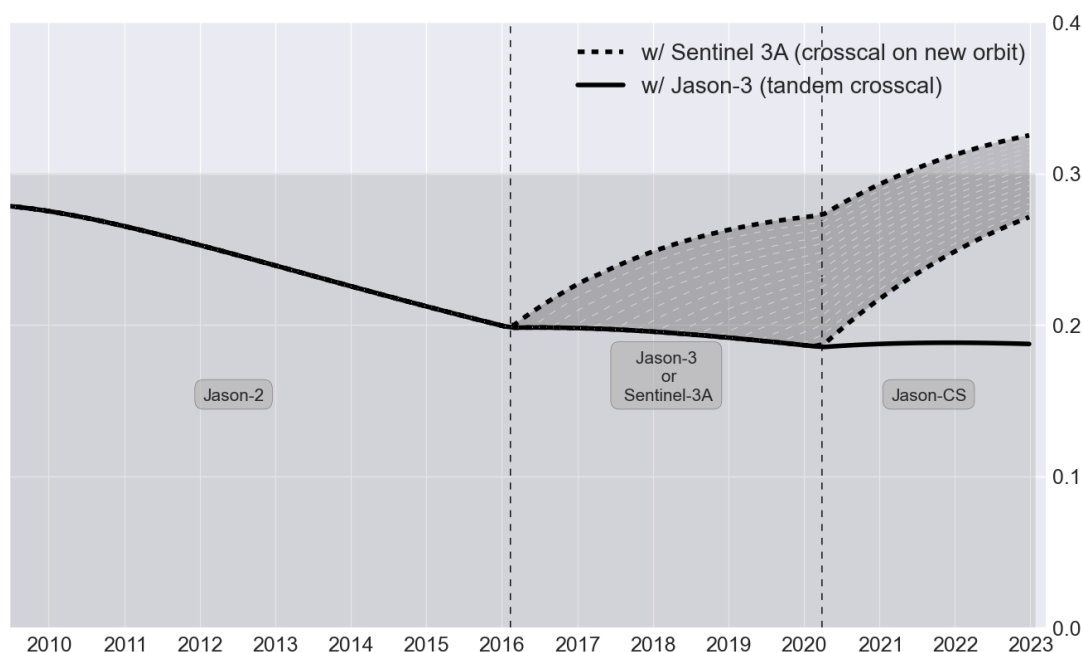


Figure 35 : Evolution of the GMSL trend uncertainty (mm/yr) in a confidence interval of 95% considering only the GMSL bias uncertainties to link altimeter missions together for 2 different satellite configurations : a) Jason-2+ Jason-3+ Jason-CS (solid line), b) Jason-2 (or Jason-2 + Jason-3)+ Sentinel-3A (dashed lines)



5.2. Estimation of an empirical TOPEX-A correction derived from altimetry and tide-gauges measurements

5.2.1. Overview

To determine the cut-off period to be applied, the uncertainty level of altimeter and tide gauge comparison has to be considered. This study has recently been performed at CLS. Trend uncertainties have been estimated versus the period length. This work has been presented in this report in section 3.3.3. A poster has also been presented at last OSTST.

The Figure 36 shows the evolution of the alti/TG drift uncertainties versus the period length for the T/P mission, derived from uncertainties presented in section 3.3.3. The uncertainties are lower than 1 mm/yr (with PSMSL network) within a confidence interval of 1-sigma (68%) for periods higher than 4 years. It converges to 0.4 mm/yr when the period reaches 10 years. However, for periods lower than 4 years, the uncertainty increases quickly: 1.5 mm/yr at 3 years, 3 mm/yr at 2 years and 7 mm/yr at 1 year.

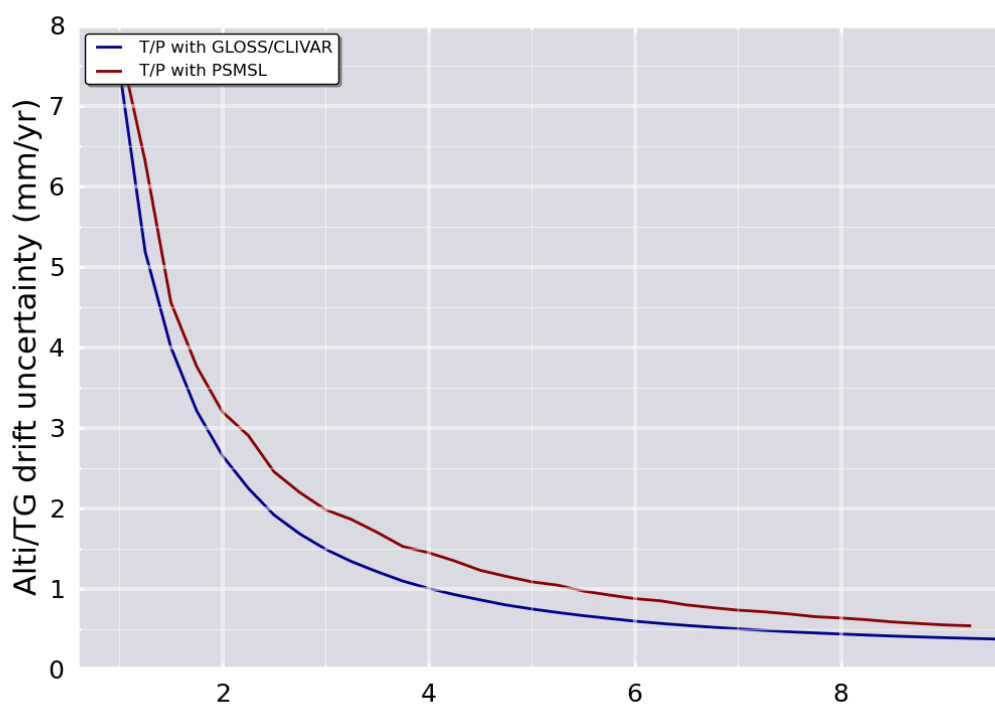


Figure 36: Evolution of uncertainty (1-sigma) versus the period length for altimetry and tide-gauges comparisons over the TOPEX-A altimeter period (GLOSS/CLIVAR and PSMSL)



Comparing the uncertainties evolution with the variations of TOPEX-A and tide-Gauges MSL differences leads to the conclusion that the signal observed for period lengths lower than about 4 years are not statically significant.

Therefore, our recommendation is to choose a cut-off period of **4 years** to have a good confidence on the TOPEX-A drift reduction.

5.2.1.1. Strategy to select data before filtering

To calculate the TOPEX-A correction, 2 strategies are possible:

- to consider only the TOPEX-A/tide gauge MSL differences before applying the low pass filter
- or apply the low pass filter over all the altimeter/tide gauge time series and then select the TOPEX-A period.

Of course, both approaches are not equivalent and will not provide the same results. In theory, we prefer the first one because TOPEX-A errors are decorrelated of TOPEX-B ones. In addition, a bias exists between both TOPEX-A and TOPEX-B times series. It was corrected, but with an uncertainty of about few millimeters that could negatively impact the estimation of the TOPEX-A correction. In practice, the disadvantage of the first approach is the extrapolation of filtering-data for the last measurements in the TOPEX-A window which could not be perfectly managed.

As this choice is not trivial, in the result section we present the results with both approaches. We will see further that the impact is relatively low.

5.2.1.2. TOPEX-A/TOPEX-B GMSL bias calculation

The TOPEX-A correction that we propose is not constrained to conserve the TOPEX-A and TOPEX-B GMSL bias. Therefore, this bias should be re-estimated after applying the TOPEX-A correction on GMSL. The bias is applied for data after TOPEX-A (February 1999) to keep the GMSL at 0 (on average) on year 1993.

In few words, the method consists in filtering TOPEX-A and TOPEX-B GMSL data with a low-pass filter (2-months-period to remove 59-day errors and noise), and the bias is deduced by calculating the first value and the last one of respectively the TOPEX-B filtered GMSL time series and the TOPEX-A one. The uncertainty of this method was estimated to 2-3 mm (Ablain et al, 2009 and 2015) but it is likely under-estimated. It should be revisited (on further study).

The GMSL bias could also be deduced from altimeter and tide-gauges comparisons applying the same approach. We have never try to test this approach until now, though it seems interesting because ocean signals are removed. This would allow (in theory) to better estimate the bias. In this study we tried to do it, and we will see in the discussion section that the result obtained are balanced.



5.2.2. TOPEX-A Correction

As mentioned previously, we proposed 2 TOPEX-A corrections:

- Altimeter/tide gauge MSL differences are selected on TOPEX-A period, then filtered out with a cut-off period of 4 years.
- Altimeter/tide gauge MSL differences are filtered out with a cut-off period of 4 years, then selected on TOPEX-A period.

On the two following figures, the TOPEX-A correction (in green) derived from altimeter and tide-gauges comparisons has been plotted for the 2 approaches. Blue curve is the initial altimeter and tide gauges comparisons and red curve, the same time series obtained after applying the TOPEX-A correction.

The TOPEX-correction (green curve) presents a V-shape signal on TOPEX-A as described by (Beckley et al, 2017). The differences between both approaches is only for the end of TOPEX-A period where in the first case the correction continues to increase whereas in the second case it decreases. A maximum of 1.6-mm differences is observed. The average drift of TOPEX-A correction is estimated to about 1.3-1.5 mm/yr.

After TOPEX-A period, the correction is not null since we applied the GMSL bias between TOPEX-A and TOPEX-B. The bias obtained is 6.1 mm with first approach and 4.5 mm with the second one. It is worth noting a residual small jump (1 mm) on the TOPEX-A correction at the TOPEX-A/TOPEX-B change. This is due to the uncertainty of the TOPEX-A/TOPEX-B GMSL bias estimation which has been estimated independently. We could correct it easily, but from our opinion it is better to conserve our independent approach to estimate the bias.

Analyzing now the blue curve, we observed that the abnormal signal variations have been reduced (by construction). However, the variance of the signal is still higher on TOPEX-A period than after (TOPEX-B/Jason). This could suggest that the cut-off period applied is too large. In annex of this document, you will find the TOPEX-A correction with a 3-year, 2-year and 1-year cut-off period and the impact on the GMSL time series. As already mentioned, to date, we rather propose this safe approach to be sure to remove only the TOPEX-A errors.

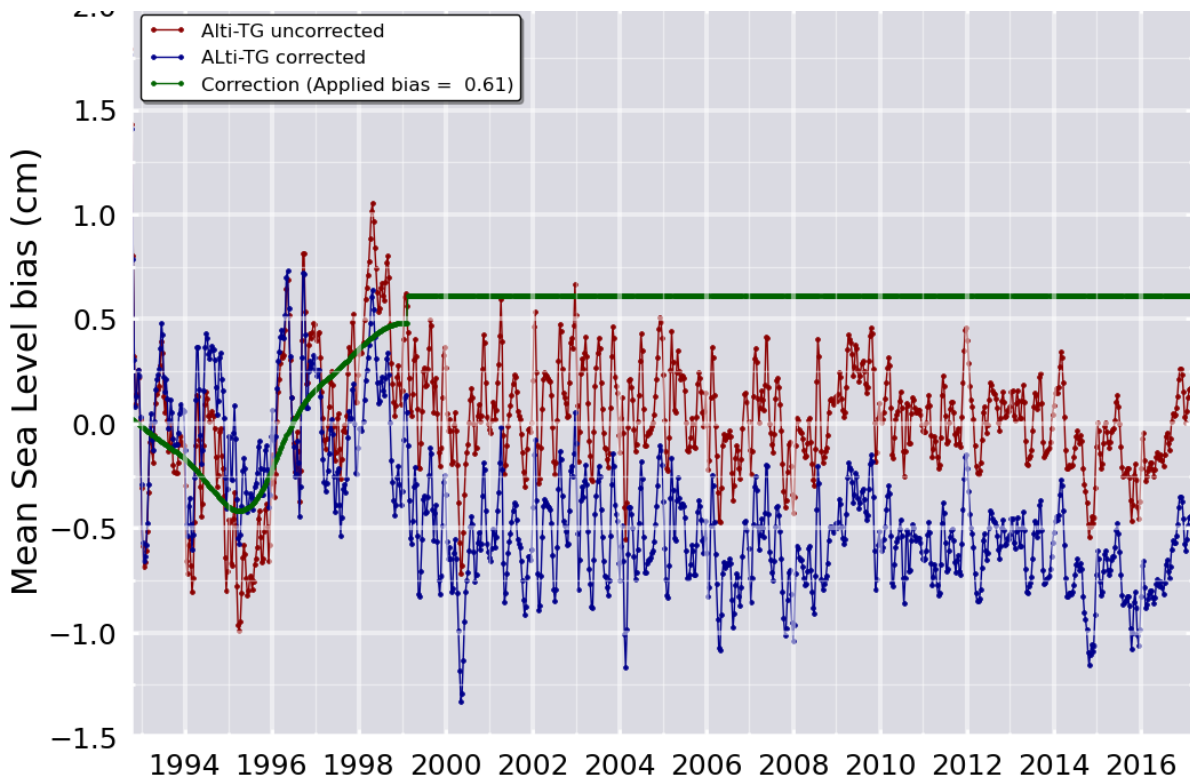


Figure 37: TOPEX-A correction derived from altimeter and tide-gauges comparisons for approach 1

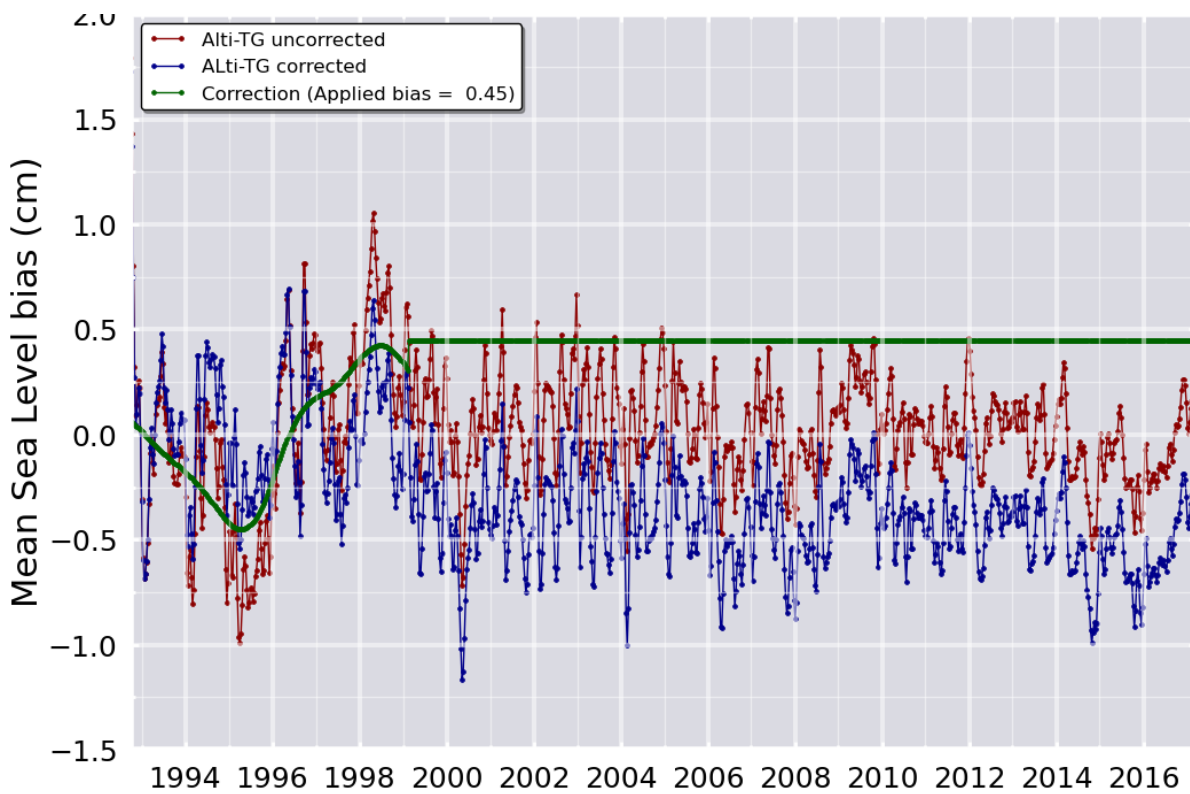


Figure 38: TOPEX-A correction derived from altimeter and tide-gauges comparisons for approach 2



5.2.3. Impact on the Aviso GMSL time series

Applying the TOPEX-A correction on the Aviso GMSL time series allows us to obtain the two following figures respectively for approach 1 and 2. The blue curve and the red one are respectively the AVISO GMSL uncorrected and corrected with our empirical TOPEX-A correction.

First of all, applying one or the other TOPEX-A correction proposed has a (very) low impact on the time series for the total GMSL increase (1.5 mm) as well as for the inter-annual signal.

Now, looking at the total GMSL rise, the impact is a reduction of about 5-7 mm over all the period. In term of trends, this is equivalent to a decrease of 0.2-0.25 mm/yr over the 25-year period. As this decrease is explained at the beginning of the time series, this highlights an acceleration of the GMSL of about 0.06 mm/yr² instead of 0.02 mm/yr² before applying the TOPEX-A correction. Focusing now on the TOPEX-A period, the GMSL evolution is significantly flatter (about -1.5 mm/y on average).

5.2.4. Inconsistency of the TOPEX-A/TOPEX-B bias calculation

As already mentioned, the TOPEX-A/TOPEX-B GMSL bias has been determined from the corrected GMSL time series. We would have been able to determine directly it from the altimeter and tide-gauge comparisons, and theoretically we should have obtained similar value taking into account the uncertainty level.

We have performed the exercise, and we obtained a different value for the TOPEX-A/TOPEX-B GMSL bias if we calculate it from GMSL or from altimeter and tide-gauge comparisons. The difference is about 5 mm (+/- 1 mm depending on the cut-off period used). To date, we are not able to explain its origin. We can just say:

- the difference of 5 mm is very likely statically significant
- this inconsistency explains the bias observed in all the figures of this document where altimetry and tide-gauges time series have been corrected with the TOPEX-A correction (look at blue curve).
- a strong regional bias between TOPEX-A and TOPEX-B MSL could generate such a discrepancy due to the poor tide-gauge coverage,

Investigations are on-going to better check and understand the reason of the inconsistency of the TOPEX-A/TOPEX-B bias calculation. It of great importance to have a better confidence in the TOPEX-A correction suggested in this document. Indeed, a 5-mm uncertainty on the TOPEX-A/TOPEX-B bias results in an additional 0.7 mm/yr uncertainty on the TOPEX-A/TOPEX-B GMSL trend. *nb: the relation is linear.*

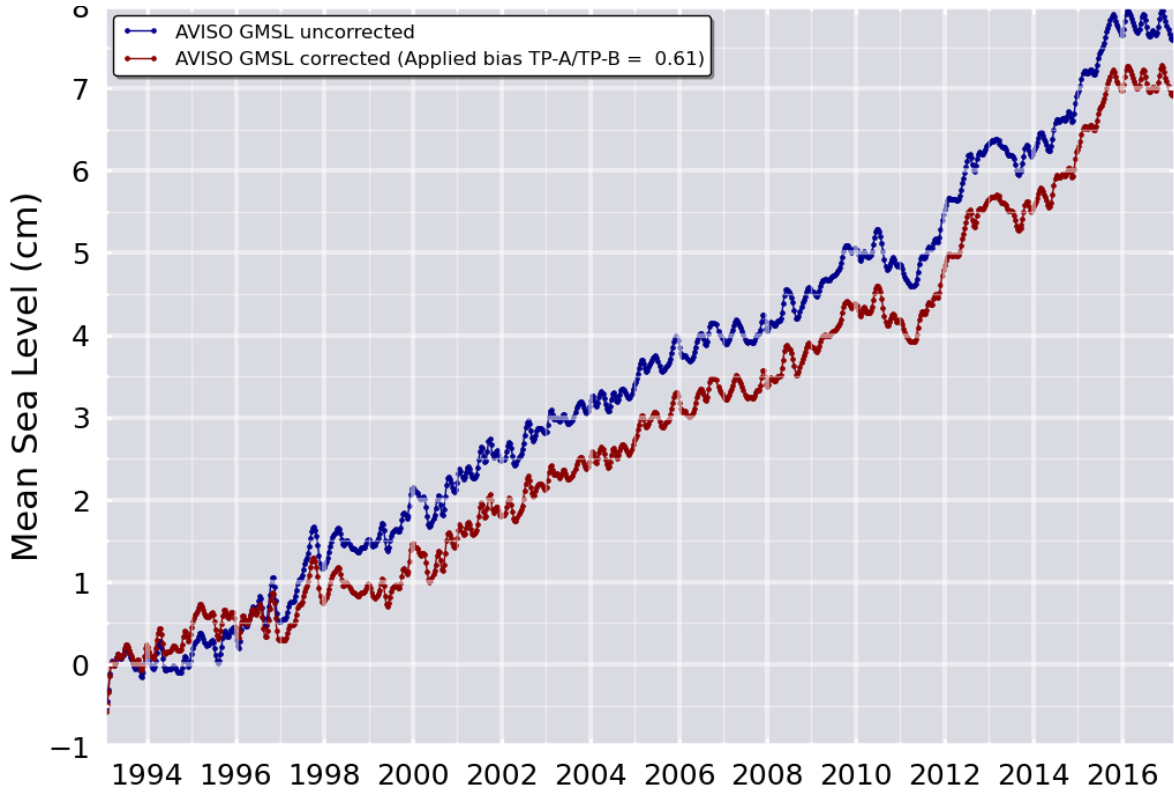


Figure 39: AVISO GMSL of reference uncorrected (blue curve) and corrected (red curve) with the empirical TOPEX-A correction for approach 1.

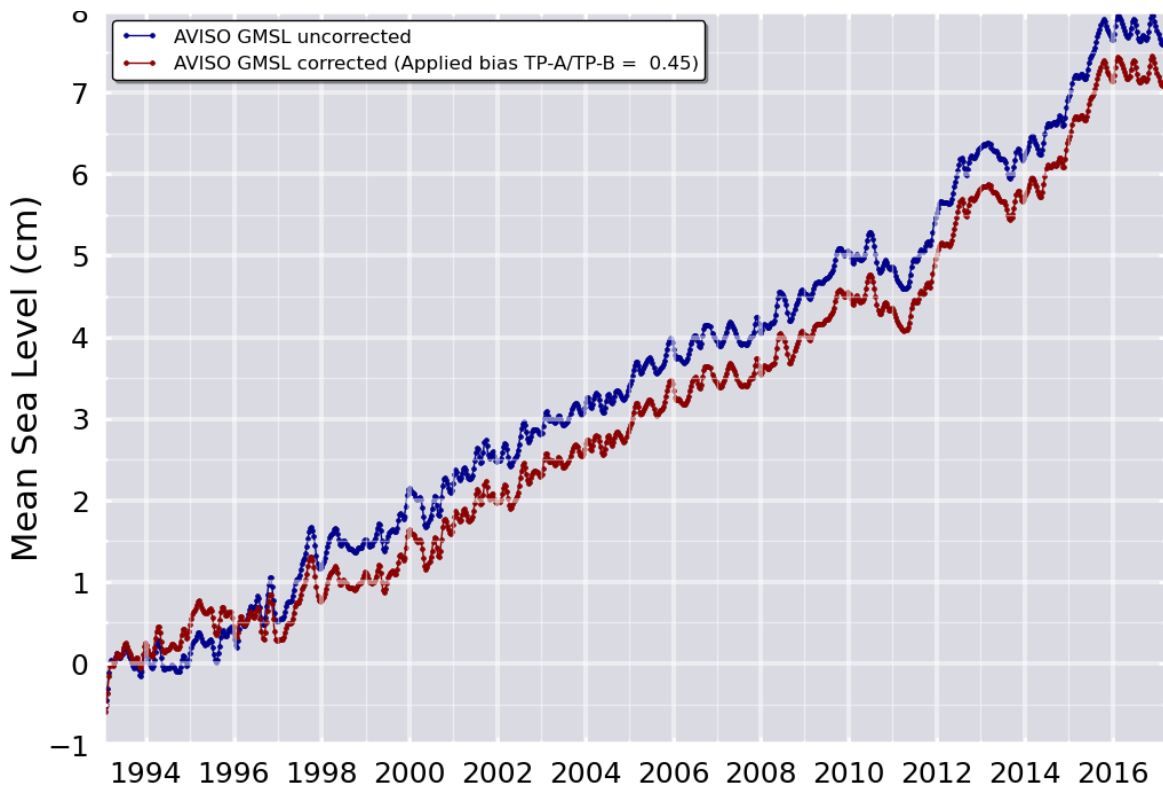




Figure 40: AVISO GMSL of reference uncorrected (blue curve) and corrected (red curve) with the empirical TOPEX-A correction for approach 2.

5.3. Determination of GMSL trend uncertainty over a 1-year period for Jason-CS requirement

5.3.1. Overview

Warning: the method proposed in this study and the ensuing results have been obtained before carrying out the analyses of GMSL drift uncertainties from tide gauges presented in section 38. Although this study should be updated with these new approach and analyses, the main conclusions presented hereafter remains true.

5.3.1.1. Context and objectives of the study

The expected stability on the GMSL slope is 0.3 mm/yr over a period of 10 years (GCOS, 2011). Currently, uncertainty is measured at 0.5 mm/yr over the total period (within a 95% confidence interval) (Ablain et al., 2015). Considering only the Jason-1/Jason-2 missions, this uncertainty drops close to 0.4 mm / year.

For the Jason-CS mission, the requirement on the GMSL slope was not expressed over a long period but over a 1-year period with an error lower than 1 mm. This requirement is inherited from 2010 OSTST meeting report but seems difficult to check over such a short period of time due to the natural variability of the ocean, due to land motion but also to observation errors (both on the altimeter system side and also on tide gauge network).

The objective of this study is therefore to demonstrate what minimal error is detectable over a 1-year period from the existing GMSL time series, taking into account oceanic variability but also altimetry errors (temporally uncorrelated and correlated). And therefore, check whether the requirement for the Jason-CS mission can be verified or not.

In this study, we will attempt to express this minimal error level in optimistic confidence intervals (68% \Leftrightarrow equivalent to 1 sigma) and more severe (2 or 3 sigma \Leftrightarrow 95 or 99%).

5.3.1.2. OSTST report

Figure below is an extract of the OSTST report (page 20). The full report is available on the AVISO server:

- http://www.aviso.altimetry.fr/fileadmin/documents/OSTST/2010/oral/final%20report/10_lisbon_OSTST_meeting_report.pdf



Requirement: Jason-3 shall measure globally averaged sea level relative to levels established during the cal/val phase with zero bias +/- 1 mm (standard error) averaged over any one year period.

Verification: Accuracy will be verified by comparison with no less than 50 tide gauges that provide the widest possible geographic coverage.

Latency: As a goal, the project will attempt to design Jason-3 to meet this level of accuracy with a latency of 2 months, in time for production of the GDR.

Explanation: Given the small autocorrelation and the 4.9 mm RMS variability in altimeter – tide gauge time series the above requirement is intended to achieve a drift accuracy over different durations as follows:

$$\text{error on mean} = 4.9 \text{ mm} / \sqrt{(23 - 1)}$$

$$\text{slope error} = \text{mean square error} / \sqrt{(\sum (t_i - t_{\text{mean}})^2)}$$

duration	error
1 year	3.5 mm/yr
2 years	1.3 mm/yr
3 years	0.68 mm/yr

It was recommended by the OSTST that this language be adopted as a goal for Jason-3 and as a strict requirement for Jason-CS.

Consequently, on Jason-CS missions we have currently the below requirements:

[SRD] R-S-01960 A, R

Sentinel-6 shall maintain the stability of the global mean sea level measurements (as recorded in the ALT-NTC Level 2 products) to levels established during the calibration/validation phase to within 1 mm (standard error) averaged over any one year period.

Note: Global mean sea level measurements are those obtained by averaging the 1-Hz sea level measurements over any repeat cycle. As such this requirement constrains the drift of a global mean sea level measurement to be less than 1 mm per year.

[SRD] R-S-02020 T, A, R

Jason-CS shall measure regionally averaged sea level (as recorded in the ALT-NTC Level 2 products) with a drift error as defined in [RD.2] of less than 5 mm/year.

Note: With "regionally averaged sea level" we mean: the average of all sea level measurements within one repeat cycle within an ocean area of approximately 40000 km².

5.3.2. Several approaches

The first approach is to use the GMSL time series provided by the Jason-1 and Jason-2 altimeter observations. This allows access to the estimation of the GMSL slope over a given period by calculating the corresponding uncertainty in a confidence interval. The level of uncertainty is the amount of interest for the study: it informs about the probability that the GMSL drift error is less (or greater) than the value obtained for a given period. To estimate this, it is necessary to consider the errors of the temporal series linked to the oceanic variability as well as the errors of the altimetry. This implies to have a good a priori statistical knowledge of these errors, and of correlated terms which are non-negligible (e.g. interannual variability of 1-2 mm over periods of 3-5 years). This will



also allow estimation of uncertainty within a precise confidence interval. The level of uncertainty obtained will therefore be highly dependent on this information.

The second approach, likely more adapted, is to use the temporal series of global average sea-level differences from altimetry and tide gauge comparisons. The altimeter GMSL drift and its uncertainty can be directly estimated over a given period. To estimate this uncertainty, it is also necessary to consider the errors of the time series, but these are easier to estimate because the effect of oceanic variability is almost totally removed since tide gauges and altimeters observe a similar signal. The level of uncertainty obtained will therefore in theory be less dependent on the information given a priori on the errors. However, we must consider the additional errors related to the tide gauges measurements (not negligible).

In addition to the main objective, the study will also make it possible to specify which of the two approaches is the most suitable for the analysis of the slope uncertainty over 1 year.

5.3.3. Mathematical formalism

Several mathematical formalisms could be applied:

- The least squares method: the slope and the uncertainty derived for this method are calculated by considering the errors on the observations independent of one another. In case of correlated errors, the results systematically lead to too small uncertainty estimation.
- Inverse method (generalized least square method): slope and the uncertainty are calculated by considering the correlated errors. This approach leads to realistic estimate of uncertainty assuming statistical a priori errors are well known.
- “Ensembliste” approach: the GMSL time series is calculated by varying the altimetry standards in input of the GMSL calculation. This allows to generate a set of GMSL time series. Hence, a confidence envelope is easily calculated calculating the standard deviation at each time measurement. This method has advantage to provide the individual uncertainties of the GMSL series, taking account of commission errors only. Failure to take into account errors of omissions leads to a overestimated uncertainty calculation. It should also be noted that the “ensembliste” approach is costly in computation time because of many possible altimetric standard combinations.



5.3.4. Altimetry GMSL drift uncertainties from tide gauge comparisons

5.3.4.1. Overview

In this section, the trend uncertainties calculation is derived from the temporal series of global mean sea-level differences between altimetry and tide gauge measurements. These comparisons are performed in the framework of SALP project supported by CNES (Valladeau et al, 2012; Prandi et al, 2016) and are regularly presented during OSTST meetings.

The GMSL differences between altimetry and tide gauges are plotted below for the Jason-1 and Jason-2 missions using the network. In red, it is the raw statistics obtained, in blue those calculated after applying a low-pass filtering over 2 months (the low-pass filter is described below) and in green after removing in addition the residual periodic (annual) signals. The calculation of the trend for Jason-2 over a period of 9 years gives a drift between the altimetry and the tide gauge of 0.1 mm/yr (with the filtered curve) but it must be remembered that the uncertainty of the method was estimated (Valladeau et al., 2012) to 0.7 mm/yr. Therefore, this drift is not statistically significant. For Jason-1, the drift observed is higher (0.3 mm/yr) but remains below the uncertainty. Dispersion of individual measurements (red curve) is also higher for Jason-1 than for Jason-2 because of larger altimetry errors on Jason-1 and better tide gauges network on Jason-2 period. Given these results, we only consider in the study the Jason-2/tide gauges time series which provides currently the best results.

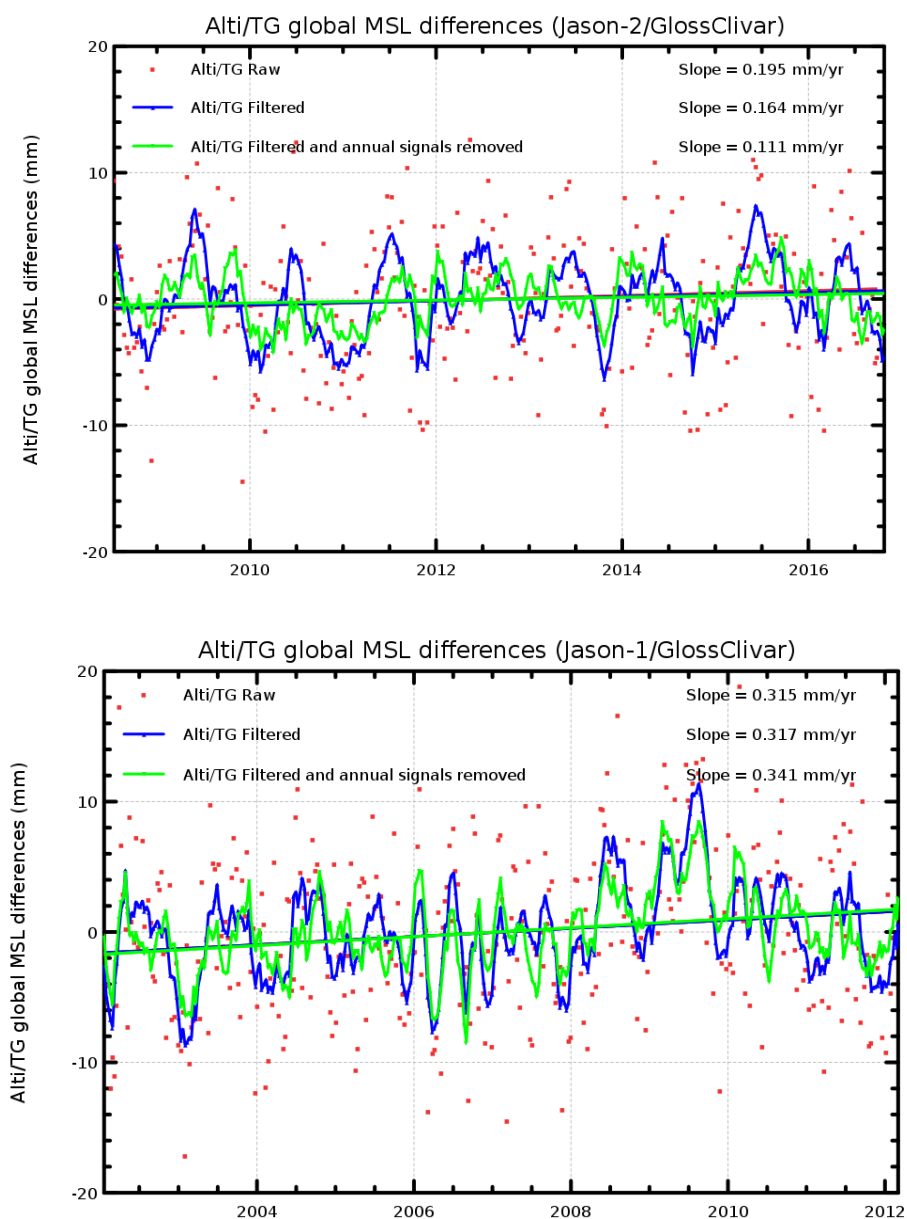


Figure 41: GMSL differences between altimetry and tide gauges for Jason-1 (on bottom) and Jason-2 (on top) using the network. Red dots are from raw data, blue curve after applying a low-pass filter (cut-off of 2 months), and green curve after removing in addition the residual periodic signals (annual).

5.3.4.2. Method

The method developed to estimate the trend uncertainties is based on the estimation of a set of local trends over a sliding window of size (P), for each Jason-2 cycle and over all the time series. Trends are basically estimated by a least square method. For this study, the window size of interest is 1 year. Then, the standard deviation of this set of local trends is calculated. Assuming the trends distribution is Gaussian (easy to check), the uncertainty level can be easily deduced in a confidence interval using the Student coefficient table.



The figure below shows the evolution of these local trends obtained considering a 1-year sliding window. They have been calculated from the raw Jason-2/tide gauges GMSL differences (red dots) and from the filtered-out ones (blue curve, low pass filter and periodic signals removed). We will discuss further the interest to filter data to estimate the trend uncertainty. The slopes obtained differ markedly between the raw curve and the filtered curve since the standard deviation is respectively 5.6 mm/yr and 2.4 mm/yr. We will interpret later the result.

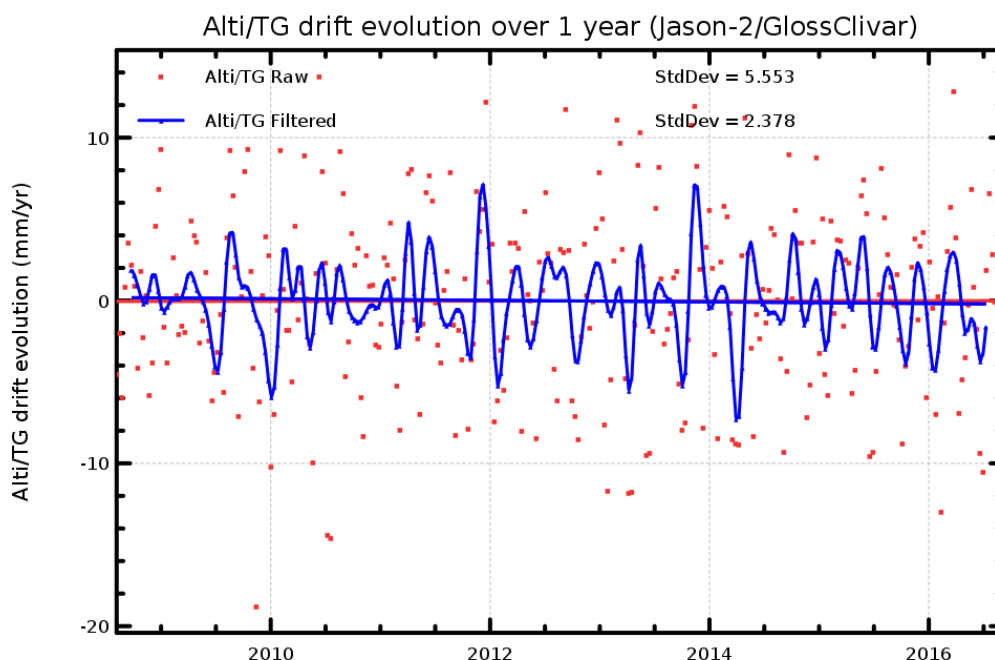


Figure 42: Evolution of 1-year trends calculated from Jason-2 and tide-gauges comparisons over all the Jason-2 period from raw time series (red dots) and the 2-months filtered time series (blue curve)

5.3.5. Results

The trend uncertainty that we would like to estimate depends on 2 main parameters: 1) the length of the period to calculate the trend; 2) the low-pass filtering applied to the raw time series.

5.3.5.1. Impact of the window size

In figure below, the standard deviation of trends has been estimated for several sliding windows sizes from 6 months to 8 years. For each estimation an error bar has been associated defined by the quadratic mean of standard formal error (from least square method). These statistics have been obtained using the raw data and the 2-months filtered time series (after removing residuals annual signals in both cases). The statistics evolves from 5.8 mm/yr for a 1-month window size to converge to about 0.3-0.4 mm/yr for period larger than 6-years considering raw data (blue dots). These



statistics are reduced respectively from 2.3 mm/yr to about 0.3-0.4 mm/yr considering the filtered data (green dots). Assuming the distribution of trends is gaussian for each window size, and making the approximation that the length of the input time series is infinite (this issue will be discussed further), these statistics are directly a measure of the trend uncertainty in a confidence interval of 68% (\Leftrightarrow equivalent to 1 sigma).

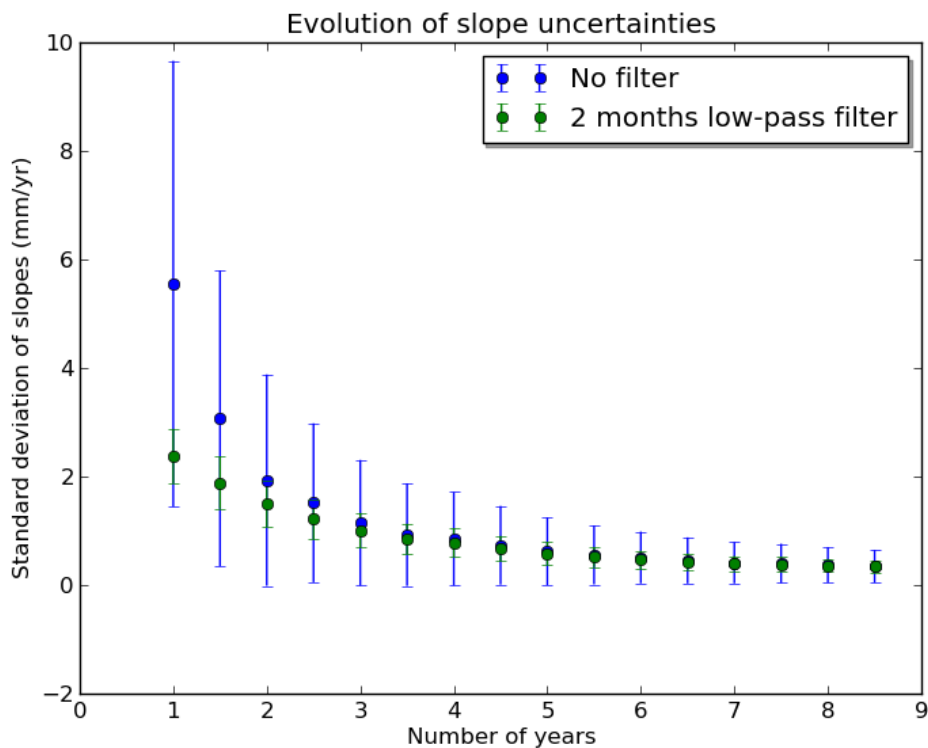


Figure 43: Evolution of the standard deviation of trends estimated for several periods from 6 months to 8 years from Jason-2 and tide-gauges comparisons (raw data in blue and 2 months filtered data in green).

5.3.5.2. Impact of the cut-off period of low-pass filter

In theory, the raw time series from altimetry and tide gauges comparisons, should be used to estimate the trend uncertainty over any periods. However, the objective of the study is to know the ability of using this time series to detect drift in altimetry GMSL. Hence, depending on the nature of the error sought, it would be appropriate to filter out the time series beforehand in order to increase the ability to detect a drift. For instance, if the altimetry error sought is assumed to be linear drift, it should be adapted to filter the data over the considered period. Conversely, if the error is a jump, the raw data must be used otherwise the jump will be attenuated by the low-pass filtering.

Hereafter, the effect of the low-pass filtering on the trend uncertainty has been calculated considering a 1-year period (of interest for the study), and for several cutoff periods. A Lanczos pass



filter is applied with a median filter (over 2 measures) beforehand. The standard deviation obtained is ranging from 5.7 mm/yr without any filtering to converge to 0.4 mm/yr for a 1-year cutoff period.

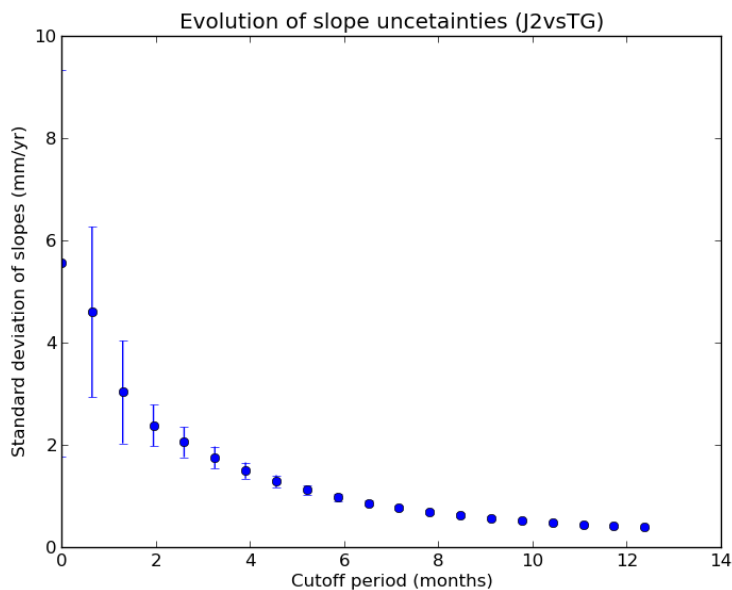


Figure 44: Evolution of the standard deviation of trends estimated over a 1-year window size for several cutoff periods of the low-pass filter from Jason-2 and tide-gauges comparisons

5.3.5.3. Analyses

The plot below shows the evolution of the trend uncertainties as a function of the length of the period (eq. sliding window size) and the cut-off period of the the low-pass filter. This gives a synthetic overview of the evolution of the trends standard deviation as a function of these 2 parameters. As the Jason-CS requirements has been given for 1 mm/yr, the plot colors have been voluntary centered around this value with distinct colors (blue and red).

The 1 mm/yr level line indicates that:

- For no filtered-out data, a minimal period of 3.5 period is necessary to be able to detect an altimetry drift of 1 mm/yr within a confidence interval of 68%
- After applying a 6-month low-pass filter, this minimal period to detect an altimetry drift is reduced to 1 year.

In case a), the altimetry drift is detectable for any source of altimetry error as a jump for instance, whereas in case b), only correlated altimetry errors over a period of 1 year (twice the cut-off period) are detectable. As past experience has shown that errors detected on altimetry were most often jumps or drifts observed over very short periods of time, the case b) is not the most appropriate approach.

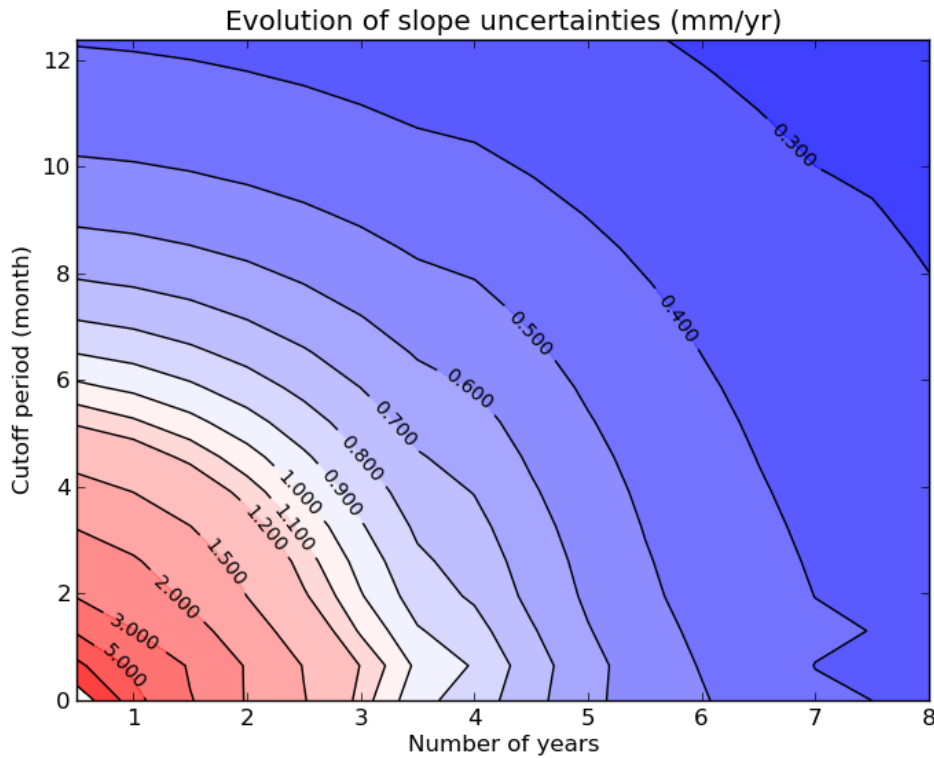


Figure 45: Evolution of the trend uncertainties by varying at the same time the length of the period (sliding window size) and the cut-off period of the low pass-filter

5.3.6. Conclusion, recommendation & discussions

5.3.6.1. Conclusion

The table below displays the trends uncertainties over a 1-year period for raw, 6-month and 1-year filtered out time series, and for different confidence intervals (68% and 90%). This demonstrates that the Jason-CS requirement (1 mm/yr over 1 year) can be verified only if altimetry errors sought are correlated on time (e.g linear drift for instance). If error is a jump or drift over a short period (few months), a 1-year period is in this this case not long enough to detect a 1 mm/yr drift.

Period (window size)	Cutoff (low pass filter)	68 % confidence interval	90% confidence interval
1 year	Raw	5.55 mm/yr	9.3 mm/yr
	6 months	0.95 mm/yr	1.6 mm/yr
	1 year	0.42 mm/yr	0.71 mm/yr



Table 11: Trends uncertainties over a 1-year period for raw, 6-month and 1-year filtered out time series of GMSL differences between altimetry and tide gauges, and for different confidence intervals (68% and 90%).

Conversely, the table below shows which minimal period is needed to detect a 1 mm/yr drift on altimetry measurements by this approach.

Altimetry drift	Cutoff (low pass filter)	68 % confidence interval	90% confidence interval
1 mm/yr	Raw	3,5 years	5.9 years
	6 months	1 year	1.7 years
	1 year	< 6 months	< 10 months

Table 12: Minimal period needed to detect 1 mm/yr altimetry drift for raw, 6-month and 1-year filtered out time series of GMSL differences between altimetry and tide gauges, and for different confidence intervals (68% and 90%).

5.3.6.2. Recommendation for the Jason-CS stability requirement

The Jason-CS requirement is achievable but only under strict conditions which should be mentioned, relative to the nature of altimetry errors sought. Otherwise, the requirement should be less strict to be applicable in any cases. The minimum period requested to detect a 1 mm/yr altimetry drift is 3.5 years in a confidence interval of 68% and almost 6 years in a confidence interval of 90 %.

5.3.6.3. Discussions

Several issues could be discussed to clarify the study:

- Jason-2/tide gauge time series used in the study can be impacted by Jason-2 altimetry errors. How to estimate the impact of these potential error on the study?
- In the study, we assume time series is infinite to define the confidence interval of uncertainty estimation. In practise it is not the case. Why this approximation has been done in the study?
- What is the impact of reducing the number of samples for the estimation of uncertainty and its confidence interval?



- d) The altimetry/tide gauge time series used in this study is provided by CLS in the framework of SALP project (supported by CNES). Using other time series provided by other groups (Mitchum et al., Watson et al., etc...), would the results be similar?
- e) It could be interesting to discuss the impact of a jump (in altimetry measurements) on the trend observed on the MSL (ref Zawadzki et al., 2016)



6. References

- AVISO : Sea Surface Height from radar altimetry, AVISO SSALTO/DUACS, <http://www.aviso.altimetry.fr/en/data/products/ocean-indicators-products/mean-sea-level/processing-corrections.html>
- Ablain, M., J. F. Legeais, P. Prandi, M. Marcos, L. Fenoglio-Marc, H. B. Dieng, J. Benveniste, and A. Cazenave. 2017. "Satellite Altimetry-Based Sea Level at Global and Regional Scales." In *Space Sciences Series of ISSI*, 9–33.
- Ablain, M., A. Cazenave, G. Larnicol, M. Balmaseda, P. Cipollini, Y. Faugère, M. J. Fernandes, et al. 2015. "Improved Sea Level Record over the Satellite Altimetry Era (1993–2010) from the Climate Change Initiative Project." *Ocean Science* 11 (1). Copernicus GmbH:67–82.
- Ablain, M., A. Cazenave, G. Valladeau, and S. Guinehut. 2009a. "A New Assessment of the Error Budget of Global Mean Sea Level Rate Estimated by Satellite Altimetry over 1993–2008." *Ocean Science* 5 (2):193–201
- Ablain, M., S. Philipps, M. Urvoy, N. Tran, and N. Picot. "Detection of long-term instabilities on altimeter backscatter coefficient thanks to wind speed data comparisons from altimeters and models." *Marine Geodesy* 35, no. sup1 (2012): 258-275.
- Atlas, Robert, Ross N. Hoffman, Joseph Ardizzone, S. Mark Leidner, Juan Carlos Jusem, Deborah K. Smith, and Daniel Gombos. "A cross-calibrated, multiplatform ocean surface wind velocity product for meteorological and oceanographic applications." *Bulletin of the American Meteorological Society* 92, no. 2 (2011): 157-174.
- Blazquez A., Meyssignac B., Lemoine J.M., Berthier E., Ribes A. and Cazenave A., Exploring the uncertainty in GRACE estimates of the mass redistributions at the Earth surface. Implications for the global water and sea level budgets. Submitted
- Cazenave A., Champollion N., Benveniste J., Chen J., *Remote Sensing and Water Resources*, 2016, p 366.
- Chambers, Don P., Mark E. Tamisiea, R. Steven Nerem, and John C. Ries. 2007. "Effects of Ice Melting on GRACE Observations of Ocean Mass Trends: ICE MELTING ON GRACE OCEAN MASS TRENDS." *Geophysical Research Letters* 34 (5):1958. <https://doi.org/10.1029/2006GL029171>.
- Chambers, Don P., John Wahr, Mark E. Tamisiea, and R. Steven Nerem. 2010. "Ocean Mass from GRACE and Glacial Isostatic Adjustment." *Journal of Geophysical Research* 115 (B11):171. <https://doi.org/10.1029/2010JB007530>.
- Chen, J. L., C. R. Wilson, D. P. Chambers, R. S. Nerem, and B. D. Tapley. 1998. "Seasonal Global Water Mass Budget and Mean Sea Level Variations." *Geophysical Research Letters* 25 (19):3555–58. <https://doi.org/10.1029/98gl02754>.
- CORIOLIS : Temperature and Salinity profiles from Argo floats, The CORIOLIS data service consortium, <http://www.coriolis.eu.org>
- Couhert, Alexandre, Luca Cerri, Jean-François Legeais, Michael Ablain, Nikita P. Zelensky, Bruce J. Haines, Frank G. Lemoine, William I. Bertiger, Shailen D. Desai, and Michiel Otten. 2015. "Towards the 1mm/y Stability of the Radial Orbit Error at Regional Scales." *Advances in Space Research: The Official Journal of the Committee on Space Research* 55 (1):2–23.



- Dee, Dick P., S. M. Uppala, A. J. Simmons, Paul Berrisford, P. Poli, S. Kobayashi, U. Andrae et al. "The ERA-Interim reanalysis: Configuration and performance of the data assimilation system." *Quarterly Journal of the royal meteorological society* 137, no. 656 (2011): 553-597.
- Dee (2011b). "Use of satellite data in atmospheric reanalysis":
<https://www.ecmwf.int/sites/default/files/elibrary/2014/14665-use-satellite-data-reanalysis.pdf>
- Dibarboure, G., M-I Pujol, F. Briol, P. Y. Le Traon, G. Larnicol, N. Picot, F. Mertz, and M. Ablain. 2011. "Jason-2 in DUACS: Updated System Description, First Tandem Results and Impact on Processing and Products." *Marine Geodesy* 34 (3-4):214–41.
- Dieng, H. B., A. Cazenave, B. Meyssignac, and M. Ablain. 2017. "New Estimate of the Current Rate of Sea Level Rise from a Sea Level Budget Approach." *Geophysical Research Letters* 44 (8):3744–51.
- Dieng, H. B., A. Cazenave, K. von Schuckmann, M. Ablain, and B. Meyssignac. 2015. "Sea Level Budget over 2005–2013: Missing Contributions and Data Errors." *Ocean Science* 11 (5):789–802.
- Ducet, N., P. Y. Le Traon, and G. Reverdin. 2000. "Global High-Resolution Mapping of Ocean Circulation from TOPEX/Poseidon and ERS-1 and -2." *Journal of Geophysical Research, C: Oceans* 105 (C8):19477–98.
- Witter, Donna L., and Dudley B. Chelton. "A Geosat altimeter wind speed algorithm and a method for altimeter wind speed algorithm development." *Journal of Geophysical Research: Oceans* 96, no. C5 (1991): 8853-8860.
- Geruo A., J. Wahr, and S. Zhong (2013) "Computations of the viscoelastic response of a 3-D compressible Earth to surface loading: an application to Glacial Isostatic Adjustment in Antarctica and Canada", *Geophys. J. Int.*, 192, 557–572, doi: 10.1093/gji/ggs030.
- GRGS solutions for GRACE datasets: <http://grgs.obs-mip.fr/grace>
- Guinehut, Stephanie, Christine Coatanoan, Anne-Lise Dhomps, Pierre-Yves Le Traon, and Gilles Larnicol. 2009. "On the Use of Satellite Altimeter Data in Argo Quality Control." *Journal of Atmospheric and Oceanic Technology* 26 (2):395–402.
<https://doi.org/10.1175/2008jtecho648.1>.
- Hayne G., S. and Handcock D. W., 1998, Proceedings of the TOPEX/Poseidon/Jason-1 Science Working Team meeting
- Johnson, Gregory C., and Don P. Chambers. 2013. "Ocean Bottom Pressure Seasonal Cycles and Decadal Trends from GRACE Release-05: Ocean Circulation Implications." *Journal of Geophysical Research, C: Oceans* 118 (9):4228–40. <https://doi.org/10.1002/jgrc.20307>.
- Henry, Olivier, Michael Ablain, Benoit Meyssignac, Anny Cazenave, Dallas Masters, Steve Nerem, and Gilles Garric. 2014. "Effect of the Processing Methodology on Satellite Altimetry-Based Global Mean Sea Level Rise over the Jason-1 Operating Period." *Journal of Geodesy* 88 (4). Springer Berlin Heidelberg:351–61
- Legeais J.F., 2015 : CalVal altimetry / Argo annual report. Validation of altimeter databy comparison with in-situ T/S Argo profiles. Ref. CLS/DOS/NT/15-007. Contrat SALP-RP-MA-EA-22406-CLS.
- Legeais, J-F, M. Ablain, and S. Thao. 2014. "Evaluation of Wet Troposphere Path Delays from Atmospheric Reanalyses and Radiometers and Their Impact on the Altimeter Sea Level." *Ocean Science* 10 (6):893–905. <https://doi.org/10.5194/os-10-893-2014>.



- Peltier, W. R. 2004. "GLOBAL GLACIAL ISOSTASY AND THE SURFACE OF THE ICE-AGE EARTH: The ICE-5G (VM2) Model and GRACE." *Annual Review of Earth and Planetary Sciences* 32 (1):111–49. <https://doi.org/10.1146/annurev.earth.32.082503.144359>.
- Purkey, Sarah G., and Gregory C. Johnson. 2010. "Warming of Global Abyssal and Deep Southern Ocean Waters between the 1990s and 2000s: Contributions to Global Heat and Sea Level Rise Budgets." *Journal of Climate* 23 (23):6336–51. <https://doi.org/10.1175/2010jcli3682.1>.
- Roemmich, Dean, and John Gilson. 2009. "The 2004–2008 Mean and Annual Cycle of Temperature, Salinity, and Steric Height in the Global Ocean from the Argo Program." *Progress in Oceanography* 82 (2):81–100. <https://doi.org/10.1016/j.pocean.2009.03.004>.
- Swenson, Sean, Don Chambers, and John Wahr. 2008. "Estimating Geocenter Variations from a Combination of GRACE and Ocean Model Output." *Journal of Geophysical Research* 113 (B8):29077. <https://doi.org/10.1029/2007JB005338>.
- Valladeau, G., J. F. Legeais, M. Ablain, S. Guinehut, and N. Picot. 2012. "Comparing Altimetry with Tide Gauges and Argo Profiling Floats for Data Quality Assessment and Mean Sea Level Studies." *Marine Geodesy* 35 (sup1):42–60.
- Zawadzki, L., and M. Ablain. 2016. "Accuracy of the Mean Sea Level Continuous Record with Future Altimetric Missions: Jason-3 vs. Sentinel-3a." *Ocean Science* 12 (1):9–18
- Zawadzki L., Taburet N., 2016 : CalVal altimetry / Argo annual report. Validation of altimeter databy comparison with in-situ T/S Argo profiles. Ref. CLS/DOS/NT/15-068. Contrat SALP-RP-MA-EA-22966-CLS.



7. Annexes

7.1. Comparing tide gauges and satellite altimetry: errors and uncertainties (Prandi et al., 2016)

Comparing tide gauges and satellite altimetry: errors and uncertainties

P. Prandi, G. Valladeau, M. Ablain
Contact: pprandi@cls.fr

Background & Goals

Evolution of Global SSH differences between altimetry and tide gauges for TOPEX/Poseidon, Jason-1 and Jason-2 missions

- > Global mean sea level rise is an essential climate indicator,
- > Altimeters measure sea level rise since ~1993 and show an increased rate of rise compared to measurements from tide gauges over the previous century,
- > Tide gauges are used as an external, independent benchmark for validation

- > The GCOS Climate User Requirement on the Global MSL trend accuracy is **0.3 mm/yr over 10 years**.
- > Several groups have estimated uncertainty on altimeter/tide gauges comparisons: **0.4 mm/yr** (Leuliette et al., 2004; Watson et al., 2015); **0.7 mm/yr** (Valladeau et al. 2012)

We are currently not able to demonstrate that the Climate User Requirements are met, mainly due to remaining uncertainties on tide gauges data

- > There is a need to refine uncertainty estimations for such comparisons.
- > Here, we review error sources and try to quantify associated uncertainties.
- > This may lead to user-driven requirements for the implementation and evolution of in-situ networks dedicated to the validation of future satellite altimetry missions.

Error sources & related uncertainties

Vertical Land Motion

- > Tide gauges relative sea level measurements are directly affected by local vertical land motion,
- > Without precise monitoring (GPS, DORIS) we cannot correct for such movements,
- > Even when GPS velocities are available, we are not able to demonstrate an improvement (spread of trend differences unchanged): we should question the linearity assumption
- > uncertainty is evaluated to **0.3 mm/yr** (lower bound)

[left] Vertical velocities of GPS stations in ITRF2016 solution

[right] distribution of SSH trend differences using different VLM solutions

In-situ geographical distribution and ensemble mean

- > Tide gauge data availability is limited in space and time,
- > Basic QC results in large unobserved areas,
- > Increasing the number of stations helps reduce uncorrelated errors,
- > Homogeneous coverage will increase the robustness of global altimeter drift estimations
- > Different averaging schemes (correcting for station density or not) might introduce artefacts
- > uncertainty is evaluated to **0.15 mm/yr**

[left] map of the GLOSS tide gauges network used in a global analysis

[right] two global average time series using different ensemble averaging strategies

Network sensitivity

- > Test small random changes in the in-situ network used,
- > Represents random unavailability of stations,
- > Even small changes can lead to large impacts,
- > Uncertainty estimated to **0.4 mm/yr**.

Impact of small changes of the in-situ network (5 and 10% of stations removed) on the global average trend

Conclusions

- > Current errors in altimetry/tide gauges comparisons prevent from establishing that altimeter data meets the GCOS Climate User Requirements,
- > A quick review of errors leads to a **0.7 mm/yr** uncertainty
- > Work is still needed to improve tide gauges network and comparison methods for the validation of future altimetry missions

Error	Uncertainty
VLM	0.3/0.5 mm/yr
Regression CI	0.2 mm/yr
Averaging	0.15 mm/yr
Network	0.4 mm/yr
Total (RSS)	0.7 mm/yr

Journées REFMAR, 2-4 Février 2016, Paris



7.2. Analytical function of the noise uncertainty

Hereafter, we provide the analytical function of the noise uncertainty versus the period length in the altimetry/in-situ time series. It is applicable for tide-gauges networks as well as for the ARGO network.

Suppose the altimetry-tide gauge situ MSL record consists of L observations of (DSLAs, time) noted hereafter $\{y; x\}$. An ordinary least square regression of the data is used to estimate the drift in this study. In other words, we model the data with $(\alpha, \beta, \varepsilon)$ such that $y = \alpha + x\beta + \varepsilon$ where α is the intercept, β the drift, ε the residuals vector.

According to the Least Square approach (and Gauss-Markov theorem), the best linear unbiased estimator $\hat{\beta}$ of the drift β is the one minimizing the sum of squared residual, $Q = \sum_{i=0}^{L-1} \varepsilon_i^2$, and the result in this simple 1-dimensional case is:

$$\hat{\beta} = \frac{Cov(x, y)}{Var(x)} \quad \text{Eq. 3}$$

In this case, the sum of squared residuals Q is distributed proportionally to χ^2 with $L - 2$ degrees of freedom. This allows to construct a t-statistic and the standard error of the estimator $\hat{\beta}$:

$$s_{\hat{\beta}} = \sqrt{\frac{\sum_{i=0}^{L-1} \hat{\varepsilon}_i^2}{(L-2) \sum_{i=0}^{L-1} (x_i - \bar{x})^2}} = \sqrt{\frac{\sum_{i=0}^{L-1} \hat{\varepsilon}_i^2}{(L-2) \cdot L \cdot var(x)}} \quad \text{Eq. 4}$$

We aim here at estimating the mathematical law of $s_{\hat{\beta}}$, w.r.t the length of the records, L , and characteristics of the TG network used to estimate the global DSLA record.

First, as ε measures the non-linearity of y , the DSLA record, it is fair to assume that the term $\frac{\sum_{i=0}^{L-1} \hat{\varepsilon}_i^2}{L}$ is proportional to the variance of the total DSLA record y :

$$\frac{\sum_{i=0}^{L-1} \hat{\varepsilon}_i^2}{L} \sim var(y) \quad \text{Eq. 5}$$

Now, if we consider that y , the global DSLA record, has been computed from N_S individual DSLA records (one per TG station) and note σ_{TG} the quadratic mean noise level of the individual DSLA records and that these noises are independent, then $var(y) = \frac{\sigma_{TG}^2}{N_S}$. With Eq. 5 :

$$\frac{\sum_{i=0}^{L-1} \hat{\varepsilon}_i^2}{L} \sim \frac{\sigma_{TG}^2}{N_S} \quad \text{Eq. 6}$$

nb: σ_{TG} is independent of L



Second, it is easy to demonstrate that:

$$\text{var}(x) \sim L^2 \tag{Eq. 7}$$

If we gather Eq. 6 and Eq. 7 in Eq. 4, then $s_{\hat{\beta}} \sim \sqrt{\frac{\sigma_{TG}^2}{(L-2)N_S L^2}}$ and finally, acknowledging that $(L-2) \sim L$:

$$s_{\hat{\beta}} \sim \frac{\sigma_{TG}}{\sqrt{N_S}} * L^{-\frac{3}{2}} \tag{Eq. 8}$$

As can be expected, the standard error of the drift estimate increases with the inconsistencies between altimetry and in-situ sea level height for each individual station of the network (σ_{TG}). However, it is inversely proportional to the length of the period (exponent 3/2) and the number of stations (square root).

7.3. Phase uncertainty estimation

The phase uncertainty is due to the presence of residual periodic signal in the linearly fitted signal which induces an uncertainty on slope estimation. This contribution to the error budget was computed by performing linear regression and computing the slope uncertainty over sinusoids of different frequency and length. Since the phase term is unknown in the residual signal, the phase uncertainty term behaves as t^{-2} , the amplitude being that of the oscillations in the residual signal.

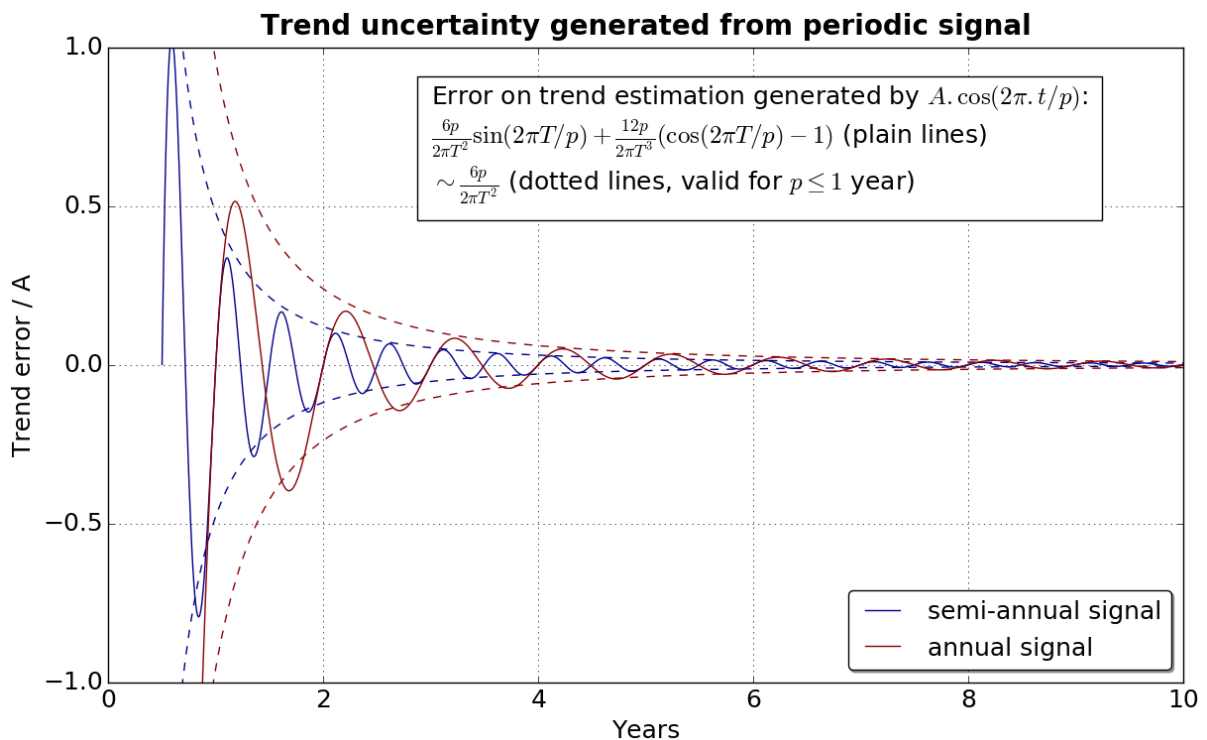




Figure 46 : Trend uncertainties associated to annual and semi-annual residual signals.

7.4. Closure budget trends and uncertainties

The phase uncertainty term was estimated for each mission using DHA referenced to 1900 dbar and the GRGS mass dataset. Such an approach is not possible for Jason-3 and Sentinel-3 missions since the duration of the obtained sla-dha-mass time series is limited to a few months using GRGS mass dataset that is only available until May 2016. For these two missions only the closure budget using CSR mass model (available until December 2016) is used. It is assumed that the phase uncertainty associated with trend estimation does not depend on the used mass solution even if annual and inter annual signals are not removed in the same way. Indeed, for processing purposes, cosines are fitted on the residual part of the closure budget using GRGS mass dataset whereas they are fitted on Altimetric data - steric and on the mass dataset using the Chambers' one. These different kinds of processing are explained by the fact that a monthly average map is available for GRGS mass model, allowing a direct alti-ts-mass colocation and computation, whereas the ones provided by Chambers et al. are averaged at a global scale. Thus, using this kind of mass models, annual and semi-annual removed signals amplitude are considered to be equals than the GRGS ones. For Jason-3 and Sentinel-3A the Jason-2 signals amplitude are used.

Mission	slope value (mm/yr)	time series length (year)	mass uncert (mm/yr)	trend uncert. (mm/yr)	phase uncert. (mm/yr)	total uncert. (mm/yr)
Jason-1	-1.11	8.33	0.16	0.46	0.04	0.86
Jason-2	-0.03	8.08	0.17	0.26	0.07	0.77
Jason-3	-1.29	0.75	2.66	6.53	8.06	10.73
Envisat	-0.07	7.17	0.17	0.47	0.10	0.87
AltiKa	1.27	3.33	0.85	1.27	0.14	1.69
Sentinel-3A	3.98	0.50	2.66	6.53	12.19	14.1
Multi-missions	-0.47	11.33	0.15	0.26	0.03	0.77

Table 13: Closure budget drift and associated uncertainty (90 % confidence level). Time-dependent uncertainties are shown as well as the total uncertainty which takes into account the non time-dependent uncertainties (related to GIA correction, 0-2000m thermosteric contribution, deep steric contribution, geocenter, land leakage). Analyses performed with CMEMS 2018, DHAs referenced to 1900 dbar and CSR mass model (Chambers et al.). GIA correction is applied to altimeter (+0.3 mm/yr).



Mission	slope value (mm/yr)	time series length (year)	mass uncert (mm/yr)	trend uncert. (mm/yr)	phase uncert. (mm/yr)	total uncert. (mm/yr)
Jason-1	-0.23	8.43	0.16	0.37	0.02	0.79
Jason-2	0.65	7.78	0.17	0.46	0.06	0.86
Envisat	0.78	7.23	0.17	0.53	0.08	0.90
AltiKa	2.97	3.12	0.89	1.83	0.31	2.18
Multi-missions	0.20	11.31	0.15	0.28	0.03	0.78

Table 14: : Closure budget drift and associated uncertainty (90 % confidence level). Time-dependant uncertainties are shown as well as the total uncertainty which takes into account the non time-dependant uncertainties (related to GIA correction, 0-2000m thermosteric contribution, deep steric contribution, geocenter, land leakage). Analyses performed with CMEMS 2018, DHAs referenced to 1900 dbar and GRGS mass model. Total GIA corrections (altimetry + mass) of 0.9 mm/yr and 0.8 mm/yr is respectively applied to Jason missions on the one hand and Envisat, AltiKa and multimissions data on the other hand (this reflects the different extent in latitude)



List of acronyms

ARGO

Argo is a global array of 3,800 free-drifting profiling floats that measures the temperature and salinity of the upper 2000 m of the ocean 7, 12, 15, 55, 64, 65, 69, 70, 107

AVISO

Altimetry website (<https://www.aviso.altimetry.fr>)

CCI

Climate Change Initiative 16, 20

CL

Confidence Level

CLS

Collecte Localisation Satellite 1, 2, 10, 85, 102, 105

CMEMS

Copernicus Marine Environment Monitoring Service 4, 6, 7, 8, 11, 18, 35, 40, 45, 46, 56, 62, 63, 64, 65, 66, 68, 69, 70, 71, 76, 77, 78, 79, 80, 81, 82, 110, 111

CNES

Centre national d'études spatiales 4, 5, 16, 17, 19, 20, 21, 22, 24, 95, 102

CORIOLIS

French operational in situ data service 56, 61, 103

CSIRO

Australia's Commonwealth Scientific and Industrial Research Organisation
4, 5, 16, 17, 19, 20, 21, 24

DHA

Dynamic Height Anomalies 3, 7, 8, 12, 55, 56, 59, 60, 61, 62, 63, 64, 65, 66, 67, 68, 69, 70, 71, 76, 77, 78, 79, 80, 81, 82, 109

DOC

Dissolved Organic Carbon 10

DORIS

The Doris system is a french civil precise orbit determination and positioning system. 37, 47



DT

Delayed Time 7, 8, 62, 66, 68, 71, 77, 82

ENSO

El Niño Southern Oscillation 20, 25, 33

ERS

European Remote-Sensing Satellite (ERS-1, ERS-2) 6, 16, 19, 20, 22, 26, 40, 41, 43, 54, 104

ESA

European Space Agency 4, 5, 16, 17, 20, 21, 24

EWH

Equivalent Water Height 66, 69, 72

GCOS

Global Climate Observing System 26, 33, 83, 92

GDR

Geophysical Data Record (Altimeter L2 product for delayed time) 56

GFZ

GeoForschungsZentrum (Germany's National Research Centre for Geosciences) 8, 55, 58, 66, 67, 68, 72, 73, 75, 76

GIA

Glacial Isostatic Adjustment 4, 5, 7, 12, 21, 25, 29, 37, 38, 59, 63, 64, 66, 67, 68, 72, 73, 74, 75, 81, 110

GMSL

Global mean Sea Level 3, 4, 5, 6, 9, 11, 12, 13, 15, 17, 18, 20, 21, 22, 23, 24, 27, 28, 29, 30, 31, 32, 33, 38, 39, 40, 42, 44, 45, 47, 48, 49, 51, 52, 53, 54, 73, 83, 84, 86, 87, 88, 89, 90, 91, 92, 93, 94, 95, 96, 97, 99, 101, 102

GLOSS/CLIVAR

Global Sea Level Observing System / Climate Variability and Predictability 3, 5, 6, 9, 35, 36, 38, 39, 40, 44, 45, 46, 49, 50, 51, 52, 53, 54, 86

GPS

Global Positioning System 5, 37, 38, 47

GRACE



Gravity Recovery and Climate Experiment 7, 8, 12, 15, 33, 55, 58, 62, 63, 64, 65, 66, 67, 68, 69, 71, 72, 73, 74, 75, 81, 103, 104, 105

GRGS

Groupe de Recherche en Géodésie Spatiale 3, 4, 7, 8, 55, 58, 63, 64, 65, 66, 67, 69, 73, 76, 77, 78, 79, 80, 81, 82, 104, 109, 111

JPL

Jet Propulsion Laboratory 8, 58, 66, 67, 68, 72, 73, 75, 76

MEI

Multivariate ENSO Index 4, 20, 22

MSL

Mean Sea Level 3, 4, 5, 6, 11, 12, 13, 15, 16, 17, 18, 19, 20, 22, 23, 25, 26, 31, 32, 33, 34, 35, 38, 40, 42, 43, 44, 45, 46, 47, 49, 52, 53, 55, 62, 74, 83, 84, 86, 87, 90, 102, 107

MSS

Mean Sea Surface 31

NASA

National Aeronautics and Space Administration 4, 5, 16, 17, 19, 20, 21, 24

NOAA

National Oceanic and Atmospheric Administration 4, 5, 16, 17, 19, 20, 21, 24

OSTST

Ocean Surface Topography Science Team 13, 85, 93, 95

PSMSL

Permanent Service for Mean Sea Level 3, 5, 6, 9, 35, 36, 37, 38, 40, 44, 45, 46, 49, 50, 52, 53, 54, 85, 86

RMS

Remote mean Square 68, 70, 71

RMSD

Remote mean Square Difference 68

RSS

Root of sum of squares 48

SARAL



Satellite with ARgos and ALtika (altimeter) 6, 7, 8, 16, 19, 20, 40, 41, 44, 53, 54, 56, 57, 60, 64, 76, 82

SALP

Service Altimétrie Localisation Précise 15, 17, 59, 63, 95, 102, 105

SL_cci

Sea Level Climate Change Initiative project (ESA) 4, 5, 17, 19, 20, 21, 24

SLA

Sea Level Anomaly 3, 5, 7, 8, 12, 25, 35, 55, 56, 59, 60, 61, 62, 63, 65, 66, 67, 68, 71, 76, 78, 82

SSH

Sea Surface Height 16, 18, 35, 37, 56, 61

T/P

TOPEX/Poseidon 17, 20, 23, 50, 51, 53, 85

TG

Tide Gauge 11, 35, 38, 39, 40, 44, 50, 51, 52, 85, 107

TOPEX

TOPography EXPerimental altimeter mission launched in 1992 3, 5, 6, 9, 11, 13, 15, 16, 18, 19, 22, 23, 24, 26, 27, 28, 29, 30, 38, 39, 40, 42, 44, 45, 49, 53, 54, 83, 85, 86, 87, 88, 89, 90, 91, 92, 104

TS

Temperature Salinity profiles 7, 12, 55, 59, 62, 66, 67, 68, 71, 75, 81

UHLSC

University of Hawaii Sea Level Center 35

VLM

Vertical Land Motion 5, 37, 38, 39, 49, 51